

See discussions, stats, and author profiles for this publication at: <https://www.researchgate.net/publication/324668879>

Optical spectroscopy of laser-produced plasmas for standoff isotopic analysis

Article in Applied Physics Reviews · June 2018

DOI: 10.1063/1.5016053

CITATIONS
190

READS
10,780

5 authors, including:



S. S. Harilal
Pacific Northwest National Laboratory

327 PUBLICATIONS 9,620 CITATIONS

[SEE PROFILE](#)



Brian Brumfield
Physical Sciences Inc.

78 PUBLICATIONS 1,367 CITATIONS

[SEE PROFILE](#)



K.C. Hartig
Pennsylvania State University

18 PUBLICATIONS 454 CITATIONS

[SEE PROFILE](#)

APPLIED PHYSICS REVIEWS

Optical spectroscopy of laser-produced plasmas for standoff isotopic analysis

S. S. Harilal,^{a)} B. E. Brumfield, N. L. LaHaye, K. C. Hartig,^{b)} and M. C. Phillips
Pacific Northwest National Laboratory, Richland, Washington 99352, USA

(Received 15 November 2017; accepted 19 March 2018; published online 20 April 2018)

Rapid, in-field, and non-contact isotopic analysis of solid materials is extremely important to a large number of applications, such as nuclear nonproliferation monitoring and forensics, geochemistry, archaeology, and biochemistry. Presently, isotopic measurements for these and many other fields are performed in laboratory settings. Rapid, in-field, and non-contact isotopic analysis of solid material is possible with optical spectroscopy tools when combined with laser ablation. Laser ablation generates a transient vapor of any solid material when a powerful laser interacts with a sample of interest. Analysis of atoms, ions, and molecules in a laser-produced plasma using optical spectroscopy tools can provide isotopic information with the advantages of real-time analysis, standoff capability, and no sample preparation requirement. Both emission and absorption spectroscopy methods can be used for isotopic analysis of solid materials. However, applying optical spectroscopy to the measurement of isotope ratios from solid materials presents numerous challenges. Isotope shifts arise primarily due to variation in nuclear charge distribution caused by different numbers of neutrons, but the small proportional nuclear mass differences between nuclei of various isotopes lead to correspondingly small differences in optical transition wavelengths. Along with this, various line broadening mechanisms in laser-produced plasmas and instrumental broadening generated by the detection system are technical challenges frequently encountered with emission-based optical diagnostics. These challenges can be overcome by measuring the isotope shifts associated with the vibronic emission bands from molecules or by using the techniques of laser-based absorption/fluorescence spectroscopy to marginalize the effect of instrumental broadening. Absorption and fluorescence spectroscopy probe the ground state atoms existing in the plasma when it is cooler, which inherently provides narrower lineshapes, as opposed to emission spectroscopy which requires higher plasma temperatures to be able to detect thermally excited emission. Improvements in laser and detection systems and spectroscopic techniques have allowed for isotopic measurements to be carried out at standoff distances under ambient atmospheric conditions, which have expanded the applicability of optical spectroscopy-based isotopic measurements to a variety of scientific fields. These technological advances offer an *in-situ* measurement capability that was previously not available. This review will focus on isotope detection through emission, absorption, and fluorescence spectroscopy of atoms and molecules in a laser-produced plasma formed from a solid sample. A description of the physics behind isotope shifts in atoms and molecules is presented, followed by the physics behind solid sampling of laser ablation plumes, optical methods for isotope measurements, the suitable physical conditions of laser-produced plasma plumes for isotopic analysis, and the current status. Finally, concluding remarks will be made on the existing knowledge/technological gaps identified from the current literature and suggestions for the future work. © 2018 Author(s). All article content, except where otherwise noted, is licensed under a Creative Commons Attribution (CC BY) license (<http://creativecommons.org/licenses/by/4.0/>). <https://doi.org/10.1063/1.5016053>

TABLE OF CONTENTS

I. INTRODUCTION	2
II. OPTICAL SPECTROSCOPY.....	4
A. Atoms	4
B. Molecules	4

^{a)}Author to whom correspondence should be addressed: hari@pnnl.gov

^{b)}Present address: Nuclear Engineering Program, University of Florida, Gainesville, Florida 32611, USA.

III. ORIGIN OF ISOTOPE SHIFT AND HYPERFINE STRUCTURE	5
A. Isotope splitting of optical transitions in atoms and atomic ions	5
B. Isotope splitting of optical transitions in molecules	6
C. Hyperfine structure	8
IV. SOLID SAMPLING USING LASER-PRODUCED PLASMAS.....	8
A. Physics of laser-produced plasmas	9



1. Nanosecond and femtosecond laser-produced plasma	10
2. Femtosecond laser filament-produced plasma	12
B. Ambient air and plasma chemistry	13
C. Line broadening mechanisms in laser-produced plasmas	14
1. Doppler broadening	14
2. Pressure broadening	14
3. Stark broadening	15
4. Instrument/artifactual broadening	15
D. LPP physical conditions suitable for isotopic analysis	16
V. OPTICAL SPECTROSCOPY MEASUREMENT TECHNIQUES	17
A. Laser-induced breakdown spectroscopy (LIBS)	18
B. Laser absorption spectroscopy (LAS)	20
C. Laser-induced fluorescence (LIF) spectroscopy	21
VI. ISOTOPIC ANALYSIS USING OPTICAL SPECTROSCOPY	24
VII. PLASMA GENERATION AT STANOFF DISTANCES	26
VIII. SUMMARY AND OUTLOOK	27

I. INTRODUCTION

Isotopic analysis is defined as the measurement of isotope ratios of selected elements within a sample of interest. Variations in stable isotope ratios or simply the presence of certain isotopes generated through nuclear decay processes can provide useful information about a sample's origin and history. Currently, isotopic analysis is used in a large number of fields, such as nuclear forensics and non-proliferation monitoring, archaeology, geology, biology, medical, and environmental applications. Isotopic analysis of samples of interest in nuclear forensics applications answer questions related to global security issues (such as nuclear fuel enrichment), while isotopic analysis can also provide answers to archaeological and anthropological questions that span the globe over both time and space. Isotopic signatures are present in biological material such as human or animal tooth and bone and in environmental monitoring.¹

The field of archaeology has several areas which require accurate isotopic detection. Isotopic analysis can be used to determine diet through analysis of the $^{12}\text{C}/^{13}\text{C}$ ratio,^{2,3} population movement based on strontium and lead isotopes, and the geographic origin of people and animals. Various archaeological materials (pottery, ceramics, rocks, etc.) can also be characterized by their isotopic compositions for classification⁴ and to determine provenance,^{5,6} making it possible to extrapolate population movement or trade patterns. Analysis of large or difficult-to-move artifacts could benefit greatly from the availability of in-field, non-contact methods that do not require subsampling or transfer of the artifact to a laboratory, allowing for the artifact to remain intact and in place. Perhaps the most recognizable application of isotopic analysis to archaeology,

though, is for the dating of materials, specifically carbon-14 dating.⁷ In addition to carbon dating, several other methods of material dating exist that involve the determination of isotope ratios, including uranium-thorium,^{8,9} potassium-argon, argon-argon,¹⁰ cesium-barium,¹¹ aluminum-magnesium,¹² iron-nickel,¹³ and uranium-lead dating.^{9,10,14,15}

There are several areas of geoscience relying on isotopic analysis, especially for geochronology. A recent review outlined the various applications of stable isotope ratios to geoscience, including chemistry, geology, and forensics.¹⁶ Several isotopes can be employed to determine the location of origin and source processes of rocks, ores, soils, clay, ceramics, etc., including strontium,¹⁷ sulfur, lead, samarium/neodymium, and osmium. Isotopic analysis, specifically of chlorine,¹⁸ carbon, and the uranium decay chains, has been used to study ocean currents and circulation. This also connects into environmental applications of isotopic detection. Stable isotope variations (such as $\delta^2\text{H}$, $\delta^{15}\text{N}$, and $\delta^{18}\text{O}$) in rainfall are strongly correlated with temperature,¹⁹ so analysis of core profiles can provide the temperature history in a region. The behavior of the core depth profile in oceans can indicate whether water movement at a given depth is dominated by advection or diffusion¹⁹ and improve knowledge of currents. Carbon and oxygen isotopic compositions can also provide information on temperature history, specifically in the reconstruction of paleoclimates.²⁰ Geological and environmental applications of isotopic detection can be extended to the analysis of extraterrestrial materials that are of interest to planetary scientists. Geochronology of different landforms such as mountains and plains helps to develop a formation timeline and reconstructs various events that may have occurred on the planet such as continental weathering.^{21,22} Specifically, strontium dating has been investigated for application to rocks on Mars, and Cl isotopic composition ($\delta^{37}\text{Cl}$) can give information on the origin of planets.²³

Various applications of isotopic analysis exist in the field of forensic science. Gunshot residue has been isotopically analyzed to distinguish different gun powders and types of ammunition²⁴ to aid in criminal apprehension and prosecution. This analysis can be extended to other explosives.²⁵ The isotopic composition can also be used to characterize illegal drugs and to identify counterfeit pharmaceuticals.²⁶ Isotopic analysis is important in the food industry for food security and conservation. Isotopic composition has specifically been used to determine fish migration patterns²⁷ and the origin of rice through Sr and Pb isotopes.²⁸

Isotopic enrichment is a fundamental measurement of nuclear fuel production, nuclear forensics, nuclear safeguards, and nuclear waste remediation. It is well-known that uranium isotopic enrichment varies largely between its use in the majority of civilian nuclear reactors and weapons, making isotopic analysis of special importance due to concerns over illicit production and trafficking of nuclear materials.²⁹ Rapid, in-field analysis of samples of interest can immediately provide information to inspectors whether further investigation of a site is necessary. Non-contact sampling provides the added benefits of reducing contamination risks to equipment and personnel. Forensic knowledge of the isotopic composition of various nuclear samples is regularly required.³⁰ Additional nuclear applications include nuclear reactor diagnostics, fuel

fabrication, Fukushima molten core analysis, waste treatment,³⁰ and treaty verification.³¹ Nuclear safeguards also involve the analysis of environmental samples for Cs to determine contamination^{32,33} and for both U and Pu isotopes³⁴ to detect any potential unsafe or misuse of nuclear technology in the nuclear industry, nuclear forensics, and for regulatory agencies.^{33,35,36} The isotopic composition of nuclear materials (beyond U isotopes) can give an indication of its origin,³⁵ which is crucial information for enforcement of nuclear regulations by agencies such as the International Atomic Energy Agency (IAEA).

There are also several other, unrelated applications of isotopic detection. Measurement of the amount of tritium embedded in a material as a function of depth is of great interest to the fusion community, specifically in plasma-facing components to determine tritium retention during and between plasma pulses.³⁷ Accurate determination and mitigation of tritium retention is not only important to the performance of the fusion device but also its lifetime. Recently, several biological and health applications have arisen in which accurate detection of isotopes is of interest. Sulfur isotope ratios have been investigated as an indicator of liver cancer.³⁸ A few examples also appeared in a recent review.³⁹ Cu isotope ratios have been analyzed in urine⁴⁰ and serum⁴¹ for diagnosis of Wilson's disease. Stable iron isotopes⁵⁴Fe and⁵⁷Fe have been spiked as tracers in formula milk to determine Fe pathways in the body through analysis of various biological samples, including blood, feces, urine, and organ tissue.⁴² Iron (using⁵⁷Fe as the tracer)⁴³ and Zn⁴⁴ were also analyzed in brain tissue samples to determine uptake pathways.

The wide variety of applications described above clearly demonstrates the necessity for accurate *in-situ*, non-contact, real-time isotopic analysis in a large number of fields. Nearly all the applications listed above currently use laboratory analysis of a sample material. Isotope-resolved mass spectrometry is a well-established analytical tool for laboratory measurements.^{16,45} Although laboratory techniques are capable of high accuracy, they are also limited by the need to physically acquire and prepare a sample, transport the sample to an analytical laboratory, and often chemically prepare and analyze the sample, all of which require time and highly skilled personnel. Development of new techniques to perform rapid isotopic analysis of solid materials in the field with no sample preparation has the potential to increase the speed of analysis, reduce measurement costs and waste, and may also open up new applications previously unobtainable by laboratory techniques.

Optical spectroscopy techniques have the potential to perform in-field, rapid, and non-contact isotopic analysis. The basis of optical spectroscopy is the probing of transitions between energy levels of an atom or molecule via absorption or emission of photons; these characteristic energy levels can be determined by measuring the photon energies (or wavelengths). Furthermore, because the measurement is performed using photons, no physical contact with a sample is required. The energies of optical transitions in atomic or molecular systems are affected by the mass of the nucleus, and thus optical spectroscopy has the potential to differentiate between isotopes based on changes in the photon energy. Isotope shifts

observed in electronic optical transitions arise primarily due to variation in the charge distribution of the nucleus for heavy elements, and due to a difference in the mass of the nucleus for the light elements when the number of neutrons is changed. The nuclear mass difference also leads to shifts in vibrational and rotational energy transitions of molecular species. However, in order to isolate optical emission or absorption arising from different isotopes, the energy separation of these transitions must be greater than the transition linewidths. Hence, one of the key figures-of-merit for using optical spectroscopy for isotopic analysis is the linewidth relative to isotope shift separation.

High-resolution optical spectroscopy is routinely used to measure electronic, vibrational, and rotational transitions in atoms and molecules. The spectral linewidths for atoms or molecules in the gas phase at moderate pressures (≤ 1 atm) and temperatures (< 1000 K) are sufficiently narrow to permit resolution of transition energies between different isotopic species. Isotopic analysis of gas-phase molecules is a relatively mature research area for atmospheric sciences, where commercial instruments utilizing near-infrared (NIR) cavity-enhanced and mid-infrared (MIR) laser spectroscopy are routinely used for molecular isotope spectroscopy of atmospheric gases (i.e., H₂O, CO₂, and N₂O).^{46–51} Unfortunately, direct optical spectroscopy of solid materials can result in broad, unresolved spectral lines from different isotopes due to interatomic interactions, which makes resolving the small isotope-induced shift difficult or impossible. Laser ablation (LA) or laser-produced plasma (LPP) provides a solution to this problem where a solid material can be brought into the plasma/gas phase where high-resolution spectroscopy can probe the isolated atoms/molecules. The added benefits of non-contact and *in-situ* detection provided by optical spectroscopic tools in conjunction with LPP production are advantageous, if not necessary for several applications (e.g., in planetary science, archaeology, and security/safeguards) where samples cannot easily be accessed or brought back to a laboratory for analysis.

In the last three decades, LPP-based technologies have gained significant ground in a wide variety of applications including nanolithography and nanotechnology, analytical and material sciences, medicine, planetary and environmental sciences, and nuclear safeguards and nonproliferation. In a LPP system, because of the transient nature of the plasma, physical conditions change dramatically during its evolution which directly influences the intensity and linewidth of atomic and molecular transitions. The incident laser parameters (pulse width, intensity, and wavelength) and the ambient environmental conditions (i.e., nature and pressure of the gas, ambient atmosphere-initiated plasma chemistry, etc.) can also affect fundamental properties of the LPP. For many years, various research organizations and universities have investigated the potential of laser-based standoff methods for the detection and discrimination of hazardous materials^{52,53} and radiological threats.⁵⁴

This review provides the recent advances in isotopic analysis employing optical spectroscopy in conjunction with laser ablation-based solid sampling. The review covers a brief description of the physics behind optical spectroscopy of atoms and molecules, the origin of isotope splitting in

atoms and molecules, hyperfine structure, the physical conditions of LPPs that are most favorable for isotopic analysis, isotope measurement methods employing LA, and the present status of optical spectroscopy as a non-contact *in-situ* tool for isotopic analysis. At the end of the review, the current status of the field will be summarized and the future outlook will be discussed.

II. OPTICAL SPECTROSCOPY

Optical spectroscopy incorporates different techniques to study the interaction of matter with light. We consider two processes occurring when a light beam interacts with a sample: absorption or emission. Various information about the sample material can be obtained by analyzing the amount of light absorbed or emitted. The type of interaction between the light and the sample depends on the wavelength and intensity of light and how the light beam affects the atoms or molecules in the sample. A brief discussion of the absorption and emission processes in atoms and molecules are given below.

A. Atoms

The electronic states of atoms have well-defined energies corresponding to the filling of atomic orbitals that result in different electron configurations. An atom can transition from one electron configuration to another through the absorption or emission of a photon or via energy transfer through inelastic collisions with other atoms and molecules. A simple schematic of absorption and emission of two electronic levels is given in Fig. 1. The frequency (ν) or wavelength (λ) of the photon involved in the absorption or emission process is directly related to the energy difference between the two electronic levels E_1 and E_2 and is given by

$$E_2 - E_1 = h\nu = hc/\lambda, \quad (1)$$

where h is Planck's constant and c is the speed of light. Since electronic levels are unique for each element in the periodic table, the emitted photon is representative of each individual element. The electronic levels in atoms are also

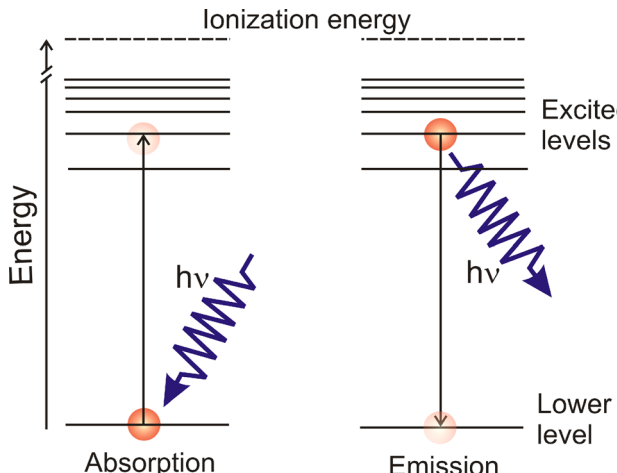


FIG. 1. Absorption and emission between two electronic levels in an atomic system.

susceptible to fine structure and hyperfine structure splitting due to spin-orbit coupling and electron-nuclear spin-spin interaction. The photons associated with electronic transitions in atoms radiate mostly in the NIR, visible (VIS), and ultraviolet (UV) wavelengths.

The spontaneous emission intensity of an electronic transition in an atom with a frequency ν depends on the atomic transition probability A (or Einstein coefficient) of spontaneous emission and the number density of the species in the upper level N_2 (density of the species in the lower level N_1 for absorption). All lines are broadened because of various broadening mechanisms. If ϕ_ν is the area-normalized line profile function, which gives the emission/absorption of a line with a central frequency ν , the spectral emission coefficient $\epsilon_{2 \rightarrow 1}$ of a line $2 \rightarrow 1$ is given by

$$\epsilon(\nu)_{2 \rightarrow 1} = \frac{h\nu}{4\pi} A_{21} N_2 \phi_\nu. \quad (2)$$

Similar to the emission coefficient, the absorption coefficient $\alpha_{1 \rightarrow 2}$ can be written as

$$\alpha(\nu)_{1 \rightarrow 2} = \frac{h\nu}{4\pi} (N_1 B_{12} - N_2 B_{21}) \phi_\nu, \quad (3)$$

where B_{12} and B_{21} are the Einstein coefficients for induced absorption and stimulated emission, respectively.

Under thermal equilibrium, the relative populations of the energy levels are given by a Boltzmann distribution. Then, the relation between the Einstein coefficients and the dependence of the number density of an electronic level to temperature (T) through the Boltzmann law are given by

$$g_1 B_{12} = g_2 B_{21}, \quad (4)$$

$$A_{21} = \frac{2h\nu^3}{c^2} B_{21}, \quad (5)$$

$$N_n = \frac{N_0}{Z(T)} g e^{-E_n/kT}, \quad (6)$$

where g , N_0 , N_n , E_n , and $Z(T)$ are the degeneracy, the total atomic number density, the number density of the selected level, the energy of the selected level, and the partition function, respectively. Thus, each atomic species absorbs or emits photons at a set of discrete and characteristic frequencies determined by the electronic energy levels and their relative populations, which depends on the excitation temperature.

B. Molecules

For molecules, the overlap of atomic orbitals leads to the formation of molecular orbitals corresponding to the chemical bonds that exist between the atoms. Similar to atoms, the different possible electron configurations of these molecular orbitals define the discrete electronic energy of the molecule. Within the limit of the Born-Oppenheimer approximation, we can construct potential energy surfaces for the different molecular electronic states where the electronic energy can be determined as a parametric function of the position of the nuclei. For polyatomic molecules, this can form a complex n-dimensional surface due to the multiple

interatomic distances, but for the simplest case of a diatomic molecule, the electronic potential energy surface only depends on a single internuclear separation. For simplicity, in this review, we consider optical spectroscopy of diatomic molecules only, considering that optical emission from diatomics is commonly observed in laser-produced plasmas. A generalized diagram of the potential energy surfaces for two electronic states of a diatomic molecule is provided in Fig. 2.

The energy level structure of a simple molecular system such as a diatomic molecule can be described using the anharmonic oscillator—non-rigid rotor model framework with the first correction terms from the harmonic oscillator rigid-rotor approximation.⁵⁵ In Fig. 2(a), the potential energy curves are provided for two electronic transitions belonging to a general diatomic molecule. The minimum point for each potential energy curve corresponds to the electronic energy (T_e). The diatomic molecule possesses both vibrational and rotational degrees of freedom that contribute to the overall energies within a given electronic state. In Fig. 2, the quantized vibrational and rotational energies for each electronic state are given. For each electronic level, there is a vibrational energy level manifold (G_v) with bound states up to the point of the dissociation energy of the molecule. For a given vibrational level, there is a corresponding rotational energy level manifold (F_J). An example of the rotational level structure for a given vibrational level is provided in Fig. 2(b). The combined energy of a rovibronic state can be expressed as the summation of the electronic (T_e), vibrational (G_v), and rotational energies (F_J)⁵⁵

$$E(e, v, J) = T_e + G_v + F_J. \quad (7)$$

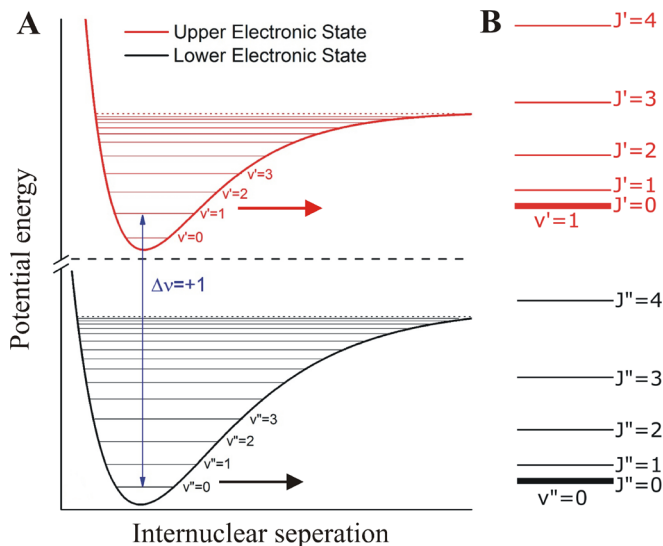


FIG. 2. (a) Energy diagram for a diatomic molecule with upper and lower state potential energies for two electronic levels, shown plotted against the internuclear separation. Vibrational (v) and rotational energy (J) levels in the upper and lower states are denoted by ' or ", respectively. The first four vibrational levels for each electronic state are labeled, and a blue arrow is drawn to show a rovibronic transition with $\Delta v=+1$. (b) An expanded view of the ro-vibrational manifold for the two vibrational levels involved in the rovibronic transition corresponding to the blue arrow in panel A. The first 4 rotational levels within each respective vibrational manifold are labeled.

The energy corresponding to an optical transition (ε) for a diatomic molecule is given by the difference of the energies for the (e, v, J) levels in the upper and lower electronic states⁵⁵

$$\begin{aligned} \varepsilon &= E(e', v', J') - E(e'', v'', J'') \\ &= T'_e + G'_v + F'_J - (T''_e + G''_v + F''_J). \end{aligned} \quad (8)$$

In this expression, the upper state and lower state energy terms are represented by ' and ", respectively.

Similarly to atomic transitions, each molecular species absorbs or emits light at a set of discrete and characteristic frequencies determined by the energy levels and their populations. In general, each molecular species has many more transitions than the corresponding atoms composing the molecule, due to the inclusion of vibrational and rotational energy levels. It is worth noting that for molecules with large moments of inertia, the rotational levels become more closely spaced and may be difficult to resolve using standard absorption and emission techniques.

III. ORIGIN OF ISOTOPE SHIFT AND HYPERFINE STRUCTURE

The optical spectra of atoms and most small molecules are composed of extremely narrow transitions that have the potential to be used for isotope-specific detection of targeted elements. Small changes in the transition frequencies can be attributed to differences in the nuclear structure of the isotopes. The predominant isotope shift effects arise from differences in mass, nuclear spin, and nuclear charge distribution. Optical transitions in neutral atoms, ions, and molecules all exhibit isotope shifts, and isotope splitting largely varies not only with the elements of interest but also with the selected optical transitions. The physics behind the isotope shift in atomic and molecular transitions is briefly given in Subsections III A–III C. The hyperfine structure (hfs) found in many electronic transitions is comparable to isotope splitting, so a brief description of hyperfine splitting in atoms is also given. A detailed account of isotope splitting^{55–61} and hyperfine splitting^{58,61–63} can be found elsewhere.

A. Isotope splitting of optical transitions in atoms and atomic ions

The isotopes of an element differ in their nuclear masses. The shift in frequency of a selected optical transition i between two isotopes of masses A and A' is conventionally divided into two components

$$\delta\nu_i^{AA'} = \delta\nu_{i,MS}^{AA'} + \delta\nu_{i,FS}^{AA'}. \quad (9)$$

The first term is the mass shift (MS) and is related directly to the difference in mass between the isotopes, while the second term is the so-called field shift (FS), which arises from differences in the nuclear charge distribution. The MS is customarily divided into a normal mass shift (NMS) due to the introduction of the reduced mass μ of the electron-nuclear system in the kinetic energy and a specific mass shift (SMS) arising from correlations in the motion of electrons and the

influence of those correlations on the nuclear recoil energy. The SMS is generally smaller than the NMS. As an example, for the ^{235}U - ^{238}U isotope pair the fractional NMS in any transition is only 2.94×10^{-8} of the given transition frequency, which corresponds to a 15 MHz (0.018 pm) isotope shift for a visible transition at 600 nm. However, for uranium atoms and ions, the SMS shifts are very small and are not expected to be practically useful for isotopic resolution. Isotope shifts of lighter and heavier elements located in the periodic table are found to be larger compared to elements with moderate masses. The isotope shifts in lighter atoms are primarily due to the mass shift, whereas the field shift scales with nuclear charge (Z) as Z^5 to Z^6 and becomes the dominant isotope shift effect in heavier atoms.⁶⁴

The isotope shifts change significantly with optical transitions based on their electronic configuration. Due to the dependence on the change in electronic charge density at the nucleus, the transitions that change the number of s-electrons will generally have the largest isotope shifts. For example, the ground state configuration of neutral uranium is $[\text{Ra}]5f^3 6d7s^2$ and the singly charged ion is $[\text{Ra}]5f^3 6d7s$: excitation of one of the optically active 7s electrons results in transitions with large isotope shifts. Histograms of isotope shifts in GHz and pm for various transitions of U I and U II are given in Fig. 3. For the 549 U I transitions over the wavelength range of 285–882 nm, the isotope shift ranges from –24 to +20 GHz (–27 to 49 pm) with an average magnitude of 8.3 GHz (7.5 pm).^{65,66} Similarly, for the 823 U II transitions over the wavelength range of 224–879 nm, the isotope shift ranges from –42 to +56 GHz (–74 to 84 pm) with an average magnitude of 11.5 GHz (7.0 pm).^{67,68}

B. Isotope splitting of optical transitions in molecules

For diatomic molecules, isotope splitting is dominated by the effects of the reduced mass μ for the pair of nuclei on the

energy level spacing for the vibrational and rotational levels in the upper and lower states of optically allowed transitions. The effect of the change in the reduced mass results in slightly different transition energies between molecular states, with an energy/wavelength splitting that can be orders of magnitude larger than splitting for atomic transitions of different isotopes. Within the anharmonic oscillator—non-rigid rotor model framework, it is possible to show how differences in the reduced mass for different diatomic isotopologues results in isotope splitting of the optical transitions. The discussion here will be focused on molecular electronic transitions in the UV-VIS, also commonly referred to as rovibronic transitions; however, isotope splitting is also regularly observed for rovibrational and purely rotational transitions in the infrared and microwave spectral regions.

The difference in the energy levels for two isotopologues can be parameterized in terms of a ratio of the reduced masses for the two different diatomic isotopologues. For a diatomic molecule, the reduced mass μ is defined by

$$\mu = \frac{m_1 m_2}{m_1 + m_2}, \quad (10)$$

where m_1 and m_2 are the masses for the first and second atoms that comprise the diatomic molecule. The ratio of the reduced masses is given as

$$\rho = \sqrt{\frac{\mu}{\mu^*}}, \quad (11)$$

where ρ is the ratio of the reduced masses for the two different isotopologues of the diatomic molecule: μ and μ^* . Using ρ , it is possible to represent the difference in rovibronic energies between two isotopologues using the following expression:⁵⁵

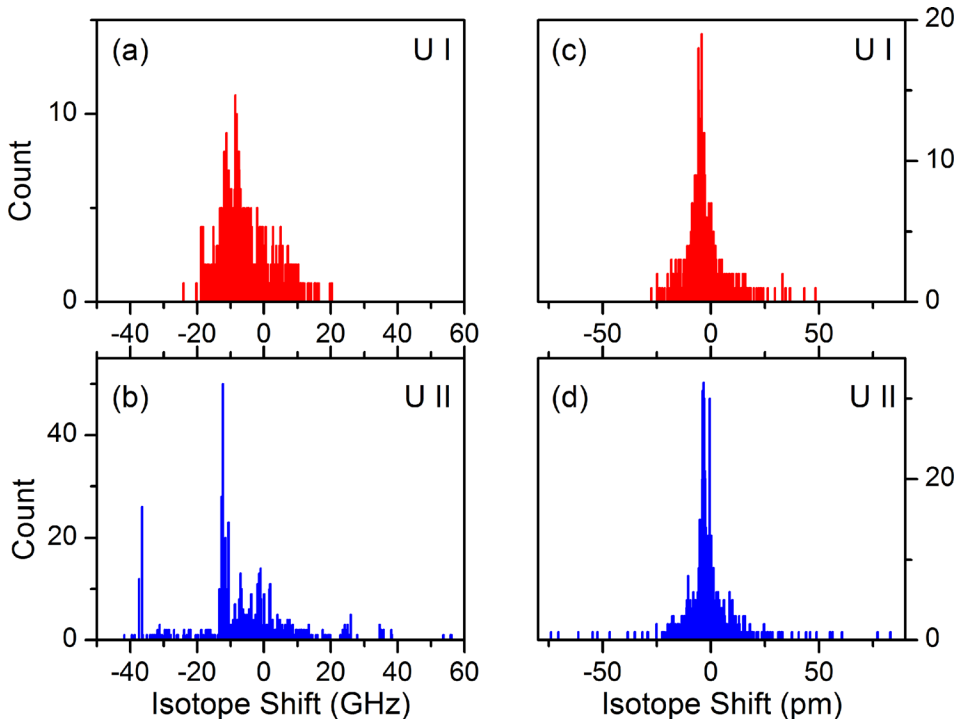


FIG. 3. Histograms of isotope shifts of U I [(a) and (c)] and U II [(b) and (d)] transitions in GHz (left) and pm (right) units.^{65–68}

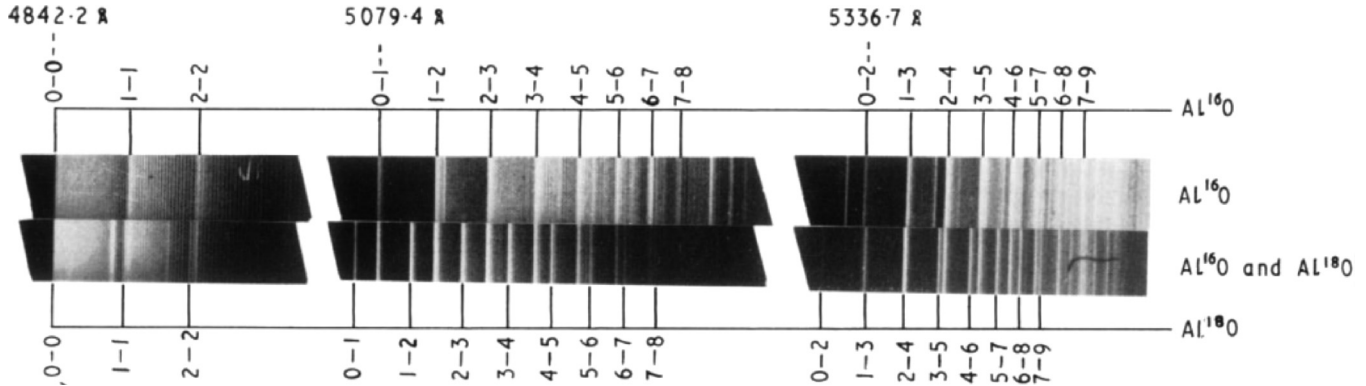


FIG. 4. Isotope shift in the blue-green $B^2\Sigma - X^2\Sigma$ electronic band of AlO. The spectral features were recorded using dc arc plasma with Al electrodes in the presence of 10 Torr oxygen ambient. To obtain the spectra of Al¹⁸O, oxygen ambient enriched in ¹⁸O to 50% was used.⁶⁹ Reprinted with permission from M. Singh and N. A. Narasimham, J. Phys. B **2**, 119 (1969) as Fig. 2. Copyright 2017 IOP.

$$\begin{aligned} \varepsilon - \varepsilon^* = & (1 - \rho) \left[\omega'_e \left(v' + \frac{1}{2} \right) - \omega''_e \left(v'' + \frac{1}{2} \right) \right] \\ & - (1 - \rho^2) \left[\omega'_e \chi'_e \left(v' + \frac{1}{2} \right)^2 - \omega''_e \chi''_e \left(v'' + \frac{1}{2} \right)^2 \right] \\ & + (1 - \rho^2) [B'_e J'(J' + 1) - B''_e J''(J'' + 1)] \\ & - (1 - \rho^3) \left[\alpha'_e \left(v' + \frac{1}{2} \right) J'(J' + 1) \right. \\ & \left. + \alpha''_e \left(v'' + \frac{1}{2} \right) J''(J'' + 1) \right] \\ & - (1 - \rho^4) [D' J'^2 (J' + 1)^2 - D'' J''^2 (J'' + 1)^2], \end{aligned} \quad (12)$$

where the energies for the rovibronic transitions for the different isotopologues are represented by ε and ε^* . In Eq. (12), the vibrational and rotational quantum numbers are represented by v and J , respectively. The first two terms describe the shift in the vibrational band head for the given rovibronic transition, while the last three terms describe the shift due to changes in the rotational energy levels. Based on Eq. (12), we expect molecular isotope splitting to increase as the quantum numbers v , J , and $|\Delta v|$ increase. There will also be a variation in the rotational splitting contribution with respect to ΔJ ; however, the values of ΔJ are limited to -1 , 0 , and $+1$ based on selection rules for allowed optical transitions. An example of the isotope shift of Al¹⁸O relative to Al¹⁶O bands is given in Fig. 4 and it clearly shows increase in isotopic shifts with increasing v , and $|\Delta v|$.⁶⁹ We can also expect the size of molecular isotope splitting to grow smaller as the mass of the diatomic species increases, as this reduces the

value of ρ . The value of ρ will also increase as the difference in the number of neutrons between the two isotopes that are in the diatomic molecule increase.

To explore the dependence of the vibrational isotope shift with respect to ρ , v , and Δv , it is instructive to consider two diatomic species with significant differences in masses: the B-X transitions for ¹⁰B¹⁶O/¹¹B¹⁶O and for ²⁰⁷Pb¹⁶O/²⁰⁸Pb¹⁶O. The molecular constants are obtained from the NIST Chemistry Webbook.⁷⁰ Summaries of the calculated vibrational isotope shifts for BO and PbO are provided in Table I. For both molecular species, we see that vibrational isotope shift can be positive or negative with respect to the upper and lower vibrational state quantum numbers for the different vibrational transitions. Comparing the relative size of the vibrational isotope shifts between BO and PbO, the vibrational isotope shift for BO is generally ~ 400 times larger when compared to the corresponding transition for PbO for the same v' - v'' transitions. Part of this difference is connected to the differences in the value of ρ , which is 1.0292 for ^{10/11}BO and 1.000173 for ^{207/208}PbO. Some of the largest isotopic shifts calculated in Table I correspond to changes in vibrational quanta greater than 1, and these larger isotope shifts should improve the detection sensitivity for the isotopologues of interest. When selecting the optimum vibrational band head, it is important to consider the Franck-Condon factors for the vibronic bands to be targeted as this will directly influence the emission intensity of the targeted vibronic bands.

When compared to the isotope splitting for atomic transitions, the effect of isotope splitting for light diatomic molecular spectra is significantly larger. As the diatomic mass increases, the change in the value of ρ becomes limited, and this results in a significant decrease in the vibrational isotope shift, to the point that it can be comparable to the expected atomic isotope

TABLE I. Calculated vibrational isotope shift (in GHz) for the B-X BO electronic transition for ¹¹B/¹⁰B and for the B-X PbO electronic transition for ²⁰⁸Pb/²⁰⁷Pb with respect to v' and v'' .

v'/v''	B-X BO electronic transition for ¹¹ B/ ¹⁰ B				B-X PbO electronic transition for ²⁰⁸ Pb/ ²⁰⁷ Pb			
	0	1	2	3	0	1	2	3
0	264	-822	-1869	-2877	0.57	-1.95	-4.44	-6.9
1	1875	789	-258	-1266	4.23	1.71	-0.78	-3.24
2	3441	2358	1311	300	7.83	5.28	2.79	0.36
3	4968	3882	2835	1827	11.34	8.79	6.3	3.87

splitting. For example, lighter elements like B provide significantly larger isotope splitting (IS) for molecules in comparison with atomic isotope splitting: for ^{10}B - ^{11}B , the IS is ~ 10 GHz⁷¹ and for ^{10}BO - ^{11}BO , the IS is ~ 4000 GHz. However, the difference in isotope splitting between atomic and molecular transitions becomes insignificant for heavier elements. In the case of U atoms, the isotope splitting of ^{235}U - ^{238}U ranges from -27 GHz to $+49$ GHz (Fig. 3), while for ^{235}UO - ^{238}UO , the IS is ~ 40 GHz. In addition, the small rotational line spacing in molecules composed of heavy elements may make it difficult to resolve individual transitions to accurately determine isotope shifts.

C. Hyperfine structure

The hfs of atomic levels arises due to the interaction of nuclear dipole moments with the fields generated by electrons at the nucleus. If the nucleus has a spin angular momentum (I), it may couple with the total electronic angular momentum (J) to give a total angular momentum of the atom (F) resulting in hfs components or transitions between two hyperfine levels. For nuclei with an even atomic number and even mass number, the spin angular momentum is zero and hence no hfs is found in their spectral lines. Hyperfine splittings are usually small; however, in certain cases, they can be larger than isotope splitting. In that scenario, isotope shifts of atoms and molecules can be entangled with hyperfine structure. A brief account of hyperfine splitting is given here, and more details about hyperfine splitting can be found elsewhere.^{61–63}

The important dipole moments associated with a nucleus are the magnetic dipole moment, which is related to nuclear spin, and the electric quadrupole moment, which is connected to the deviation from the spherical charge distribution. The total amount by which the energy level splits (ΔE_{hfs}) is given by

$$\Delta E_{\text{hfs}} = \frac{AC}{2} + \frac{3BC(C+1) - 4BIJ(I+1)(J+1)}{8IJ(2J-1)(2I-1)}, \quad (13)$$

where

$$C = F(F+1) - J(J+1) - I(I+1). \quad (14)$$

A and B are hfs constants which will be unique for each isotope in each particular electronic level representing the electronic-nuclear magnetic dipole and electric quadrupole coupling and have units in Hz. The first term in Eq. (13) represents the magnetic dipole hfs and the second term represents the electronic dipole correction. The selection rules constrain the number of allowed transitions within the hfs. Since photons carry only one unit of angular momentum, the differences in electronic or atomic angular momentum quantum numbers are restricted to $\Delta J = 0$ and ± 1 and $\Delta F = 0$ and ± 1 , with $J0 \leftrightarrow 0$ and $F0 \leftrightarrow 0$ transitions forbidden. Isotope splitting and hyperfine structures of two special cases (Rb and U) are briefly discussed here.

There are two naturally occurring isotopes for rubidium: ^{85}Rb and ^{87}Rb . The ground state of Rb is $5^2\text{S}_{1/2}$ and the first excited state is split into two by the spin-orbit interaction ($5^2\text{P}_{1/2}$ and $5^2\text{P}_{3/2}$); each of these levels is split further by the

hyperfine interaction. The isotope splitting, the energy levels along with associated total angular momentum quantum numbers F for Rb isotopes (^{85}Rb and ^{87}Rb), and the simulated spectrum are given in Figs. 5(a) and 5(b) for $5^2\text{S}_{1/2} - 5^2\text{P}_{3/2}$ 780 nm D2 transition. The total angular momentum (F) given in Fig. 5(a) corresponds to the sum of nuclear and electron angular momentum values. There are six allowed transitions per isotope with $\Delta F = \pm 1, 0$. The composite spectrum given in Fig. 5(b) has overlapping isotope lines from ^{85}Rb (blue) and ^{87}Rb (red), including multiple hyperfine transitions (sharp lines).

Unlike Rb isotopes, the uranium isotope ^{235}U has significantly more complex hyperfine structure.^{63,72–74} The neutral uranium atom has 92 electrons with six outside the closed [Ra] core. In the ground-state configuration [Ra] $5f^36d7s^2$, any of these six outer electrons can be optically active, and complex angular momentum coupling between them leads to a large number of states within the same orbital configuration. Further, the coupling of the high-angular-momentum d - and f -electrons leads to extended and overlapping fine-structure patterns. Mixing and perturbation between these overlapping structures result in extremely complex energy level structures and correspondingly complex spectra. The resulting states can have wide-ranging total angular momentum J from 0 to > 9 (the ground state has $J=6$), and for ^{235}U coupling with nuclear spin ($I=7/2$) which can lead to a complex hyperfine structure. Modeled absorption spectral features of ^{238}U and ^{235}U including 22 allowed hyperfine transitions of ^{235}U are given in Fig. 6 for the U I 394.38 nm transition. Hfs is absent in ^{238}U because $I=0$. Because of the presence of the hfs, the ^{235}U exhibits a broadened spectrum with lower amplitude in comparison with the ^{238}U spectrum. Further details about U hfs can be found elsewhere.⁷⁵

IV. SOLID SAMPLING USING LASER-PRODUCED PLASMAS

Isotopes of atoms or molecules have the potential to be detected by optical methods if the isotope shifts are large enough to be distinguished using spectroscopic tools. Optical absorption and emission spectra of solid materials directly are useful to identify the elemental composition; however, the spectral features are too broad to permit determination of isotopic composition due to the small isotope shifts. Therefore, it is necessary to generate a vapor cloud from the solid that represents the composition of the solid sample of interest with a reduced number density of atoms for subsequent analysis using optical spectroscopy. Fortunately, LPPs can be used for solid sampling of any material of interest. LPPs are generated by focusing a high-intensity laser onto the surface of a medium, wherein absorption of laser photons causes sufficient heating of the medium to produce a plasma. Spectroscopic analysis of atomic line absorption and emission from the induced plasma are then used to deduce the composition and isotopic information. However, a LPP is a highly transient system with large gradients in temperature and density, and the level populations of atoms/ions and molecules change significantly during its evolution.^{76–80} As a consequence, the time and location used to probe a LPP with an optical diagnostic is critical to optimize

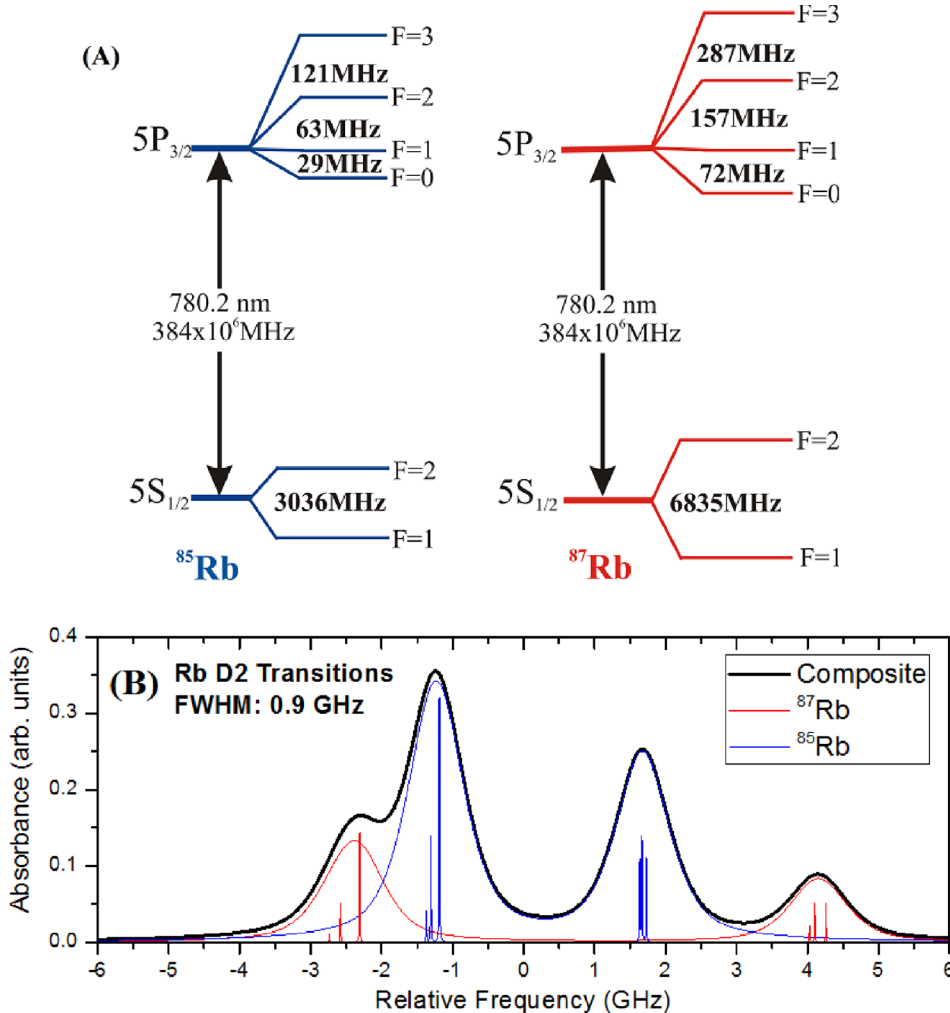


FIG. 5. (a) Energy level splitting in ^{85}Rb and ^{87}Rb showing hyperfine transitions. (b) Simulated Rb D2 isotope transitions along with a convoluted spectrum with a resolution of 0.9 GHz (1.82 pm). The composite spectrum (black) has overlapping spectral lines from ^{85}Rb (blue) and ^{87}Rb (red), including multiple hyperfine transitions (sharp lines).

the conditions for isotopic analysis. In Secs. IV A–IV D, a brief description of the physics of LPPs and the various parameters influencing LA sampling are given with an emphasis on identifying the suitable conditions in ns laser, fs laser, and filament ablation plumes for isotope spectroscopy using electron transitions in ions/neutral atoms and vibronic transitions in molecules.

A. Physics of laser-produced plasmas

LA is defined as the removal of material from a target of interest by direct absorption of laser energy. The amount of mass removed during LA, typically $\sim\text{ng-pg}$, vaporizes and subsequently generates a high-temperature and high-density plasma ($\sim 10\,000\text{--}50\,000 \text{ K}$ and $\sim 10^{19} \text{ cm}^{-3}$ at the onset)^{81,82} which contains excited atoms, ions, and molecules. Extensive studies of the fundamental properties of LA have been conducted in the last 50 years since the discovery of lasers in the 1960s.^{76,83} Even though the LPP process looks simple, the physics involved in LPP creation and its subsequent evolution is notoriously complex and contains many simultaneous processes, including sample heating, melting, vaporization, ejection of particles, plasma creation, plasma heating, and expansion.⁸⁴ The LPP plume properties vary significantly with space and time. The transient nature of LPP plumes can be understood from the time-resolved self-emission images given in Fig. 7.⁸⁵ Briefly,

the entire process of LA can be subdivided into three sub-processes: (i) plasma generation, (ii) laser-plasma interaction, and (iii) plume expansion.⁸⁶ All these processes are directly influenced by the target material (physical and chemical properties,⁸⁷ laser parameters (wavelength, pulse width, fluence at the target, etc.),^{88–90} and environmental conditions (nature and pressure of the ambient gas,^{91–94} magnetic fields,^{95–97} etc.). Hence, the parametric space of the LA process is large and can be used positively to optimize conditions for various applications including isotopic analysis by properly tuning the physical conditions of the produced plasma.

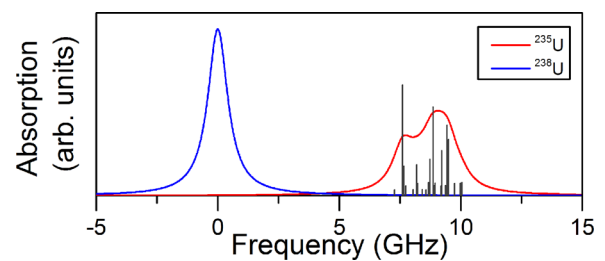


FIG. 6. Modeled absorption spectra including hyperfine structure for ^{235}U (red) and ^{238}U (blue) for U I 394.38 nm transition. The total area of the peaks is equal for the ^{238}U and ^{235}U transitions, where each transition is a Lorentzian with a 1 GHz FWHM. Relative strengths of 22 individual hyperfine transitions are also given (sharp black lines).

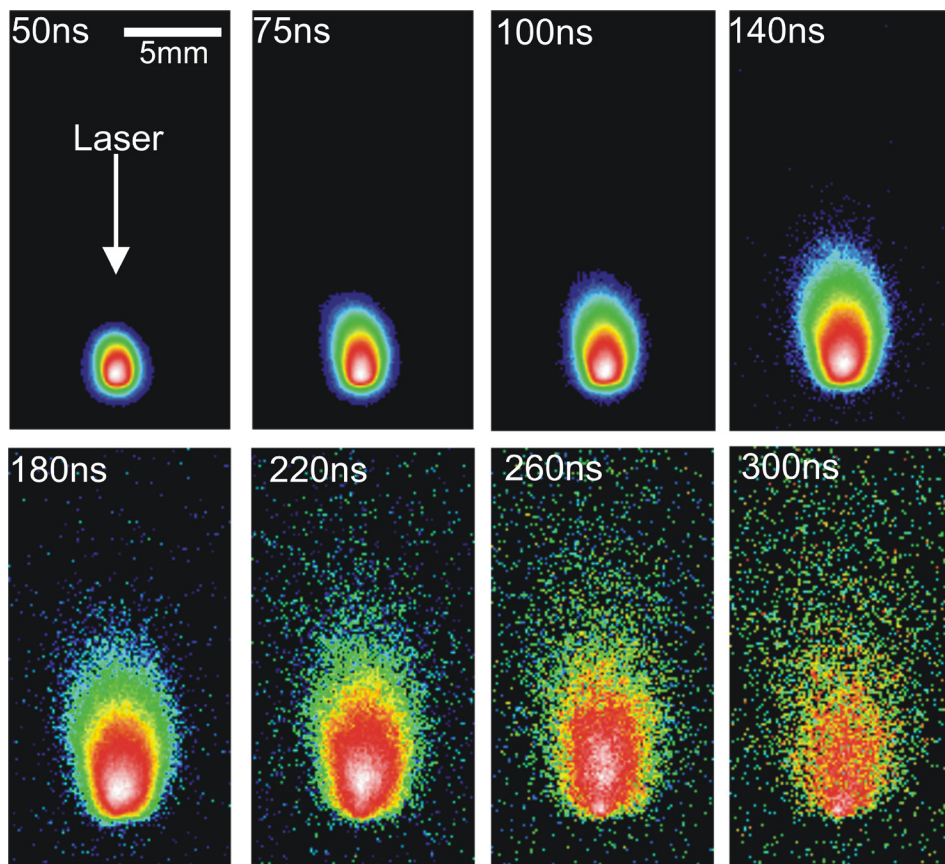


FIG. 7. The time evolution of self-emission from a ns LPP from an Al target in vacuum. The exposure time used was 2 ns. The timings in the images represent the time after the onset of plasma formation. All of the images are normalized to their maximum intensity. Plume behavior indicates free expansion.⁸⁵ Reprinted with permission from Harilal *et al.*, J. Appl. Phys. **93**, 2380 (2003) as Fig. 2. Copyright 2018 AIP Publishing LLC.

The interrelated laser parameters that influence plasma generation conditions include pulse duration, energy, and wavelength. Many of the present applications of LA have been developed in the past using “long pulse” nanosecond (ns) pulsed lasers (mostly Nd:YAG or excimer lasers). However, especially in the last decade, “ultrafast” femtosecond (fs) laser technology has evolved significantly and has been employed for many LA applications due to some potential advantages over traditional ns lasers such as reduced damage to the sample, less susceptibility to sample matrix and elemental fractionation effects, reduced optical continuum emission, and colder plasma generation conditions.^{89,98–100} If the fs laser power is higher than the critical power for self-focusing, filaments will be generated in the beam; this provides the potential to use fs laser filaments to generate plasma at longer-range standoff distances.^{101,102} Given that the research effort in the LA area is huge, the physics of LA generation conditions are briefly mentioned here with an emphasis on the differences in ns, fs, and filament plume physical conditions. The following discussion is directed to useful conditions in LA plumes generated by various methods for optical spectroscopy, which are essential for further development of any analytical measurement technique including standoff detection of isotopes.

1. Nanosecond and femtosecond laser-produced plasma

The evolutionary history of atoms, ions, and molecules in a LPP is dependent on the physical conditions of the plasma. The nature of laser irradiation, specifically the laser pulse duration (τ_p), affects the physical conditions of the

plasma which in turn influence the linewidth and shape of an optical transition. The physics of ablation energy threshold, plasma generation, expansion, persistence, etc., are heavily dependent on the initial conditions of the laser-target interaction and hence the τ_p of the laser too. Even though the only difference between ns- and fs-LA is the difference in laser pulse duration, the mechanisms leading to energy absorption and target ablation are entirely distinctive for both cases. Figure 8 gives the various processes taking place during ns- and fs-LA with approximate timescales.^{89,103,104} The energy density of ns- and fs-LA discussed here is concentrated on LA applications in analytical science rather than values typically used for ultrahigh-intensity applications such as high energy density physics, fusion, extreme ultraviolet (EUV) or x-ray light sources, and collimated electron or proton beams.

At the initial stages of laser-matter interaction, regardless of the τ_p , the laser photons will be coupled to the electrons in the system. For long pulse ns lasers, the absorption process is linear and obeys the Beer-Lambert law driven by a thermal process. However, nonlinear processes become significant during ultrafast laser absorption because of high peak intensities. Electron impact ionization and strong electric field ionization are the major processes for free electron generation during fs-LA. It is important to understand that laser photon absorption processes, as well as ablation physics, will be different for metals and dielectrics. For example, in metals, free electrons in the conduction band absorb energy through inverse Bremsstrahlung (IB) absorption. For dielectrics, valence band electrons absorb photons and generally decay to their initial state and re-emit the photon.

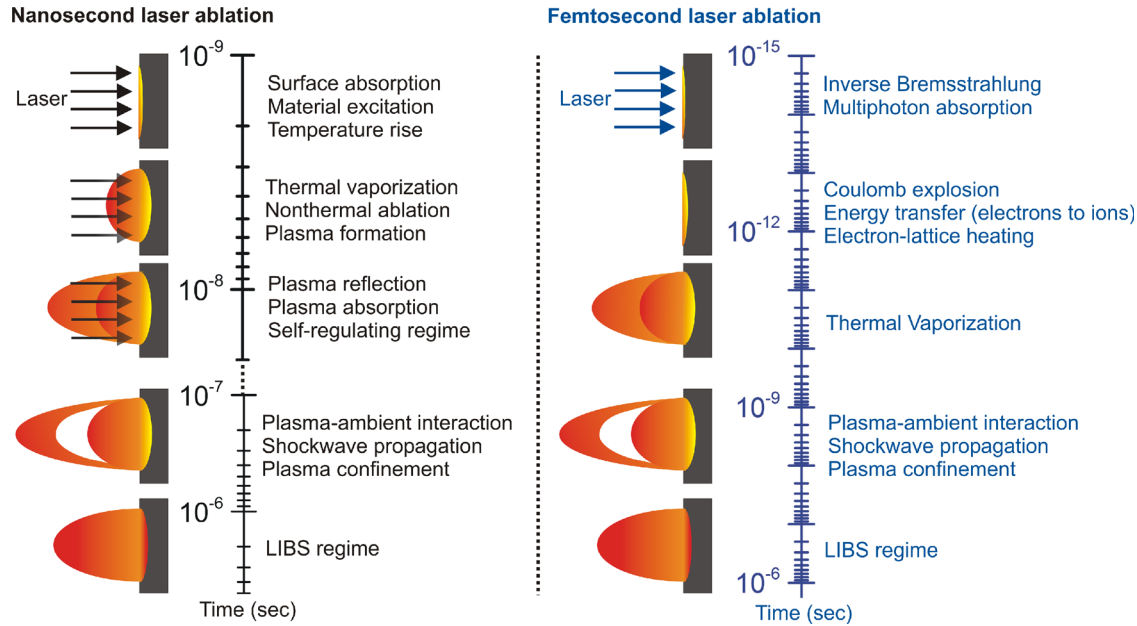


FIG. 8. Approximate timescales of ns and fs energy absorption and laser ablation along with the various processes occurring during and after the laser pulse are given.

Because of this, the ablation threshold will typically be higher for dielectrics compared to metals.¹⁰⁵

The differences in various processes occurring during ns- and fs-LA can be understood by comparing the duration of the laser pulse τ_p with the characteristic relaxation times, such as the electron-to-ion energy transfer time (τ_{ei}), electron heat conduction time (τ_{heat}), and the hydrodynamic or expansion time, all of which typically occur on the order of several ps after the onset of laser absorption. Hence, for ns-LA, various processes like ionization, sample heating, vaporization, etc., occur during the laser pulse ($\tau_p \gg \tau_{ei} \sim \tau_{heat}$), while in the case of fs-LA, these phenomena do not occur until after the end of the laser pulse ($\tau_p < \tau_{ei} \sim \tau_{heat}$). In ns-LA, the plasma is formed during the laser pulse and a significant portion of the laser pulse will be used for plasma heating instead of target ablation. However, for fs-LA, heat diffusion is frozen during the interaction of the laser beam with the target material and shock-like energy deposition leads to ablation. Hence, fs-LA offers greatly reduced thermal damage and heat affected zones on the target due to negligible heat conduction and hydrodynamic motion during the laser pulse.¹⁰⁶ Other noticeable differences reported for fs-LA in comparison with ns-LA include lower temperature plasma generation with predominantly neutral atomic emission,^{89,107} reduced continuum emission,^{81,108} reduced emission persistence,⁸¹ narrower angular ion distribution,¹⁰⁹ and nanoparticle emission.^{110,111} The lower temperature conditions present for fs-LA also lead to the generation of molecules at earlier times of its evolution in comparison with ns-LA.^{84,89,98,112}

Previous studies have shown that the laser fluence threshold for ablation (F_{th}) approximately follows $F_{th} \sim \tau_p^{1/2}$ for ns- and ps-LA.¹⁰⁵ However, for fs pulses, the electron temperature dominates the electron-phonon temperature and hence the photon absorption depth governs the heated volume instead of heat diffusion depth (heat diffusion depth is

proportional to $\tau_p^{1/2}$). A strong deviation from the usual $\tau_p^{1/2}$ scaling of F_{th} for pulses below ~ 10 ps in dielectric materials is reported Perry *et al.*,¹¹³ which is also confirmed by theoretical analysis by Gamaly *et al.*¹⁰⁵ In general, the F_{th} for fs-LA is found to be lower than for ns-LA.¹⁰⁵

Apart from the τ_p , the laser wavelength λ affects the ablation properties greatly, especially in the case of ns-LA.^{114,115} Considering the long duration of the laser pulse in comparison with plasma generation conditions, laser-plasma coupling, which is governed by two λ -dependent absorption mechanisms (IB and photoionization), cannot be avoided in ns-LA. The calculated ratio between IB absorption coefficients for different Nd:YAG laser wavelengths ω , 2ω , and 3ω is approximately 9:2:1.¹¹⁶ In contrast, the role of fs λ on LA is not well understood. In fact, it is a controversial subject and fs laser λ s are thought to have little influence on LA; however, studies have shown that the λ of fs-LA affects both threshold and efficiency of ablation.^{117,118}

It is well-known that thermal processes dominate ns-LA for material removal. However, when a material is excited using fs laser pulses, because of very short pulse duration compared to characteristic time scales, an extreme nonequilibrium state is generated. At very early times, the absorption of fs laser photons leads to the presence of very hot electrons while keeping the lattice and ions at colder temperatures. Such strong electronic excitation during fs LA may lead to nonthermally induced phase transitions.¹¹⁹ With time, the lattice temperature may exceed the melting temperature which typically happens in \sim ps timescale. According to Stoian *et al.*¹²⁰ for fs LA, there are two competing mechanisms resulting in material removal and ablation: Coulomb explosion and thermal vaporization. In Coulomb explosion, the excited electrons ejected from the target surface after laser absorption create an electric field due to charge separation between the ejected electrons and the highly ionized atoms. The generated electric field pulls

the ions out of the target resulting in the removal of the first few monolayers (several nanometers) of the lattice within the skin depth. Coulomb explosion dominates at low laser intensities near to the F_{th} , leading to gentle ablation. Thermal vaporization leads to an order of magnitude higher ablation rate per pulse compared to Coulomb explosion.¹²⁰ However, the topic of Coulomb explosion is intensively debated for the ablation of metals during fs LA considering the strong electric fields at the surface can be compensated by the presence of conduction band electrons from the bulk of the material.¹¹⁹

The hydrodynamic expansion features of the plasma are also governed by initial plume conditions, which are different for ns- and fs-LA, as well as environmental conditions. The role of the ns laser impact area on plume hydrodynamics has been reported widely.^{121–124} In ns-LA, larger spot sizes lead to plume-sharpening effects caused by ion acceleration from enhanced laser-plasma coupling.¹²⁵ According to Anisimov,¹²⁴ the expansion of ns laser-generated ellipsoidal plumes is faster along the axis with smaller initial dimensions. Changes in ion angular distribution caused by a rectangular beam “flip over” have been reported for both ns-¹²⁴ and fs-LA.¹²⁶ Previous studies documented that fs-LA plumes are highly collimated in comparison with ns-LA plumes at atmospheric pressure, which was explained as pressure confinement due to strong overheating of the laser impact zone caused by the low optical penetration depth and greater power per unit volume.^{89,127} It has to be mentioned that for a fixed spot size, the collimation properties of fs-LA (angle of particle ejection) may be slightly different than ns-LA because of changes in the angular distribution of ions¹⁰⁹ that could affect the confinement properties of the plume when plume expansion happens at ambient pressure levels.

The differences in ablation mechanisms during interaction between materials and ns and fs laser beams lead to distinct differences in ablation efficiency and crater shape.¹⁰⁶ Since laser-plasma coupling is negligible in fs-LA, for a fixed laser fluence, the ablation efficiency will be significantly higher for fs-LA compared to ns-LA for NIR wavelengths.¹⁰⁹ However, high ablation efficiency can be possible even with ns-LA by using shorter wavelengths where IB processes are negligible. For ns-LA, it has been found that the mass ablation rate⁸⁸ is proportional to $\lambda^{-4/3}$. Since the time scale of ns-LA is longer than the heat diffusion times, shock waves propagating through the melt layer and ablation-induced reactive forces initiate splashing of the melt layer. For fs-LA, since all these processes happen on short time scales (\sim ps), the heat load to the surrounding material is minimized. Hence, the craters formed by fs-LA will be cleaner with well-defined edges, while the ns-LA craters show significant irregularities in the crater rims because of re-solidification of splashed melt layers.¹²⁸ The craters generated by previous pulses may also affect expansion dynamics of the plumes generated by subsequent pulses.¹²⁹ The ablation focal conditions (in front, on, or behind the target) may also have an influence on laser-target coupling conditions regardless of the τ_p .^{130,131}

2. Femtosecond laser filament-produced plasma

There is significant interest in using ultrashort laser filaments for remote sensing of atmospheric gases and aerosols,

lightning control, laser-produced plasma spectroscopy, coherent anti-Stokes Raman scattering, and the generation of THz radiation.^{98,132} The filaments generated during fs laser propagation can travel over a very large distance without suffering from diffraction effects and can potentially be used to generate plasmas at large standoff distances. Such self-guided filaments, on the order of $100\text{ }\mu\text{m}$ in diameter, can be generated over hundreds of meters to kilometers.^{102,133–136} So far, it has been reported that filaments can propagate as far as a few kilometers in the atmosphere using the Teramobile facility.^{102,136} However, formation or propagation of filaments alone is not sufficient to generate ablation of a solid target; the fluence at the target must also be above the ablation threshold. The physics behind filament generation are briefly mentioned here; a detailed description of filament generation can be found elsewhere.^{137,138}

A schematic of the filament generation,¹³⁷ a photograph of filament propagation, and a cross-sectional view of the filament are given in Fig. 9. An ultrashort pulse of sufficiently high peak power can undergo self-focusing via the nonlinear Kerr effect when propagating through a transparent medium such as air. This self-focusing of an energetic pulse can cause weak ionization of the surrounding air, thereby forming a plasma. The created plasma acts to defocus the beam, decreasing the intensity. The balance or equilibrium between the focusing and defocusing of the beam leads to the formation of self-guided laser channels or filaments.^{137,139,140} Self-focusing occurs during propagation of an ultrafast Gaussian-shaped laser beam in a medium such as air when the input laser power P_{in} exceeds the critical power (P_{cr}), which is given by^{137,138}

$$P_{cr} = \frac{3.72\lambda^2}{8\pi n_0 n_2}, \quad (15)$$

where n_0 is the linear refractive index and n_2 is the nonlinear refractive index coefficient. Plasma generation sets an upper

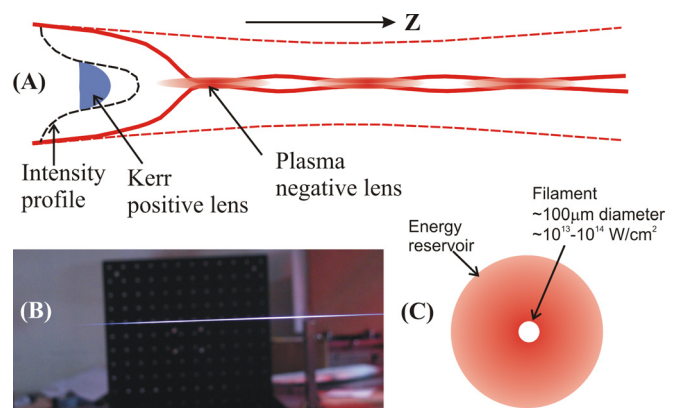


FIG. 9. (a) A schematic of the vertical slice of a propagating filament. The Kerr effect generates a positive refractive index profile which overcomes the diffraction of the beam, leading to focusing of the beam and plasma generation. The negative refractive index generated by the electrons in the plasma defocuses the beam. (b) Photograph of a filament. The laser beam is propagating from left to right. (c) The filament and energy reservoir. The filaments are typically $\sim 100\text{ }\mu\text{m}$ in diameter and carry $\sim 10^{13} - 10^{14}\text{ W/cm}^2$. The filaments are clad by an energy reservoir carrying a significant fraction of the energy and whose diameter varies from $\sim 60\text{ }\mu\text{m}$ to several mm.

limit for the intensity of a filament in the air. For a laser operating at $\lambda = 800$ nm in air, $P_{cr} \sim 3$ GW. The change in the index of refraction due to a plasma Δn_p can be expressed as

$$\Delta n_p = -\frac{\omega_p^2}{2\omega^2} = -\frac{e^2 \rho_e}{2m_e \epsilon_0 \omega^2}, \quad (16)$$

where ω_p and ω are the plasma and laser frequencies; e , m_e , and ρ_e are the electron charge, electron mass, and filament electron plasma density, respectively; and ϵ_0 is the electric permittivity of free space. The maximum intensity I inside a self-guiding filament channel in the air can be approximately obtained by balancing the index of refraction due to electron plasma generation with the nonlinear index of refraction $n_2 I$

$$n_2 I + \Delta n_p = 0, \quad (17)$$

$$I = \frac{e^2 \rho_e}{2n_2 m_e \epsilon_0 \omega^2}. \quad (18)$$

Equations (15)–(18) provide the key elements of the formation and stabilization of laser filaments. When the power level of the laser used for filament generation is ~ 1 – $10 P_{cr}$, a single filament will be formed which typically carries 10%–15% of the total pulse energy (\sim a few mJ), and is clad by the rest of the laser energy which acts as a photon bath or energy reservoir (Fig. 9).¹⁴¹ However, as the laser intensity increases, especially when the laser pulse power reaches 10–100 P_{cr} , multiple filaments can co-exist.¹³⁶ In that scenario, the filament beam will propagate nonlinearly with a turbulent exchange between nucleating and dying filaments and the photon bath itself.¹⁴²

Inside the filament, the peak intensity is clamped at $\sim 5 \times 10^{13}$ W/cm², which is powerful enough to ablate solid targets. There are numerous studies that exist in the literature comparing the differences between ns- and fs-LA, with an emphasis on differences in emission properties; however, studies comparing the emission features under various fs laser focusing conditions (or filament) are limited. It is well-known that the properties of any laser-generated plasma strongly depend on laser irradiation conditions, and hence it is anticipated that the plume generated by fs laser filaments will differ from plasmas generated by focused fs pulses. Studies have shown that the emission features of plasma plumes change significantly for ablation occurring at different distances along the filament channel, which is explained as changes in ablation efficiency along the filament channel caused by the effectiveness of using the reservoir energy for ablation.^{138,143} It has been reported that there is a substantial reduction in evaporated mass for filament-induced ablation compared to sharply focused fs-LA.^{144,145}

There are two approaches routinely used to generate filament plasmas: loosely focusing a fs laser beam using a long focal length lens (typical for laboratory-based filament generation) or propagating the laser beam to larger distances where self-focusing is the only mechanism driving self-collapse (lens-free filaments). It has been found that loosely focused filaments generate ablation plumes with higher temperature and density along with increased persistence

compared to plumes generated by lens-free filaments.¹⁴⁶ This can be correlated to differences in the use of the reservoir energy stored around the filament [Fig. 9(c)] for target excitation and plasma generation.¹³⁷ Because of the dynamic balance between self-focusing and plasma defocusing in filamentation generation, the filament generation conditions are important as they ultimately determine the filament diameter, intensity, electron plasma density, and geometry of the energy reservoir around the filament. Since these filament beam properties determine the ablation and plasma conditions, they, in turn, have a strong effect on the observed optical emission properties.¹⁴⁶

B. Ambient air and plasma chemistry

The cover or buffer gas present during plasma generation and expansion affect physical conditions in the plasma greatly,^{91–93,147–158} which in turn influence the linewidth of any optical transition as well as its persistence. Ambient gas promotes cooling of the LPP because of enhanced collisions and controls the entire LA lifecycle from plasma generation to particle condensation. LA plume expansion into vacuum conditions is less complex compared to its expansion in the presence of a reactive gas like air. In the latter scenario, the plasma chemistry will redefine the plume hydrodynamics and evolution of the chemical composition of the plume. Moreover, the presence of a cover gas causes effects such as plume splitting, sharpening, confinement, and the formation of shocks and internal plume structures.^{85,159–162} In the presence of moderate to high ambient pressures, a shock wave will be formed at the interface between the plume and ambient medium at the start of ablation and continue to expand until the back pressure from the ambient gas matches the pressure of the plasma plume.¹⁶³ The presence of an ambient medium can also help to extend the plasma lifetime by regulating temperature and density instead of the rapid decay of those parameters seen in the free expansion of LA plumes in vacuum or low-pressure conditions.⁸¹ However, this increase in temperature and density due to confinement also broadens the linewidths of optical transitions.

Molecular species in LA plumes are generally formed at later times ($\sim 2 \mu\text{s}$ – $50 \mu\text{s}$), and their formation is explained as due to atomic collisions and recombination, which is prevalent when the plasma has cooled down to lower temperatures. The presence of a cover gas expedites the cooling process through plasma-ambient species collisions. Even though the LA process is extensively used in a variety of applications, it is still not fully understood *when and where* these molecules are formed. Currently, significant efforts are ongoing to improve the understanding of molecular formation thermodynamics in LA plumes.^{157,163–173} Even though the composition of air shows a larger percentage of nitrogen molecules compared to oxygen molecules, the reactivity of plume species with N₂ is poor due to its extremely high bond dissociation energy. However, many elements quite readily react with O₂ to form oxides. Hence, the oxygen molecules present in the atmospheric air medium may affect emission and absorption processes in laser ablation plumes greatly due to chemical reactions through the oxidation process.¹⁷⁴ Results have highlighted that the strong shockwaves formed

at the plume edge during LA expansion in air mediate the temporal evolution of molecular formation in LA plumes.¹⁶³ A systematic study for elucidating the effect of O₂ in the ambient environment on metal laser ablation plasmas showed that the presence of oxygen in the ambient environment reduces the persistence of both emission and absorption signals through an oxidation process that depletes the density of atomic species within the resulting LPP plume.¹⁶⁹ The molecular formation mechanisms in LA plumes and their correlation to isotopic analysis has been reported.^{175,176} Investigations on C₂ and CN molecular formation in LA plumes have been performed by several research groups.^{164,166}

C. Line broadening mechanisms in laser-produced plasmas

One of the important parameters for using optical spectroscopy for isotopic analysis is linewidth to line separation. Optical transitions, both atomic and molecular, are not immune to environmental factors and hence never provide precisely sharp line structures. While LA is a powerful technique for generating ions, atoms, and molecules from a solid material, the species are generated in a high-temperature and high-electron density environment. These conditions lead to significant spectral line broadening, which may reduce the ability to resolve small isotope splittings.

Among the various line broadening mechanisms, natural broadening will be inherent in the system due to a finite lifetime of all excited states in an atomic system. States involved in an electronic transition are broadened in accordance with the Heisenberg uncertainty principle in the time-energy formulation: $\Delta E \cdot \Delta t \geq \hbar/2$. For an atomic transition, the natural linewidth full width half maximum (FWHM) is defined by the Heisenberg limit and can be expressed in terms of the transition wavelength

$$\Delta\lambda_{1/2}^n = \frac{1}{2\pi c\tau}, \quad (19)$$

where τ is the excited state spontaneous emission lifetime; if both the upper and lower energy states in the transition have lifetimes, they are combined according to $\frac{1}{\tau_c} = \frac{1}{\tau_1} + \frac{1}{\tau_2}$. If the lower level is ground state, there can be no radiative decay and hence its contribution to line broadening is zero. Natural broadening has a *Lorentzian lineshape*, is independent of transition frequency, and is homogeneous; that is, it applies equally to all members of an ensemble. For an allowed atomic transition with a 10 ns lifetime, the corresponding width is 16 MHz. Compared to other broadening mechanisms discussed in Secs. IV C 1–IV C 4, natural broadening is typically negligible.

Prominent broadening mechanisms that influence spectral linewidths in a LPP are Doppler, pressure, and Stark effects. An in-depth knowledge of these line broadening mechanisms in a LPP system is ultimately important to employ optical spectroscopy for isotopic analysis. A brief discussion of various line broadening mechanisms is given below. A detailed description of spectral line broadening in plasmas can be found in Griem¹⁷⁷ or Kunze¹⁷⁸ or Konjevic.¹⁷⁹

1. Doppler broadening

Doppler broadening arises from the Doppler shift of light emitted or absorbed by a moving particle depending on its velocity with respect to the direction of observation/excitation. In the non-relativistic approximation, this is given by $\delta\nu_D = v_0(\frac{v}{c})$, where v_0 is the rest transition frequency and v is the particle velocity. In a gaseous ensemble of particles with a random Boltzmann distribution of velocities, the resulting broadening is inhomogeneous and has a *Gaussian lineshape* with FWHM

$$\Delta\lambda_{1/2}^D = \lambda \sqrt{\frac{8kT_D \ln 2}{Mc^2}}, \quad (20)$$

where T_D is the temperature in K, M is the atomic mass in kg, k is the Boltzmann constant, and c is the speed of light. If we assume a temperature¹⁸⁰ of 7000 K and a 400 nm transition for ²³⁸U, the resulting Doppler width is 2.9 GHz or 1.55 pm. Since Doppler width scales with $T_D^{1/2}$, it may affect the linewidth significantly at higher temperatures.¹⁸¹

2. Pressure broadening

In the presence of a buffer gas, collisions of an atom, ion, or molecule in an excited state (radiator) with other atoms, molecules, or ions (perturber) can cause randomization of the wavefunction phase and collisional quenching of the radiator, which effectively results in shortening the coherence lifetime of the excited state. The averaged effect of these collisions results in additive *Lorentzian* broadening of the lineshape in combination with lifetime broadening and also shifts the center wavelength of the optical transition. This is commonly referred to as van der Waals broadening. The pressure-induced broadening and shift of the spectral line center can be calculated using the following formulas:

$$\Delta\lambda_{1/2}^p = \sum_i \sigma_i(T_0) P_i \left(\frac{T_0}{T} \right)^{n_i}, \quad (21)$$

$$\Delta\lambda_{shift}^p = \sum_i \delta_i(T_0) P_i \left(\frac{T_0}{T} \right)^{k_i}, \quad (22)$$

where $\Delta\lambda_{1/2}^p$ is the HWHM broadening from pressure broadening of a single optical transition for a radiator in a gas mixture composed of a number of different perturbing atomic, ionic, or molecular species and $\Delta\lambda_{shift}^p$ is the shift in the center position of the optical transition. The summations on the right side of Eqs. (21) and (22) reflect that each perturbing species contributes differently to pressure-induced broadening and shift of the radiator transition. Within the summation, $\sigma_i(T_0)$ is the HWHM pressure broadening coefficient for the i^{th} perturber at a reference temperature of T_0 and P_i is the partial pressure of perturber i . Similarly, $\delta_i(T_0)$ corresponds to the shift in the line position. The units of pressure broadening and shift are given in nm per unit pressure (e.g., nm/atm). The sign of $\delta_i(T_0)$ can be negative or positive,

corresponding to a blue or red shift in the spectral line center. Scaling the temperature dependence of the broadening and shift of the spectral line with respect to T_0 is given by $(T_0/T)^{n_i}$ and $(T_0/T)^{k_i}$, where the temperature-dependent exponent n_i (k_i) is specific to the i^{th} perturber. Values for n_i and k_i are positive, and Eq. (21) indicates that as the temperature increases, pressure broadening decreases. This behavior occurs because the decrease in the number density of perturbers has a stronger dependence on the gas kinetic temperature than the increase in collision frequency associated with a higher gas kinetic temperature.

Values of $\sigma_i(T_0)$, n_i , $\delta_i(T_0)$, and k_i can be obtained from high-resolution spectroscopy studies where the number density of perturbers and gas kinetic temperature are controlled or from theoretical calculations. For example, Anderson *et al.*¹⁸² has confirmed values in this range for the 254 nm resonance line of Hg in air, nitrogen, and CO₂ and found broadening of approximately 7 GHz/1.5 pm at atmospheric pressure and room temperature. It is important to note that the gas kinetic model of collisional broadening predicts that collisional broadening will decrease with increasing temperature and is proportional to T^b , where b varies between -0.3 and -0.7 at constant pressure. This has been accurately confirmed in experimental studies,¹⁸³ and thus we expect collisional broadening of approximately 1.5 GHz at a temperature of 7000 K for the mercury resonance line.

Resonance broadening is a special form of collisional broadening occurring between like particles, with one collision partner in an excited state that is connected to the ground state by an allowed transition and the other in the ground state. In this case, a dipole interaction increases the effective collision radius, and the resulting broadening can be estimated from¹⁷⁸

$$\Delta\lambda_{1/2}^R \cong 9 \times 10^{-34} \left(\frac{g_1}{g_2} \right)^{\frac{1}{2}} \lambda_r^3 f_r N_1, \quad (23)$$

where λ_r is the wavelength (nm) of the observed line, f_r is the oscillator strength, g_2 and g_1 are the statistical weights of its upper and lower levels, and N_1 is the ground state number density in m⁻³.

3. Stark broadening

Stark broadening arises from collisions with ions and electrons and is sometimes considered a special form of collisional broadening; however, the mechanism is quite different. As the name implies, the proximity of an ion or electron to another particle (either neutral or ion) undergoing an optical transition creates a local electric field which in turn causes Stark mixing of the states involved in the transition with other (nearby) electronic states. Stark broadening is one of the primary diagnostic tools for investigating plasmas, and the theory is correspondingly well-developed.^{184,185} In general, the Stark effect can have a linear or quadratic dependence on the field. However, nearly all atoms/ions except hydrogen experience a quadratic Stark effect.

According to Griem,¹⁷⁷ the broadening (FWHM) and shifts of an atom transition due to Stark effect are given by

$$\Delta\lambda_{1/2}^s = 2w \left(\frac{n_e}{10^{16}} \right) + 3.5A \left(\frac{n_e}{10^{16}} \right)^{\frac{1}{4}} \left[1 - \frac{4}{3}N_D^{-\frac{1}{3}} \right] w \left(\frac{n_e}{10^{16}} \right), \quad (24)$$

$$\Delta\lambda_{\text{shift}}^s = D \left(\frac{n_e}{10^{16}} \right) \mp 2A \left(\frac{n_e}{10^{16}} \right)^{\frac{1}{4}} \left[1 - \frac{4}{3}N_D^{-\frac{1}{3}} \right] w \left(\frac{n_e}{10^{16}} \right), \quad (25)$$

where w is the electron-impact parameter which can be incorporated at different temperatures, A is the ion broadening parameter, and N_D is the number of particles in the Debye sphere. The first term in Eqs. (24) and (25) are the broadening and the shift due to electron impact, while the second term is the ion correction factor. The Stark broadening due to electron contribution has a *Lorentzian lineshape*. However, the Stark lineshape can be slightly asymmetric, especially for neutral atoms, because of the presence of the ion broadening component. Stark broadening is a well-established method for measuring the electron density of laser-produced plasmas.^{77,146} NIST maintains an active bibliographic database of papers related to atomic line broadening¹⁸⁶ because of their importance in plasma and astrophysics. Though Stark broadening impact parameters are readily available for low- and mid-Z elements,¹⁸⁷ limited resources are available in the literature for high-Z elements.

4. Instrument/artifactual broadening

All spectrographs or monochromators carry an instrumental profile which represents the form of the broadening. The shape of the instrumental profile depends on several parameters associated with spectrometers which include widths of the entrance and exit slits, pixel width in the case of a multi-channel detector, diffraction phenomena, quality of the system components, aberrations, alignment, etc. Thus, the shape of the instrumental profile varies from system to system since it is a convolution of several individual terms. For emission analysis using laboratory-based monochromators, insufficient resolution of the spectroscopic system to measure the actual lineshape may be detrimental. For example, a 0.5 m standard spectrograph with 2400 grooves/mm grating results in instrumental broadening \sim 0.04 nm at 500 nm, and this increases to \sim 0.16 nm with the use of 600 g/mm grating.

Apart from broadening caused by various line broadening mechanisms, a measured lineshape from LPPs can be artificially broadened by other factors such as opacity effects (self-absorption), power broadening, and instrumental broadening. In these scenarios, the broadening of a line is caused by the way in which the measurement is made. The absorption processes in the plasma may lead to broadening of an emission line during radiative transfer. This is because absorption is strongest at the line center and weakest at the wings of the spectral profile. For inhomogeneous plasmas like LPPs at atmospheric pressure, a central dip in the line profile can be seen (self-reversal) for optically thick lines which is caused by absorption in the cooler outer layers or coronal regions.^{188,189} Such self-absorption and/or self-reversal in LPP can cause an artificial inflation in measured linewidths as well as a decrease in peak height. The spectral width of the atomic absorption

line can also be increased at high probe laser intensities by an effect known as power broadening.¹⁹⁰ In power broadening, the probe laser intensity is strong enough to perturb both absorption and emission from atomic and molecular states and thereby modify the frequency distribution of the absorption coefficient.

D. LPP physical conditions suitable for isotopic analysis

A LPP is a transient system with physical conditions typically characterized by temperature and density gradients. Under thermodynamic equilibrium, the intensity of emission or absorption of a line transition is related to both the number density of the concerned species as well as the temperature. Because of rapid changes in the physical conditions, the maximum concentrations of ions, atoms, and molecules occur at various times during the LPP evolution.^{77,92,150,191} For example, LA plumes are hotter and denser at the earliest times of its lifespan where emission from ions dominates, followed by atoms. Molecules are formed at later times.

Isotopic analysis using optical spectroscopic tools should be performed when the linewidth of the transition is less influenced by various broadening mechanisms. The physical conditions of a LPP change significantly with many experimental parameters which in turn influence the linewidth of a transition. Figure 10 gives the estimated linewidths and shifts with respect to plasma temperature for Stark, Doppler, and van der Waals collisional broadening for the Rb 780 nm transition.¹⁸¹ The Doppler linewidth estimate is straightforward [Eq. (20)] and proportional to the square root of the temperature. For the Rb 780 nm transition, Doppler broadening increases from 4 pm to 8.5 pm when the temperature of the plasma increases from 5000 K to 20 000 K. The Stark linewidths and shifts are proportional to the number density of electrons and are a weak function of the temperature of the system, especially when the temperature is $\geq 10\,000$ K. The van der Waals collisional

broadening may become dominant at low temperatures and/or when the ambient gas pressure approaches atmospheric levels. For example, the estimated van der Waals broadening for the Rb transition at 780 nm is ~ 8 pm when the number density of foreign species is $\sim 10^{18} \text{ cm}^{-3}$.

Considering the existence of high-temperature and high-density regimes in LPPs at early times after plasma formation, Stark broadening will be the predominant line broadening mechanism compared to Doppler and pressure broadening. Typically, ns-LA plumes attain critical density in the earliest times of their evolution, and their density drops with time.⁸² The Stark broadening due to electron impact will be significant when the electron densities of the plasmas are $\geq 10^{16}/\text{cm}^3$ (Refs. 177 and 185), and these conditions exist in LPP plumes until $\sim 10 \mu\text{s}$ for ns-LA and $\sim 2 \mu\text{s}$ for fs-LA.⁸¹ The Stark broadening and shift change with line selection and are largest for hydrogen lines. For example, the measured Stark widths of H_α , H_β , and H_γ transitions in a laser-plasma system can be approximately several nm when the density of the plasma system is $> 10^{17}/\text{cm}^3$.¹⁹²

Doppler broadening is found to be insignificant compared to the Stark effect at early times of the LPP evolution; however, it may be influential at late times of plasma evolution especially when the experiments are performed at low-pressure. For isotope splitting measurements performed under atmospheric pressure conditions, pressure broadening may influence the linewidth greatly. Zameroski *et al.*¹⁹³ and Pitz *et al.*¹⁹⁴ reported the pressure broadening and shift of Rb D2 and K D1 transitions, respectively. Taylor and Phillips¹⁹⁵ compared the Doppler and pressure broadening for the 860.79 nm U I transition from 1 to 760 Torr pressure levels of air and found that the Doppler broadening was relatively constant in this pressure range (1.17 GHz or 2.89 pm), while the pressure broadening increased from 0 to 1.59 GHz (3.92 pm).

As mentioned previously, the persistence and physical conditions of the LPP change significantly between plasmas

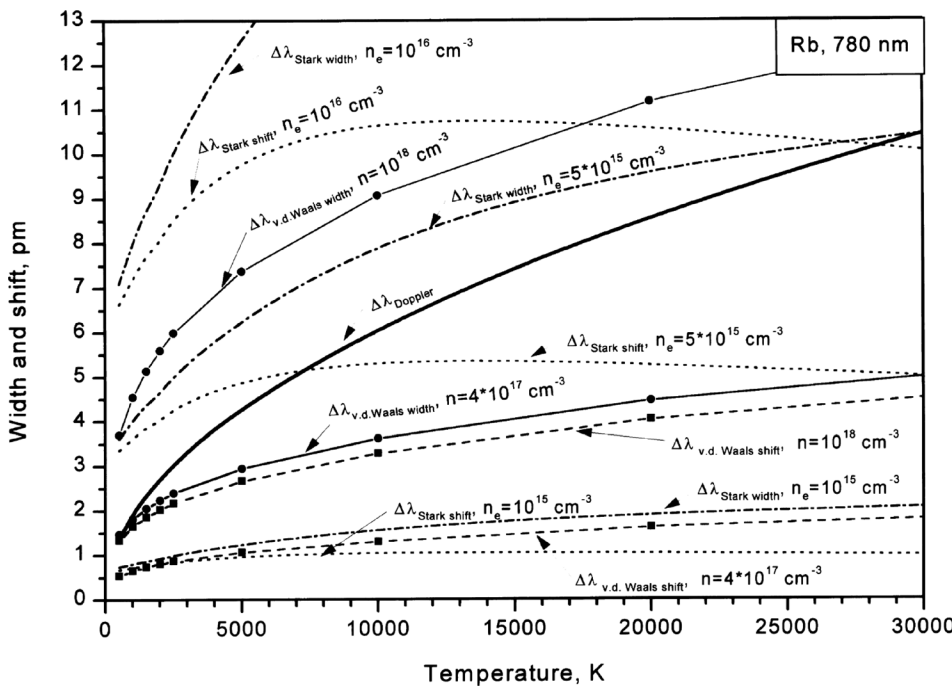


FIG. 10. The estimated contributions of various line broadening mechanisms for the Rb 780 nm line as a function of temperature.¹⁸¹ Reprinted with permission from Gornushkin *et al.*, Spectrochim. Acta B **54**, 1207 (1999) as Fig. 2. Copyright 2017 Elsevier.

created by ns, fs, and filament ablation. The selection of the measurement timing window with respect to the onset of plasma formation is very important for isotopic analysis for both absorption- and emission-based analysis. Previous studies have shown that under similar laser fluence conditions, the temperature and density decay are much faster for fs LPPs than ns LPPs.⁸¹ Filament ablation plumes are found to have the lowest persistence where atoms and molecules exist only for a short time because of the lower temperature initial conditions in comparison with fs-LA and ns-LA.^{146,191}

Emission-based techniques require thermal excitation, leading to the requirement of a higher-temperature and higher-density environment, which ultimately increases the spectral linewidths due to Stark and Doppler effects. At later times, the spectral linewidth measurement using emission spectroscopy is limited by the instrumental broadening of standard spectrographs used in laboratories. High spectral resolution is ultimately necessary to resolve closely spaced isotopic lines. For example, a 0.5 m standard spectrograph with a 2400 grooves/mm grating and a 25 μm slit provides a resolving power of $\sim 12\,000$ which is not adequate to resolve the small isotope shifts generated by most atoms. Combining instrumental broadening and the crowded spectral features seen from targets containing high-Z elements such as U, the emission-based isotopic analysis is always a challenge, even though chemometrics can help to overcome some of these limitations.¹⁹⁶ In this regard, there are certain advantages offered by absorption-based methods for isotopic analysis. Absorption spectroscopy methods probe the ground state atoms which exist in the gas phase for a longer period of time ($\sim 100\text{s}$ of μs) than excited states as the plasma cools. Though the absorption spectrum may be influenced by both Doppler and pressure broadening in the LPP system at later times, the magnitude of broadening may be on par or lower in comparison with isotope splitting for many of the elements. Hence, probing of the plasma at later times using absorption spectroscopy inherently provides narrower lineshapes as opposed to emission spectroscopy.

V. OPTICAL SPECTROSCOPY MEASUREMENT TECHNIQUES

Even though the primary focus of this review is optical spectroscopic techniques applicable to rapid, non-contact measurement of isotopes from solid targets, there exist a variety of laser spectroscopy tools that can also be used for isotopic analysis of gas-phase molecules which are outside the scope of this review.^{197,198} Among the various laser spectroscopic tools, laser absorption spectroscopy (LAS) in the infrared spectral region is perhaps the most widely used tool for isotopic analysis. Some of the advantages of absorption spectroscopy employing tunable lasers are high spectral resolution, negligible detector noise because of the higher spectral power density of the lasers, and high detection sensitivity.¹⁹⁷ The sensitivity of LAS depends both on the experimental scheme and modulation techniques.^{195,199–201} The most appropriate combination of laser source and detection scheme depends on many parameters specific to each application.

The principal reason for using a LPP is that the solid sample, even located at a standoff distance, should be vaporized

so that the neutral atoms, ions, or molecules present in the gas phase can be used for isotopic distinction under normal environmental conditions. Passive and active optical spectroscopic tools can be used to analyze LA plumes or isotope shifts in atomic transitions. Passive spectroscopy exploits the emission from a thermally excited transition, while active spectroscopy involves the use of an external electromagnetic source (typically a laser) to perturb the population of ions or atoms contained in the plasma so as to measure their absorption or alter their emission. Optical emission spectroscopy (OES) is routinely used for LA plume analysis (commonly called laser-induced breakdown spectroscopy or LIBS)^{78,202–205} because of its experimental simplicity and multi-elemental observation capability. Emission analysis is very useful for inferring physical conditions of the plasma such as temperature, density, ionization fraction, and opacity.^{90,92,150,162} However, the emission from atoms and ions in the plasma observed in LIBS experiments is strongest at early times in the plasma evolution, times at which the spectral lines are also the broadest. LAS and laser-induced fluorescence (LIF) spectroscopy are the most common active spectroscopic tools for LA characterization. Since the ground state population is exploited in active techniques like LAS or LIF, lineshapes can be monitored at late times in the plasma evolution where the temperatures of the plasma are lower in comparison with the LIBS regime.

The major building block of all LA-based optical spectroscopic tools is the choice of the laser for ablation. The energy of the selected laser should be capable of inducing a plasma from the sample of interest. It is recommended to keep the laser fluence at the target well above the ablation threshold to minimize stochastic plasma events. The produced plasma expands normal to the target surface regardless of the angle of incidence of the laser. Other important laser parameters relevant to LA-based optical spectroscopic tools are wavelength, repetition rate, and pulse width. The most common choice of laser is the fundamental wavelength (1064 nm) from Nd:YAG with pulse duration \sim a few ns. This laser can be operated at 532 nm, 355 nm, or 266 nm with the use of harmonic crystals and dichroic mirrors. However, as mentioned in Sec. IV, the physical properties of the plasma generated by ns laser ablation depend strongly on the laser wavelength as it determines the laser-target and laser-plasma coupling. NIR ns-LA provides hotter plasma conditions at a reduced ablation rate, while UV ns-LA provides more efficient material removal and vaporization and also generates reduced continuum emission. Ablation using ultrafast fs lasers provides certain advantages over ns lasers [lower temperature plasma, reduced continuum and heat-affected zone (HAZ), etc.], though it comes with an additional cost (cost and complexity of the laser, bulkiness, etc.). Other laser options for LIBS experiments are excimer, N₂, CO₂, and fiber lasers.^{206–209}

Selection of the repetition rate of the laser for plasma generation and subsequent spectroscopic detection is directly related to the speed of the signal acquisition system and electronics. Typically, the flashlamp-pumped solid-state lasers or discharge-based lasers (excimer, CO₂, N₂) provide repetition rates ~ 1 –500 Hz. However, higher repetition rate is possible with a diode-pumped solid-state laser or fiber laser. If the same target location is used for repetitive ablation, the craters

formed at the ablation area will influence the efficacy of ablation as well as the plasma physical conditions. So, to minimize the errors associated with target drilling, the sample can be translated. A brief description of LA-based optical spectroscopic tools (LIBS, LAS, and LIF) is given in Subsections **V A–VC**.

A. Laser-induced breakdown spectroscopy (LIBS)

Currently, LIBS is the most popular application of LA combined with OES due to its simplicity, robustness, stand-off capability, real-time analysis with no sample preparation requirement, minimal sample destruction, and broadband detection.^{79,204,205} Because of these, LIBS has been used in numerous applications ranging from geology, heritage, nuclear, and environmental to detection of biological agents and explosives.^{78,79,90,203–205,212,222} Several reviews and textbooks exist on the science and applications of emission spectroscopy of LA plumes.^{79,223} The basic building blocks of a LIBS instrument are a suitable laser for luminous plasma generation, the necessary collection optics, a spectrometer, and a detector. A schematic of the LIBS setup is given in Fig. 11. Several articles discuss the selection of lasers for LIBS experiments, in particular, the ablation wavelength and pulse duration.^{162,224} Compared to Ar ambient, the presence of air may result in a reduced persistence in atomic emission due to oxide formation.¹⁶⁹

Considering the transient nature of LPPs, space- and time-resolved diagnostic measurement techniques are essential for retrieving the distributions of ions, neutrals, molecules, temperature, and density.^{225–227} However, in many LIBS analytical applications, plasma emission is spatially and temporally integrated, resulting in a loss of information on the spatial and temporal distribution of ions, neutrals, and molecules. As a consequence, only averaged values for properties such as electron densities and plasma temperatures are obtained. The spatial information of the plasma can be gathered by imaging the plasma on the entrance slit of an imaging spectrograph. In the other scenario, the entire plasma volume can be imaged onto a fiber, which can be used to

transport the radiation to the detector. In the latter case, the average emission features of the plasma are obtained from the detector which is the method usually employed for stand-off analysis.

The optical system used to transfer the radiation from the plasma to the detector defines the spatial resolution and signal collection efficiency. Both lens and/or mirrors are used for this purpose, although the use of mirrors avoids chromatic aberration which is typical of focusing lenses. However, whatever arrangement is selected, the space-resolved data provide line-of-sight integrated measurements. The Abel inversion approach can be used to overcome this issue, which converts the axially and laterally resolved data into radially resolved data.²²⁸

In LIBS, the intensity of line radiation is recorded against the wavelength. One of the criteria for isotopic analysis is the resolution of the detector system. The spectrograph and detector used to analyze the collected light determine the resolution, the spectral bandwidth, and the time resolution. There is a trade-off between the resolution of the spectrometer, the spectral bandwidth, and throughput. A traditional Czerny-Turner spectrometer provides high throughput, but the spectral bandwidth and resolution depend on the length of the spectrograph as well as the grating groove number density. However, a rotating turret with several gratings can be used to overcome some of this limitation. Echelle spectrographs are capable of covering the entire UV-VIS spectral region (200–900 nm) with excellent spectral resolution, though with reduced throughput in comparison to Czerny-Turner spectrographs. Hence, to obtain a single shot LIBS spectrum, the Czerny-Turner design is preferred over an Echelle spectrograph.

The detector coupled to the spectrograph determines the time resolution of the system. Regular charge-coupled device (CCD) cameras can be used for time-integrated dispersed light collection, while intensified CCDs (ICCDs) provide time resolution down to a few ns. The intensifier uses a multichannel plate that acts as a shutter as well as a photomultiplier. Temporally resolved spectral features of the transient LIBS plume can be obtained by synchronizing the ICCD with various moments of the plasma during its evolution using a delay generator. The spectral bandwidth and resolution available from an emission analysis system also depends on the CCD array and pixel size, respectively. Before the advent of ICCDs, the photomultiplier tube (PMT) was routinely used as a detector and the LIBS spectrum was obtained by scanning the monochromator. The use of PMTs as detectors, which provides large detection

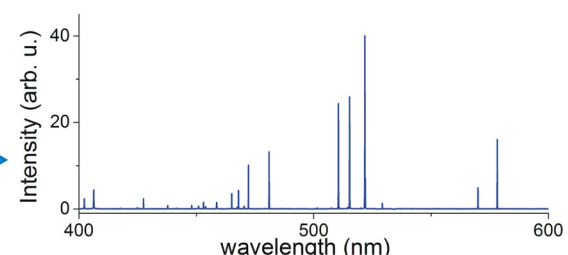
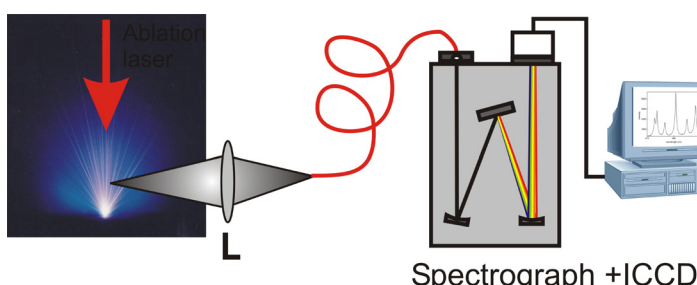


FIG. 11. Schematic of the LIBS experimental setup (L, lens). The red arrow represents the ablation laser. A Czerny-Turner spectrometer coupled to an ICCD is used as the detector system. A representative emission spectrum from brass target obtained using the LIBS technique is also given on the right side of the figure.

bandwidth and dynamic range compared to an ICCD, is very useful to obtain the time-dependence of emission from atoms, ions, and molecules in a LA plume.^{163,226} Such measurements also provide delay as well as decay times from emission of the constituent species at a specific point within the plasma which are very useful parameters related to the evolution of laser ablated materials.^{107,229,230}

Typically, the LA plumes generated with a ns laser and a power density of approximately a few GW/cm² are particularly hot (≤ 5 eV) and dense ($\leq 10^{18}/\text{cm}^3$) at early times (~ 0 –30 ns).^{77,150} This high-temperature and high-density regime present at early times in LA plumes will lead to continuum emission contributed by free-free and free-bound transitions and spectral broadening of the emission lines mainly caused by Stark effect. As the plasma evolves, it will cool down and emission from line radiation predominates with improved signal-to-background ratios (SBR) and signal-to-noise ratios (SNR). An example of LIBS spectra collected at various times after the onset of a fs LPP on a brass target is given in Fig. 12. The spectral features clearly show that at early times the lines are significantly broadened because of the Stark effect, while at later times the line shape is constrained by instrumental broadening.

Emission from ions, neutral atoms, and molecules can be detected using LIBS; however, their emission times with respect to the onset of plasma formation vary significantly. The acquisition time window is one of the most important considerations for LIBS-based studies, taking into account the transient nature of the laser-generated plumes. This consideration includes the delay of the emission collection window with respect to the laser pulse (gate delay, τ_d) as well as collection window time (gate width, τ_w). Since the time evolution of emission from continuum, atoms, ions, and molecules vary significantly with the plasma generation conditions, the selection of τ_d and τ_w are important to optimize the SNR and lower the relative standard deviation (RSD). For both ns- and

fs-LA, the early stages of LA are dominated by continuum emission (though their time scales are different).²³¹ The continuum radiation for a typical LIBS experiment using a NIR Nd:YAG laser persists up to $\sim 1 \mu\text{s}$.²³² For fs-LA, the continuum radiation is short-lived, ≤ 100 ns.²³¹ The suggested temporal windows for atomic and molecular emission detection from ns, fs, and filament ablation plasmas are given in Fig. 13. Apart from the method of plasma generation, the optimum temporal gating parameters can vary considerably with factors such as laser power density, laser wavelength (especially for ns-LA), sample composition (trace or bulk), the observed emission lines, and the nature and pressure of the ambient gas.

For quantitative analysis using LIBS, matrix-matched calibration standards are often used. An alternative approach is to use calibration-free LIBS, where basic plasma physics properties are used to model the emission and thereby infer the composition of the plasma.^{90,212,214} The reported detection limits for LIBS vary over many orders of magnitude but are often at the part-per-million level for many elements.^{78,233} However, the analytical merits of LIBS are not as good when compared to other commonly used elemental detection methods, especially for trace elemental detection, such as ICP-OES, ICP-MS, and GC-MS. Recently, extensive research has been carried out to improve the figures of merit of LIBS; some proposed methods for improvement include microwave-excited LIBS,^{234,235} double-pulse LIBS,^{236,237} cavity-enhanced LIBS,¹⁹⁹ spatially confined LIBS,²³⁸ spark excitation,²³⁹ nanoparticle-enhanced LIBS,²⁴⁰ and resonance-enhanced LIBS.^{79,241} These methods usually improve the SNR of the LIBS measurement; however, they come with an increase in experimental complexity.

LIBS performance has been dramatically improved through increased coupling of the laser energy to the target and the vaporized material, leading to a more efficient production of atoms in an excited state.²³⁶ As mentioned previously in Sec. IV, there are certain advantages to using fs lasers for LIBS instead of using ns lasers; these include lower excitation temperatures, lower continuum emission, reduced HAZ, etc. Reduced continuum emission shows good promise for improving the limit of detection for major and trace elements in the sample as well as the use of non-gated detectors for analysis.²⁴² On the other side, ns LIBS provides higher emission persistence in comparison with fs LIBS.¹⁹¹ Considering the timescales of interaction with the target material will be similar for fs and filament LIBS, significant differences in physical conditions of the generated plasma are not expected. However,

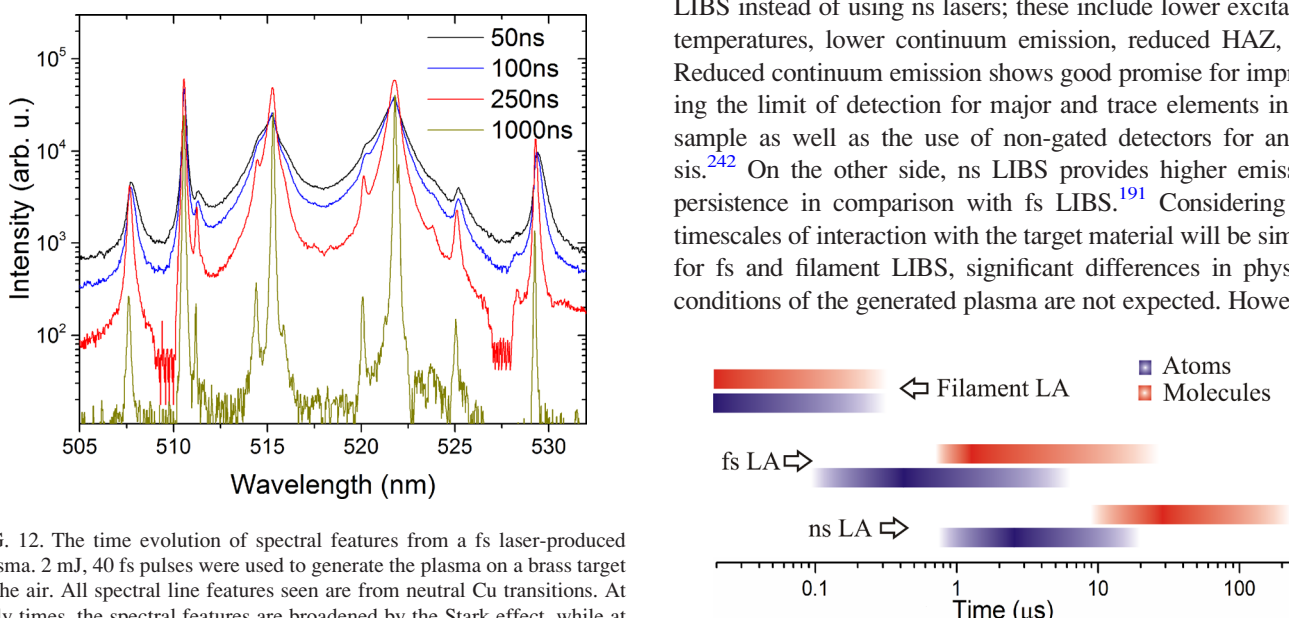


FIG. 12. The time evolution of spectral features from a fs laser-produced plasma. 2 mJ, 40 fs pulses were used to generate the plasma on a brass target in the air. All spectral line features seen are from neutral Cu transitions. At early times, the spectral features are broadened by the Stark effect, while at late times the spectral linewidths are limited by instrumental broadening. Significant background emission can also be seen at early times of plasma evolution.

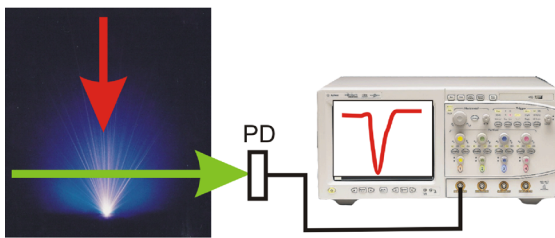
FIG. 13. Suggested signal analysis time window for emission analysis from ns, fs, and filament LIBS plumes in air ambient.

the energy coupling between the laser and target will be different for fs and filament LIBS. In fs LIBS, the stronger energy coupling leads to increased ablation and hence higher emission intensity and persistence compared to filament LIBS.¹⁴⁶ Typically filaments carry a fraction of the energy of the propagating fs laser beam and the rest of the energy is stored in the energy reservoir which clads the filament. Hence, the energy coupled to the target in filament-generated plasmas is decreased compared to focused fs LPPs, eventually resulting in weaker plasmas generated by filament ablation.¹⁴⁶

B. Laser absorption spectroscopy (LAS)

Absorption spectroscopy is a well-established technique for identifying and quantifying gaseous species; this is done by measuring the intensity decrease in laser light tuned to the atomic or ionic transition that is transmitted through the sample plume. In the last two decades, several groups have used LAS of a LPP to measure the ground state population, inherent linewidth in the plasma, isotope splitting, etc.^{195,243–246} LAS of LPPs is an active diagnostic tool, meaning it requires a second laser which should be resonant with a selected transition. A schematic of the LAS set up is given in Fig. 14. The basic building blocks of a LA-LAS setup are a pulsed laser to generate the LPP, a tunable probe laser, a detector to analyze the transmitted intensity, and electronics (i.e., pre-amplifier and analog-to-digital converter (ADC)). The ideal absorption spectroscopy laser source would have a wide range wavelength tuning and narrow spectral linewidth to enable measurement of transmission over multiple atomic, ionic, and molecular resonances. Laser sources that meet these criteria are continuous wave (cw) dye, external-cavity diode, and Ti:sapphire lasers.

For a standard LA-LAS setup, the ablation laser beam will be oriented normal to the sample surface, while the probe laser beam will be directed through the plasma parallel to the sample surface and perpendicular to the ablation laser. To reduce the interaction region with the LPP, the probe laser is typically focused through the LPP. LAS inherently monitors the plasma properties at a certain location of the plasma where the cross-section of the probe laser beam intersects the LPP. The transmitted beam through the plasma is focused onto a photodiode, converting the transmitted intensity into a time-dependent voltage signal that is measured using an ADC.



$$A_b(\lambda, t) = -\ln\left(\frac{I(t)}{I_0}\right)$$

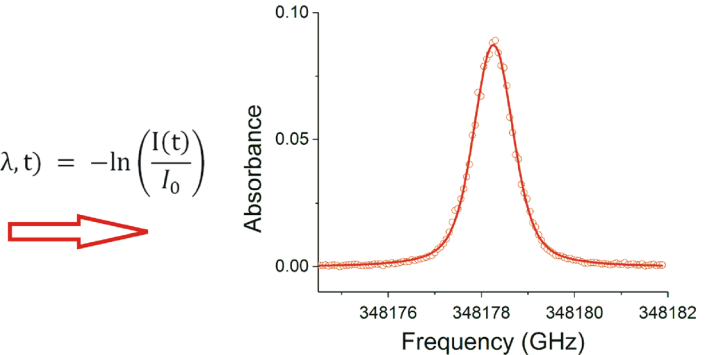


FIG. 14. Schematic of LAS of LA plume is given (PD, photodiode). The red and green arrows represent the ablation laser and probe laser, respectively. In LAS, the absorbance signal is obtained from the recorded transmitted signal. An example of an excitation or absorbance spectrum is also given (right) which is obtained by tuning the probe laser across a resonance transition.

Because the evolution of the LPP occurs on ns to μ s time-scales, an ADC system with a response bandwidth > 1 MHz is a requisite. This time-sampling requirement for the ADC is generally met by using a high-speed digital oscilloscope or stand-alone data acquisition (DAQ) board. The data acquisition system will be synchronized with the ablation laser with a trigger signal from the ablation laser.

For absorption measurements, the reduction of light intensity transmitted through the plasma is monitored. Unlike emission intensity, which is proportional to the number density of atoms in the upper level, the absorption signal depends on the lower state population of atoms or molecules. The Beer-Lambert law provides the relation between the transmitted and initial light intensity as

$$I(t) = I_o e^{-A_b(\lambda,t)}, \quad (26)$$

where $A_b(\lambda, t) = \sigma(\lambda, t)N_1(x, t)l$ is the absorbance, which is the product of the absorption cross-section σ at the frequency of light, the path length l through the sample, and N_1 , the number density of interacting species in the lower energy state which is a function of the position x along the line-of-sight and the time of measurement; $I(t)$ is the intensity of the probe laser incident on the detector at time t ; and I_o is the intensity of the probe laser in the absence of absorption, which may be obtained from a reference detector, or ideally from the time immediately prior to the arrival of the ablation pulse. The absorbance $A_b(\lambda,t)$ can therefore be defined as

$$A_b(\lambda, t) = -\ln\left(\frac{I(t)}{I_0}\right). \quad (27)$$

In LAS, when using a cw laser source, the spectral resolution is dictated by the spectral width of the probe laser, which is much smaller than typical linewidths in the LPP. Current commercially available tunable Ti:sapphire and tunable diode lasers provide linewidths in the range ~ 0.1 – 10 MHz, which is sufficient to resolve isotope shifts of most atomic transitions. For a fixed probe laser wavelength, the time-resolved absorbance is recorded for each ablation pulse, and absorption over multiple pulses may be averaged. To record an absorption spectrum using cw lasers, the wavelength of the laser is stepped or scanned across a spectral feature to record time-dependent absorption over a range of

wavelengths. The scanning requirement places a limit on the spectral bandwidth which may be acquired in a given time period for LAS. Moreover, an acquisition typically occurs over multiple ablation pulses while the laser is scanned, which may lead to measurement noise due to shot-to-shot signal variations due to changing plasma conditions between pulses.

Because LAS can actively probe the electronic ground energy state of an atomic (or ionic) population, analysis of plasma evolution at low temperatures and late times is possible where the Stark broadening effect is negligible. Analysis of cooler plasmas with limited spectral broadening enables various applications of interest, such as the determination of isotope ratios from the isotope shift in the spectra.^{244,247–251} Absorption linewidths in LPP plumes are typically limited by Doppler and van der Waals broadening, both of which can be made smaller by performing experiments in reduced pressure environments. This is the reason why nearly all previous studies of LAS to measure isotopes in LPPs were performed under an inert buffer gas at reduced pressures (< 25 Torr).^{246,247,249,250} Taylor and Phillips¹⁹⁵ have shown that atomic absorption linewidths for uranium are found to be narrower than isotope shifts of many U transitions even at atmospheric pressure (Fig. 15). Their measurements show a factor of ~ 2 increase in linewidth of U I 861 nm when the air pressure was increased from a few Torr to atmospheric pressure levels. These results highlight that LAS is suitable for isotopic analysis of LA plumes at late times in the plasma lifecycle even at ambient atmospheric pressure.

Several studies have applied LAS to LA plumes in low-pressure ambient environments for the investigation of several elements, including rubidium,²⁴⁴ uranium,^{247–250} gadolinium,²⁵¹ strontium,²⁵² plutonium,³⁰ and calcium.¹⁸¹ Experiments have also been conducted at atmospheric pressure for uranium.¹⁹⁵ The use of cavity ring-down spectroscopy (CRDS) to study the lineshapes of atomic and molecular transitions was demonstrated in Refs. 199 and 201. We note for completeness that absorption measurements may also be

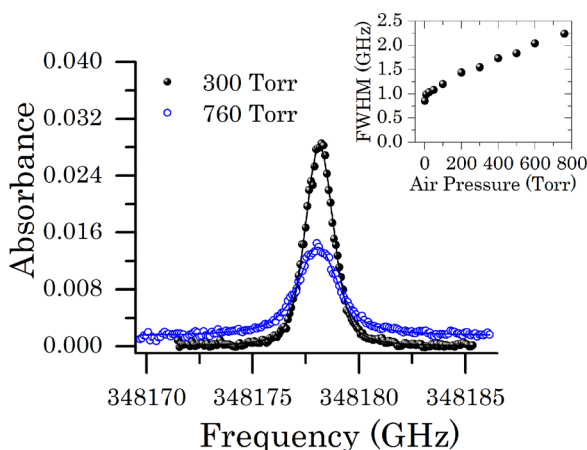


FIG. 15. The absorbance spectrum of the ^{238}U 861 nm transition in air at 300 and 760 Torr at $7\ \mu\text{s}$ time delay after the onset of LPP evolution. A 1.3% uranium-containing filter glass was ablated using pulses from a ns Nd:YAG laser. The pressure dependence of linewidths is given in the inset.¹⁹⁵ Reprinted with permission from Taylor and Phillips, Opt. Lett. **39**, 594, (2014) as Fig. 2. Copyright 2017 Optical Society of America.

performed using incoherent light instead of tunable lasers. In this case, UV and vacuum ultraviolet (VUV) absorption spectroscopy measurements were performed on LPPs using a dual-laser plasma system.^{253–255} In the dual plasma absorption spectroscopy scheme, the continuum emission from a high-Z LPP was used to probe photo-absorption spectra in the second plasma.

Absorption measurements using cw lasers can directly provide path-integrated (column) number densities of a selected transition and are able to record quasi-three-dimensional spatial mapping.^{256,257} Bushaw and Alexander²⁵² studied the dynamics of atoms and ions in a LA plume and reported splitting of the absorption spectrum at an early stage of plume evolution. According to them, many ground state atoms are accumulated into a contact layer between the laser plasma and cover gas, and when the probe beam passes parallel through the sample with a certain height, the beam interacts with atoms of two different velocity groups in the two opposing layers. Using this method, they estimated the lateral velocity of atoms in the plume by measuring the magnitude of the Doppler splitting.

Similar to thermally excited LIBS emission, the selection of acquisition time with respect to the plasma onset is also important for absorbance measurements and varies significantly for ns laser, fs laser, and filament ablation conditions. Since LAS is a transmission-based technique, the high-density gradient observed in a LPP system hinders the absorption measurements at early times of its evolution due to photo-thermal deflection as well as the high opacity of the plasma. Moreover, considering the highly sensitive nature of the measurement, signal saturation is also expected especially for bulk samples.⁷⁵ Approximate LAS acquisition time windows used for atomic/ionic transitions in LA plumes are given in Fig. 16. Presently, the LAS measurement of molecules in LA plumes is nonexistent in the literature and hence its acquisition time window is not provided.

C. Laser-induced fluorescence (LIF) spectroscopy

Among the various optical spectroscopic methods, fluorescence spectroscopy incorporates aspects of both atomic absorption and emission. Hence, LIF is capable of addressing some of the limitations in the figures of merit of LIBS (precision, detection limits, line broadening, etc.) and LAS (excitation geometry). In fluorescence spectroscopy, like atomic absorption, the lower state atoms in the plasma plume are

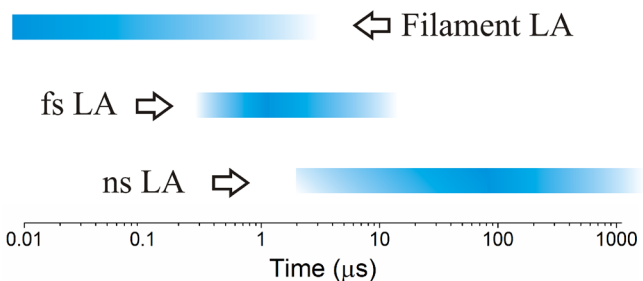


FIG. 16. Suggested acquisition temporal windows for absorbance measurements of atomic transitions in LPP plumes are given for ns laser, fs laser, and filament ablation plumes.

excited using a tunable laser. However, instead of directly monitoring the amount of light absorbed in the process, the emission resulting from the decay of the resonantly excited atoms is measured. A schematic of laser-induced fluorescence spectroscopy of a LPP is given in Fig. 17(a) along with a typical excitation spectrum [Fig. 17(b)]. Similar to LAS, the LIF or excitation spectrum is obtained by scanning the tunable laser across a resonant transition. In a LIF spectrum, the emission intensity is plotted against the excitation wavelength.

Two LIF schemes can be possible after a resonant absorption process – resonance and non-resonance fluorescence [Fig. 17(c)]. In resonance fluorescence, the resonant and LIF photons have the same wavelength. The resonance LIF provides strong LIF signal, but interference from scattered light may be problematic. In non-resonance LIF, relaxation of the excited atom is through other lower energy levels coupled to the resonantly pumped upper energy level. The latter approach is very useful for reducing the effect of scattered light from the resonant excitation beam.^{258,259}

The building blocks of LIF experiments to probe a LPP are similar to a LA-LAS experiment. For excitation, tunable lasers with a wide wavelength tuning range and narrow linewidth are preferred. Both pulsed [dye, optical parametric oscillator (OPO)] and cw [dye, diode, Ti:sapphire] lasers can be used for LIF excitation of selected transitions in a LA

plume, though most of the reported work used pulsed laser sources. For pulsed sources, depending on the pulse duration, the spectral bandwidth of the laser pulse may be smaller or larger than the linewidth of the optical transition, although for measurement of an excitation spectrum it should be smaller. For a pulsed LIF excitation source, the LIF signal varies linearly with laser energy at lower laser energy density levels where most of the ground state atoms are ready to be pumped to the excited state. However, as the energy density increases, optical saturation of LIF is expected due to bleaching of the lower level population.^{260,261} Instead, optical saturation may be minimal with the use of a cw excitation laser source considering the lower peak power. Moreover, continuous pumping of the ground state atoms is possible during the entire duration of the plume lifespan with the use of a cw LIF laser.²⁵⁹

Traditionally, LIF experiments have been performed using a PMT as the detector [Fig. 17(a)]. The LIF signal is collected when the excitation beam is in resonance with a transition, and an excitation spectrum can be obtained by scanning the LIF laser across a resonance transition. For measurements that require high time-resolution, PMTs and photodiodes are preferred as they provide higher dynamic range and larger detection bandwidth than an ICCD. However, time gating of the detector will be useful to separate thermally excited and

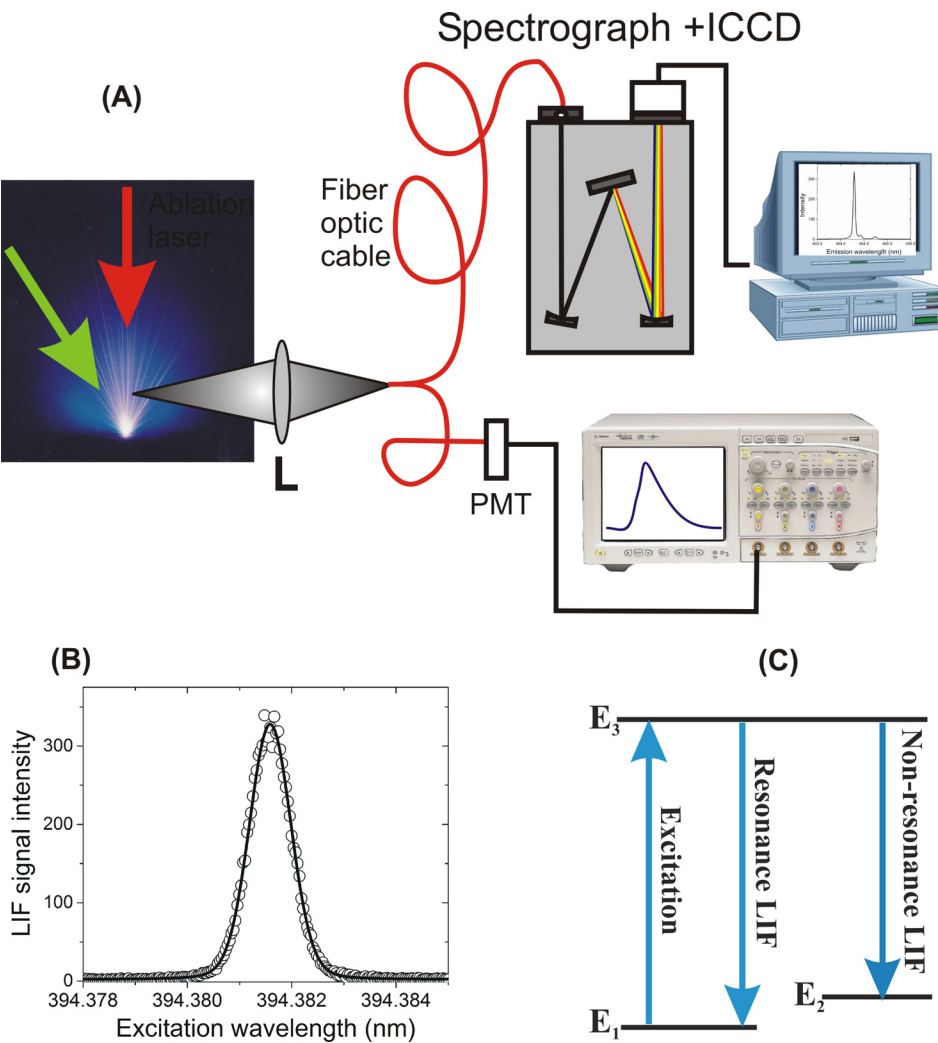


FIG. 17. (a) A general schematic of the LIF spectroscopy of a LPP is given. The red and green arrows represent the ablation and LIF laser beams. In the LIF setup, two detection schemes are given. For a general LIF setup, the fluorescence signal is collected using a PMT detector when the LIF beam is scanned across a resonance transition. For two-dimensional fluorescence spectroscopy, a spectrograph in conjunction with an ICCD is used. (b) An example of a LIF excitation spectrum. (c) Resonance and non-resonance LIF schemes.

LIF emission. The use of a spectrograph and ICCD as a detector provides additional information such as wide spectral features which will be useful for monitoring both LIF and thermally excited transitions. 2D-fluorescence spectroscopy (2D-FS), a versatile technique that combines emission and absorption features of the plasma, is also very useful for canceling various shot-to-shot noises (flicker) happening in a laser ablation plume.⁷⁵ The pump beam scattered light can be avoided if the wavelength difference between fluorescence and excitation transitions falls outside the spectral bandwidth of the spectrograph.

LIF of LA plumes was first reported by Measures and Kwong;^{262,263} they reported improved detection limits, reduced matrix effects, and a linear calibration curve in comparison with LIBS. In their experiment, a nitrogen laser-pumped tunable dye laser was tuned to the optical transition wavelength of an analyte of interest in a LPP plume. Niemax *et al.*²⁶⁴ used a pulsed dye laser for LIF and demonstrated calibration of LIF data by internal standardization with metallic and gas matrices. They also extended this work by using a cw diode laser for LIF excitation and reported uranium isotope ratios in solid samples.²⁵⁰ In the past, LIF of LA plumes was used for various trace element determinations including Pb in metallic reference materials,²⁶⁵ Pb in liquids,^{266,267} Co in soil, steel, and graphite,²⁶⁵ isotopic analysis of Li,²⁶⁸ heavy metals in soils,²⁶⁹ trace boron in nickel-based superalloys and steels,²⁷⁰ Al, Cr, Fe, and Si in steel,²⁷¹ and Pb in a Cu matrix.²⁶¹ The use of LIF on LA plumes provides an improvement in sensitivity, typically several orders of magnitude,²⁶⁷ and selectivity compared to LIBS.

While LIF techniques are commonly used in areas of combustion and plasma research, LIF has not seen widespread use in the characterization of LPPs. Several groups have used UV lasers for LIF [named plume LIF (PLIF)]²⁷² or laser ablation laser-excited atomic fluorescence (LA-LAEF)²⁷³ and pulsed OPO's to resonantly excite a certain transition in the LIBS plume (called resonance-enhanced LIBS or RE-LIBS).^{274,275} For example, Wang *et al.*²⁷² used an ArF laser to induce fluorescence of a laser ablation plume. In their experiments, the excitation energy is channeled to electronic excitation energies of various atomic transitions. In such LIF pumping schemes, the fluorescence is detected from nearby excited levels which are reached through thermal collisions because of the high temperature in the system. In RE-LIBS, the probe laser was used to resonantly excite the host atoms, and energy exchange occurs through collisional transfer. Goueguel *et al.*²⁷⁴ used an OPO laser pulse for collisional LIF excitation. Such PLIF or RE-LIBS methods are useful to increase the detection limits of trace elements, typically two orders of magnitude better than that of LIBS.^{261,269,272,275} Several research groups explored RE-LIBS analysis for trace metal detection, namely, Pb in aqueous solution.^{261,266,274,276–278} However, LIF schemes, such as PLIF, LA-LAEF, and RE-LIBS, are not intended to measure the absorption with high resolution; instead, the LIF beam is used to improve the magnitude of emission. It is necessary to use tunable lasers to obtain high-resolution spectral features employing LIF spectroscopy.

Shen *et al.*²⁷⁹ investigated LIF of uranium atoms and atomic ions in the afterglow of LA plumes generated from uranium-bearing glasses under atmospheric pressure air and showed (1) measurements of the U⁺ ion at 409.5 nm yielded better detection limits than using the neutral atom, (2) detection limits of ~0.05% uranium content in the glass samples, (3) substantial improvement in detection limits over passive LIBS, and (4) time delay studies showed that the LIF signal persisted much longer than the LIBS plasma thermal emission, with the signal dropping to only half intensity at 10 μs after plasma formation. On first take, point (4) is quite remarkable for reactive uranium atoms and ions under atmospheric conditions where they might be expected to rapidly react/recombine with oxygen or water, particularly since prior studies at low pressure (1–5 mbar)²⁸⁰ showed that emission from uranium atoms was strongly quenched by traces of oxygen.

Miyabe *et al.*²⁸¹ investigated the dynamic behavior of LA plumes in the presence of ambient gas at moderate pressures using LIF and noticed that a significant portion of ground state atoms and ions accumulate in the contact region between the plume and ambient gas. Simultaneous optical absorption and LIF measurement was used for 3D mapping of number densities of ions and neutrals in a laser ablation plume in vacuum by scanning the pulsed dye laser frequency.^{256,257} Nakata *et al.*²⁸² studied quenching effects during LIF measurement of LA plumes using 2D photography. Orsel *et al.*²⁸³ used LIF to study oxidation of Al in LA plumes using spatiotemporal mapping. LIF was previously used to image nanoparticles in LA plumes with the help of an atomization laser beam.²⁸⁴ It has been recently demonstrated that LIF of LA plumes is also well-suited for standoff detection.²⁸⁵ For standoff analytical applications of a LPP employing LIF, both the ablation laser as well as the LIF laser beams should be propagated through an air medium and generate a plasma on the sample of interest located at a certain distance. Compared to thermally excited emission, which is concentrated to the hot and dense regions of the plume, LIF can utilize the plume periphery where cooler atoms of the plasma are concentrated.

The general parameters of LIF spectroscopy for probing and sensing are the excitation spectrum, emission spectrum, and fluorescence lifetime or decay rate. Nearly all LIF studies were performed using pulsed laser excitation. However, recent studies of LA plumes in air demonstrate that cw lasers are useful for continuously exciting the ground state population during the entire lifetime of the sampled plume (Fig. 18),²⁵⁹ which significantly enhances the persistence of LIF emission. Moreover, the use of cw tunable lasers for LIF excitation provides narrower linewidths compared to pulsed OPOs and hence are better for selective excitation and isotopic analysis, simpler parametric optimization due to the absence of interpulse delay, and the LIF signal can be scaled by increasing the laser power. 2D-fluorescence spectroscopy (2D-FS), which provides a two-dimensional contour plot of measured emission over a wide range of excitation and emission wavelengths, is a relatively new technique and has recently been demonstrated in a highly transient LPP by measuring simultaneous absorption and emission from coupled electronic transitions of Al in air and uranium at various pressures ranging from 10 Torr to 760 Torr.^{258,259}

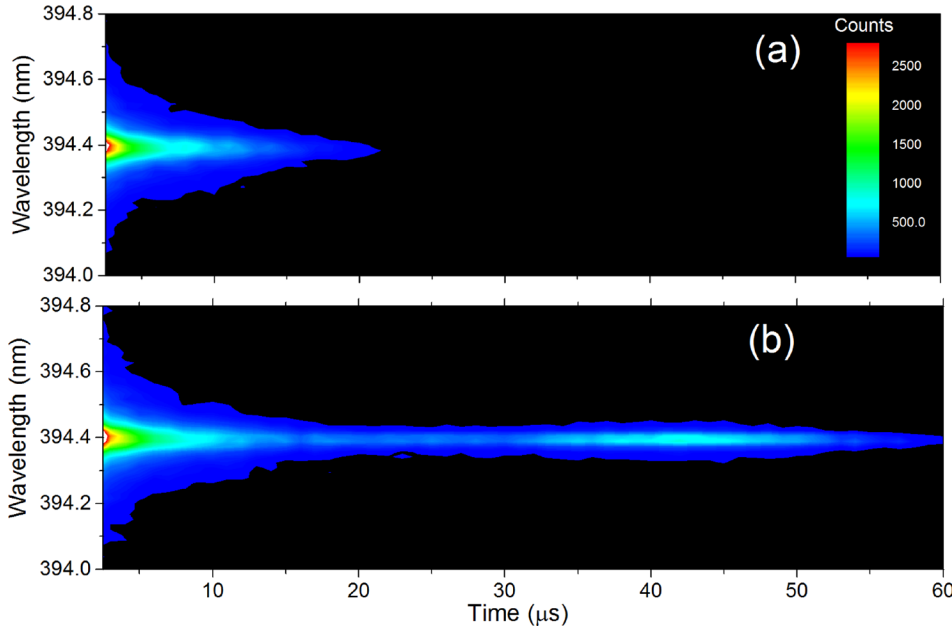


FIG. 18. (a) Time evolution of (a) LIBS and (b) LIBS + LIF when the LIF excitation laser is tuned to the 396.15 nm Al I transition. A Q-switched ns Nd:YAG laser operating at 1064 nm was used to produce plasmas on an Al target in the air. Reprinted with permission from Harilal *et al.*, Opt. Lett. **41**, 3547 (2016) as Fig. 2. Copyright 2017 Optical Society of America.

Molecular LIF is routinely used in molecular spectroscopy for various applications; however, only a few articles exist about LIF excitation of molecules in LA plumes in the literature. Nagli and Gaft²⁸⁶ used LIF of various molecules to increase the sensitivity of the LIBS method. They noticed the decay times of the LIF process are similar to their excitation pulse width and explained the shortening of the lifetime due to collisional quenching of the molecular excited state or thermal quenching due to high-temperature conditions existing in the LPP system. Other researchers also reported molecular LIF of LA plumes for molecules such as AIS, CuO, SiO, C₂, and CN.^{287–290}

VI. ISOTOPIC ANALYSIS USING OPTICAL SPECTROSCOPY

As mentioned in Sec. III, nearly all atomic and molecular transitions exhibit isotope shifts; however, the magnitude of the isotopic spectral shifts vary significantly with the mass of the species as well as with the selected optical transition. For example, in the case of uranium, ²³⁵U–²³⁸U isotope shifts can be as high as ~80 pm but are on average only ~7.5 pm for U I neutral and U II ion transitions.^{65,67} Ideally, for isotopic analysis using optical spectroscopy, the selected optical transition should have a high transition probability ($g\alpha$) along with large isotope splitting (IS). These desired attributes greatly limit the number of candidate transitions; however, multi-line chemometric approaches or partial least squares (PLS) multivariate regressions are capable of mitigating part of this limitation when calibration samples are available.¹⁶⁷

Among the various optical spectroscopic tools, LIBS has been used widely to detect isotopes, especially for nuclear materials. Some of the lines selected for isotopic detection using LIBS are U I 682.693 nm (IS 17.9 pm),⁷⁴ U II 424.437 nm (25.129 pm),²⁹¹ Pu I 594.522 nm (13 pm),²⁹² Li D I 670.790 nm and D II 670.775 nm (17 pm),²⁹¹ and H and D 656.11 nm (179 pm).²⁹¹ H and D line transitions

provide the largest isotope splitting, and the isotopic splitting can be detected even using a spectrograph with moderate resolution (~5000). Recently, several groups started using LIBS to monitor deuterium retention in plasma-facing components (PFC) in next-generation fusion devices.^{293–298} Similarly, emission spectroscopy is a good tool for monitoring Li isotopic information in nuclear energy and Li battery energy storage devices. Such an *in-situ* characterization of materials including isotopic information will be a versatile tool for these next-generation energy industries.

Because of the large isotope shift of actinide elements compared to lighter elements, LIBS has been used by several groups to analyze the isotopic enrichment of U and Pu.^{196,291,292,299} Many of these studies were performed at reduced pressures to decrease various line broadening effects large, high-resolution spectrographs were used to improve spectral resolution. Metallic uranium targets were studied under low-pressure conditions (~20 mTorr air) using a 1-meter spectrograph;²⁹⁹ by using a spatially and temporally resolved LIBS signal, clear resolution of ²³⁵U was observed for enrichments down to a few percent. Similar studies on plutonium²⁹² used a cover gas of helium at ~97 Torr and a 2-meter spectrograph in a double-pass configuration. They were able to clearly resolve the ²³⁹Pu and ²⁴⁰Pu isotopes in an oxide sample with nearly equal abundances of the two isotopes. For similar measurements on a hydride sample with a 94:6 (²³⁹Pu:²⁴⁰Pu) ratio it was possible to resolve the minor ²⁴⁰Pu isotope at near the noise level. Chinni *et al.*³⁰⁰ have investigated the overall spectral features of U plasmas, behavior in atmospheric air and time-resolved persistence of U I and U II signals therein, measurement in soils and on surfaces, double-pulse ablation enhancements, and remote detection at distances up to 30 meters.

Uranium isotopes have been measured using LIBS in a number of recent studies, many under ambient air conditions which showed the potential use of these techniques in standoff or non-contact measurements.^{74,299,301} Doucet *et al.*¹⁹⁶ used a 0.55 m spectrograph to detect U and H isotopes at atmospheric

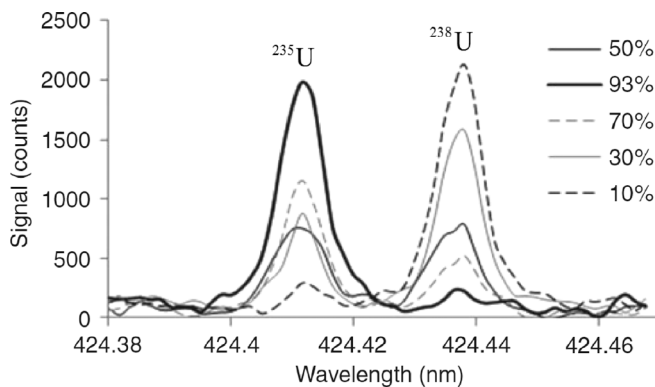


FIG. 19. Isotope splitting measured for U_2O_3 samples with varying enrichment levels using LIBS in the air at atmospheric pressure conditions. A ns duration laser was used for ablation of glass targets with various U enrichment.²⁹¹ Reprinted with permission from Cremers *et al.*, *Appl. Spectrosc.* **66**, 250 (2012) as Fig. 10(a). Copyright 2017 SAGE Publication Ltd.

pressure conditions; however, isotope splitting was only partially resolved due to spectral broadening and the relatively low resolution of the spectrograph ($\lambda/\Delta\lambda \sim 20\,000$). Cremers *et al.*²⁹¹ used a high-resolution spectrograph with a resolving power of $\sim 75\,000$ to measure enrichment ratios of various U samples in air at atmospheric pressure, and they were able to clearly resolve the 25 pm isotope splitting of U II 424.437 nm (Fig. 19). While isotope ratios can be determined from overlapping spectral lines, isotopic precision and detection sensitivity for the minor isotope generally improves with increasing ratio of peak separation to peak width.⁷⁴

It is often desirable to perform LIBS measurements in the air at ambient pressure conditions to avoid the need to load a sample into a vacuum chamber. The presence of air, being a reactive gas which contains oxygen molecules, leads to oxidation processes of expanding plumes and molecular formation. The use of molecules for isotopic analysis is very promising for lighter molecules, considering the isotope splitting can be several orders higher in comparison with isotope splitting in atomic transitions. For example, the isotope shift of ^{10}B and ^{11}B atoms is ~ 2 pm while the diatomic oxides ^{10}BO and ^{11}BO provide an IS of ~ 5 nm. Similarly, for Sr isotopes, the IS between ^{86}Sr and ^{88}Sr is ~ 0.25 pm, while the molecular species ^{86}SrO and ^{88}SrO exhibit an IS ~ 148 pm. In 1998, Niki *et al.*³⁰² used emission from $^{10/11}\text{BO}$ to study isotope shifts during LA of a boron-containing sample in 3 Torr air, and they were able to resolve the large isotope shift of BO molecules using a spectrograph with a low resolving power $\lambda/\Delta\lambda \sim 1250$.

There are extensive studies recently on isotopic analysis employing molecules generated during laser ablation at atmospheric conditions by various groups^{176,242,303–308} and is referred to as laser ablation molecular isotope spectroscopy (LAMIS).^{176,309} An example of the isotope shift observed in $^{12}\text{C}_2$, $^{12}\text{C}^{13}\text{C}$, and $^{13}\text{C}_2$ is given in Fig. 20.³⁰⁵ So far, LA has been used for isotopic analysis of BO (^{10}BO and ^{11}BO),^{176,302} C_2 ,¹⁷⁶ CN,¹⁷⁶ ZrO ,¹⁷⁶ SrO ,¹⁷⁶ CaCl ,¹⁷⁶ OH,¹⁷⁶ UO (^{235}UO and ^{238}UO),^{167,307} UO (U^{16}O and U^{18}O),³⁰⁸ and AlO (Al^{16}O and Al^{18}O)¹⁷⁵ molecules.

Using LAS, several groups were able to resolve the hyperfine structures and isotope shifts of ^{85}Rb and ^{87}Rb and

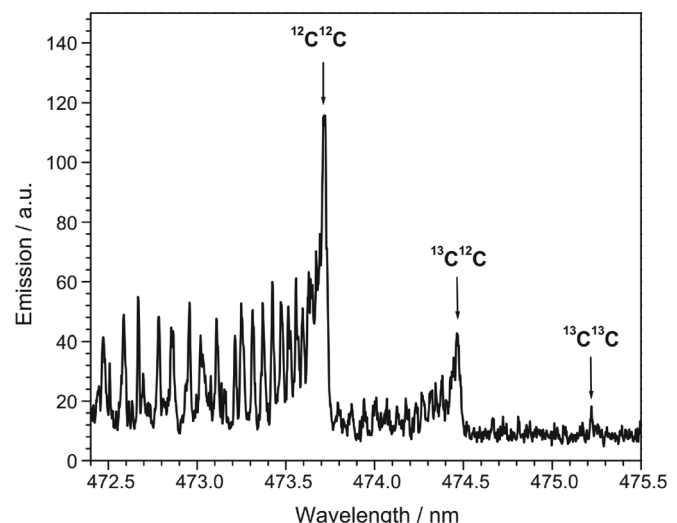


FIG. 20. The Swan bands (1–0) of the three isotopologues of C_2 . LA was performed on a benzoic acid sample using fundamental radiation from a ns Nd:YAG laser.³⁰⁵ Reprinted with permission from Dong *et al.*, *Spectrochim. Acta B* **100**, 62 (2014) as Fig. 1. Copyright 2017 Elsevier.

^{6}Li and ^{7}Li at lower pressure furnace conditions.³¹⁰ Winefordner and co-workers²⁴⁴ extended the application of LAS in the isotopic analysis of solid materials using laser sampling. In their study, they used LAS to resolve the isotope structure of the 780 nm Rb D₂ transition and to measure the ^{85}Rb - ^{87}Rb isotope ratio under low-pressure conditions (0.15–10 Torr). Niemax and co-workers^{247,249} demonstrated isotope-selective detection of uranium by LA of a solid sample followed by diode laser absorption spectroscopy of the ablated material. Miyabe *et al.*^{30,248} reported optimal conditions of LAS for uranium and plutonium isotopic analysis at reduced pressures. They used natural and enriched uranium samples²⁴⁶ and found that a delay time of $2.5\ \mu\text{s}$ at a probing distance of ~ 2.5 mm were the optimal conditions with a pressure of 6 Torr He. Their results also showed a double peak structure for ^{235}U , ascribed to the hyperfine structure of that isotope. Miyabe *et al.*³⁰ also used LAS to measure isotope shifts of Pu; an example of the measured hfs structure and isotope splitting of a Pu ion transition is shown in Fig. 21.

LAS of LA plumes was used for isotopic analysis of a micron-sized gadolinium sample and demonstrated the ability to resolve and quantify (< 10% relative uncertainty) the 0.2% abundance ^{152}Gd isotope in particulate samples.²⁵¹ These studies showed that compact diode laser devices can effectively replace the large-scale grating spectrographs used in direct LIBS studies while providing significantly better resolution, as well as having active interrogation which should provide significant signal enhancement for isotopic detection applications. Phillips *et al.*⁷⁵ performed isotopic analysis on a neutral U transition at 394.38 nm using time-resolved LAS and showed the linewidths for U isotopes even at atmospheric pressure conditions were < 3 GHz (1.6 pm). This indicates that absorption-based methods can be used for isotopic analysis of various elements with small isotope splitting.

Isotopic analysis employing LAS of LA plumes is typically restricted to probing a single electronic transition in the

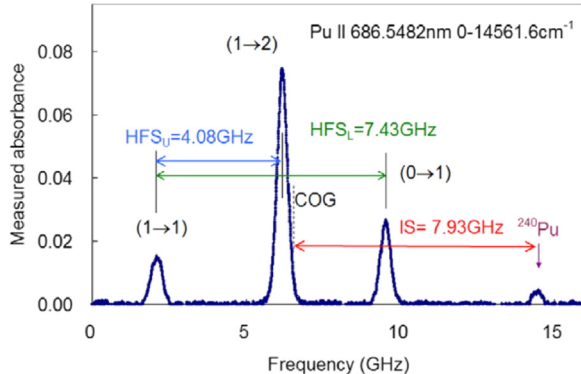


FIG. 21. The absorption spectrum of a Pu ion transition around 686.5 nm. A 532 nm laser was used for ablation of a PuO_2 pellet sample, and an external cavity diode laser (ECDL) was tuned across the selected Pu ion transition in 6 Torr He. The hfs of ^{239}Pu and isotope splitting of ^{240}Pu are marked in the figure.³⁰ Reprinted with permission from Miyabe *et al.*, Spectrochim. Acta B **134**, 42 (2017) as Fig. 4. Copyright 2017 Elsevier.

plasma; this limitation is due to wavelength selection and tunability range available for the probe laser. In comparison, LIBS provides a broadband detection capability, although with reduced spectral resolution. This limitation of LAS can be overcome with the use of frequency combs. Bergevin *et al.*³¹¹ demonstrated the versatility of dual-comb spectroscopy, offering high spectral resolution and broadband detection, to analyze Rb isotopes and K transitions. In these experiments a ≥ 13 nm spectral bandwidth with simultaneous ≤ 1 pm spectral resolution was acquired in a LPP with single shot ablation. Merten and Johnson²⁴³ used OPO pseudo-continuum to record the absorption spectrum from a laser-produced plasma which provided emission that was wider than the absorption line profile, but narrow enough to allow the use of an Echelle spectrograph without order sorting. They used this technique to measure the lithium isotope ratio.

As mentioned previously, LIF spectroscopy incorporates aspects of both atomic absorption and emission. Similar to LAS, LIF spectroscopy provides both selectivity and sensitivity—desired conditions for isotopic analysis. However, limited studies are available in the literature for isotopic analysis employing LIF of LPPs. Smith *et al.*²⁶⁸ used LIF of LA plumes at moderate pressure levels (10 mTorr to 1 Torr) for isotopically selective measurements of lithium in a solid sample of lithium oxalate. In their experiments, a dye laser with 10 pm FWHM was scanned across the Li I 670 nm transition with a 15 pm separation between isotopic fine components. Smith *et al.*²⁵⁰ extended this study to uranium isotopic analysis with two modes of operation: (i) a rapidly scanned diode laser for selective excitation of ^{235}U and ^{238}U via LIF and (ii) time-integrated detection of LIF signals from the individual isotopes during the single-shot duration of the LA event. These studies highlighted the utility of LIF after LA sampling for isotopic detection in the field and can be extended to other actinide elements.

Phillips *et al.*⁷⁵ demonstrated the use of 2D-FS with fs-LA to measure uranium enrichment in solid samples. Natural uranium (NU) and highly enriched uranium (HEU) samples were clearly distinguished based on the 2D-FS maps with good separation of the ^{238}U and ^{235}U isotope peaks (Fig. 22).

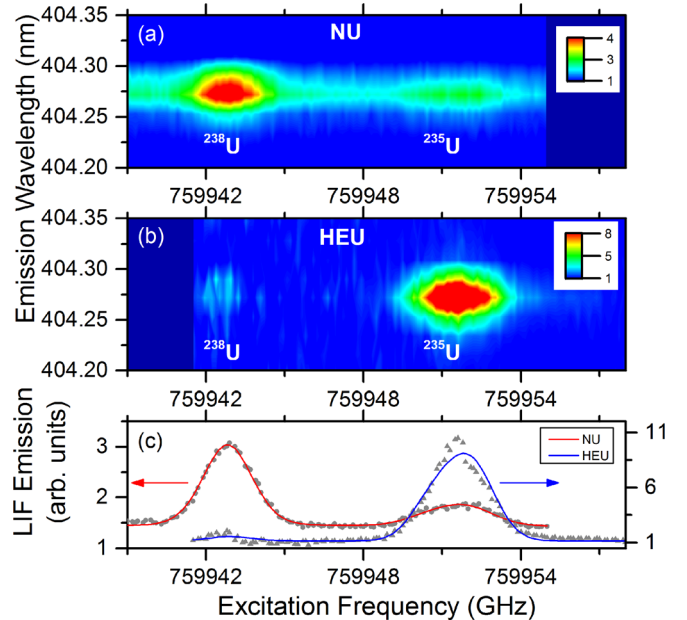


FIG. 22. (a) 2D-FS intensity for NU sample. (b) 2D-FS for HEU sample. (c) LIF excitation spectrum for NU (red) and HEU (blue) samples. The samples were ablated using 40 fs pulses in 50 Torr Ar.⁷⁵ Reprinted with permission from Phillips *et al.*, Sci. Rep. 7, 3784 (2017) as Fig. 2. Copyright 2017 Nature Publications.

Since 2D-FS represents simultaneous absorption and emission spectral features, normalization using the emission spectra was employed to reduce shot-to-shot measurement noise and to improve the SNR in the LIF excitation spectra. These results highlighted the usefulness of 2D-FS to measure U enrichment in a fs-LA plume at reduced pressure and up to atmospheric pressure levels.

VII. PLASMA GENERATION AT STANDOFF DISTANCES

The aim of this section is to provide the current status as well as to understand the advantages and limitations of laser choices for generating plasmas at standoff distances. For the creation of LPPs at a standoff distance, the ablation laser beam should be propagated through an air medium and generate a plasma on the sample of interest located at a certain distance. The generated plasma may have to emit copious amounts of radiation in the spectral region of interest for efficient collection of the signal by the detector located at a standoff distance. Ideally, it is important to create a LPP with suitable physical conditions with maximum size, brightness, and long emission persistence to obtain the best SNR from standoff distances.

The factors influencing standoff plasma generation and detection include the energy coupling of the laser beam with the target (which depends on the focusing conditions and distance), the radiation properties of the plasma, and the collection solid angle. According to geometrical optics, a Gaussian laser beam can be focused to a spot size (approximate) w_D

$$w_D = \frac{2\lambda r}{\pi D} M^2, \quad (28)$$

where r is the standoff distance, D is the laser beam diameter at the focusing optics, and M^2 represents the laser beam

quality parameter. Based on Eq. (28), the spot size at a stand-off distance is governed by the laser beam properties such as aberrations caused by the optical system, as well as by diffraction of the laser beam. Assuming minimal aberration in the system, the focal spot size increases with focusing distance as a consequence of diffraction. For field experiments, unlike laboratory-based systems, one has to account for atmospheric turbulence which leads to spreading of the laser (irradiance fluctuations) and pointing stability (beam wander).³¹² Hence, the atmospheric scintillation during laser propagation may limit the maximum usable beam diameter at a stand-off distance. Apart from that, the required power density for ablation at stand-off distances also depends on the sample physical properties, analyte concentration, and environment.

For emission detection and analysis, the amount of light collected from the LPP zone is limited by the etendue of the system. Though a LPP from any target is emitting in a 2π solid angle, the emission intensity at the detector is limited by the solid angle of the collection optics with a $1/r^2$ dependence. A telescope can be used to collect the light emission remotely, which is then resolved into a spectrum using an optical spectrometer. The resolution of a spectrograph depends on the grating size, groove density, and size of the spectrograph. However, the throughput of the spectrograph decreases with improvement in resolution. Hence, optical throughput of the detector system is recognized as a major limiting issue. In this regard, interference spectrometers, which offer high throughput and high spectral resolution, are very promising.^{313,314}

The majority of stand-off plasma generation research presented in the literature has used ns lasers.^{315–323} There exist several excellent review articles on this topic.^{317,324,325} While this type of ablation laser pulse is feasible for short-range measurements on the order of \sim 10–100 meters,³¹⁸ very high laser energies (several Joules) may be required to extend the reported range. Most of the reported ns laser-based stand-off systems used fundamental radiation from a Nd:YAG laser (1064 nm), and operations up to 120 meters have been demonstrated using \sim 1 J of laser energy and a Galilean telescope for focusing and light collection.^{312,324} A ns-LA system with stand-off distances up to \sim 7 m was also used for Mars planetary exploration where atmospheric pressure levels are lower (7 Torr CO₂).^{326,327}

Improving the laser energy coupling to the target is especially important for stand-off detection applications, where weak LPP emission is difficult to collect due to losses that scale with the stand-off distance. Double-pulse LPP generation has been shown to enhance emission intensities and persistence, and improve detection limits.³²⁸ The double-pulse approach has been realized with different geometries and laser sources. Two main geometry variations have been investigated for double-pulse LA: orthogonal and collinear. In the collinear configuration, both laser pulses propagate on the same axis and are incident perpendicular to the target surface and hence suited for stand-off LA applications.^{329–333}

Focused femtosecond lasers can also be used to generate plasmas at stand-off distances, and researchers have used such a laser system for LIBS studies for distances up to \sim 25 m.³³⁴ However, it may be beneficial to use ns lasers instead

of fs lasers if focusing optics are used to generate plasmas at stand-off distances considering the availability of inexpensive and high peak energy lasers with a smaller footprint. With the use of high-energy ns lasers (currently lasers with > 10 J are available from commercial vendors), higher stand-off distances for plasma generation than already demonstrated should be achievable.

Under the proper conditions, high-intensity ultrashort pulses propagating through the atmosphere may undergo filamentation,^{137,139} and these filaments can propagate over hundreds of meters to kilometers.^{133–135} Currently, significant efforts are underway to use fs filaments to generate plasmas at stand-off distances, and this technique has been named remote filament-induced breakdown spectroscopy (R-FIBS). R-FIBS on copper and steel plates has been demonstrated at 90 m stand-off distances.³³⁵ These studies used 80 fs pulses with 250 mJ energy from the Teramobile laser system,³³⁶ which produced multiple filaments within the beam. A UV laser was used to perform R-FIBS experiments at 10 m stand-off distances.³³⁷ R-FIBS has also been used to investigate biological samples³³⁸ and graphite.³³⁹ Xu *et al.*³⁴⁰ performed detailed studies of R-FIBS on metallic targets, showing several advantages over traditional ns-LIBS and projecting that performance out to km-scale distances should be possible. Rohwetter *et al.*¹⁰¹ demonstrated filament plasma generation at 180 m, although the elemental analysis was not performed due to limitations of the detection system. So far, filaments have been used for remote laser ablation of a solid sample for up to \sim 500 m.¹⁰² In their experiments, high-intensity filaments were used to damage Ge samples. With the current advent of the shorter pulse (<30 fs) and high power (10–100 TW) lasers larger stand-off distances may be feasible, though further research in this direction is necessary.

VIII. SUMMARY AND OUTLOOK

This review has summarized the current status of optical spectroscopy tools in conjunction with LPPs for isotopic analysis. Presently isotopic analysis is carried out in laboratory settings using mass spectrometry. However, rapid, in-field and non-contact isotopic analysis of solid materials is essential for a large number of applications including national security and nuclear non-proliferation. Optical spectroscopy of LPP plumes is well-suited for filling this scientific gap. But, using optical spectroscopy for isotopic analysis brings several challenges that are still under investigation by various research organizations. A key challenge is detecting small isotope splitting seen in the optical transitions of atoms and molecules combined with sufficient limits of detection for minor isotopes in a sample.

Isotope splitting in atoms and molecules varies significantly between elements and even between various optical transitions, so the selection of isolated transitions with the largest isotope splitting is key. Isotope shifts of lighter and heavier elements are found to be larger compared to elements with moderate masses. For lighter-elements (e.g., H), the mass effect contributes a large isotope shift, while field effects contribute significant isotope splitting for heavier elements such as U. But, optical spectroscopy of atoms may not

be a good tool for isotopic analysis for elements in mid-range masses due to small isotope shifts.

Spectroscopic analysis of molecules offers a new paradigm for isotopic information from light diatomic molecules. The vibrational and rotational transitions in molecules can provide isotope splitting that can be orders of magnitude greater than atomic splitting and will be useful for numerous applications. Currently, significant efforts are underway to use molecular isotopic signatures for numerous applications. However, the vibronic transition isotope shift found in molecules decreases with an increase in diatomic mass to the point that it can be comparable to the expected atomic isotope splitting for heavy elements.

LPPs provide an ideal platform for *in-situ* isotopic analysis with no sample preparation. However, for isotopic analysis using LPPs in conjunction with optical spectroscopy, it is important to create a plasma plume with the appropriate physical conditions, maximum size, and long excited or ground state atom/molecular emission/absorption persistence. It is well-known that the LPP is a notoriously complex system and its physical properties may change significantly with time and space and have a direct correlation to numerous experimental parameters. The physical conditions in a LPP plume and the time evolution of atomic, ionic, and molecular species are interrelated, so fine-tuning the experimental parameters to generate suitable conditions for isotopic analysis is very important. The physical conditions also affect the various line broadening mechanisms in a plasma. The potential for high-resolution spectroscopic methods to remotely measure isotope ratios via atomic or ionic transition isotope shifts will depend critically on the interplay of the isotope shift and hyperfine structure with broadening mechanisms including Doppler, collisional, and Stark effects. Hence, an in-depth understanding of “*when and where*” to look to obtain isotopic information in a LPP system is critical.

Thermally excited emission spectroscopy or LIBS is a strong measurement approach for isotopic analysis provided the splitting is larger than the various broadening mechanisms in the plasmas and the instrumental broadening. In fact, passive emission spectroscopy is well suited for certain applications considering its simplicity and rapid analysis. However, when the isotope splitting becomes $< 10 \text{ pm}$, the usage of emission spectroscopy is cumbersome because of the need for the high-resolution spectrographs. Currently, significant efforts are underway to develop compact spectrographs with resolution greater than 10^5 , although maintaining high resolution combined with high throughput and a large spectral window is always a challenge.³⁴¹ The optical throughput in the spectrograph system is also one of the limiting issues to using emission spectroscopy for standoff analysis. Large telescopes can be used to mitigate this issue. The use of interference spectrometers, which offer high resolution and high throughput, will also be useful to overcome some of the limitations of dispersive spectrometers.

In comparison with thermally excited emission spectroscopy, there are certain advantages to using tunable laser absorption spectroscopy for isotopic analysis, especially with laser-solid sampling. Absorption-based measuring tools (LAS and LIF) probe the lower state population of an atomic

or molecular transition which persists as the plasma cools. Absorption-based methods may therefore be performed at very late times of LPP evolution corresponding to a regime of minimal spectral broadening in electronic transitions. However, in the past, LAS or LIF methods were not routinely used for isotopic analysis partly due to unavailability of reliable tunable lasers. With the recent advent of tunable, high power and ultra-narrowband laser technologies (diode, quantum cascade, and Ti:sapphire lasers)—which operate with minimal mode hopping and improved performance in terms of tuning range, linewidth, power, and operation temperature—laser spectroscopy can be expected to play an important role in future sensing applications. Also, the recent development of frequency comb technology is very promising, which provides a very large bandwidth combined with high spectral resolution, and may provide isotopic information even from a single-shot laser ablation.³¹¹ LIF of LA plumes combine the advantages of both emission and absorption spectroscopic tools for isotopic analysis. The recent developments of 2D-FS as a LA tool, obtaining simultaneous absorption and emission profiles, can provide non-contact and standoff capability for isotopic analysis.^{75,259}

Currently, ns lasers are routinely used for solid sampling allowing for rapid, non-contact optical spectroscopy measurements, and standoff distances are only limited by the focusing difficulty raised due to diffraction of the laser beam. One can use fs laser filaments, which are somewhat immune to diffraction, to generate plasmas at very large standoff distances. The ultrashort laser plasmas inherently provide lower-temperature conditions which aid faster formation of molecules as well as a rapid cooling of atomic populations. However, energy coupling of the filament with solid samples located at a standoff distance may be a technical limitation of this approach. Higher energy ultrafast laser pulses may be necessary to propagate and generate filament ablation at large standoff distances. However, ultrafast lasers at higher power levels generate multiple filaments, and further research efforts are needed in this direction to understand the interaction between the plasmas generated from multiple points (colliding plasma plumes) and subsequent emission features. On the other side, focused ns lasers provide better energy coupling to the target in comparison with filament ablation. The availability of compact and high energy solid state ns lasers (currently, $> 10 \text{ J}$ table top and compact lasers are available) along with adaptive optics for focusing and light collection, bring certain room for improvement in terms of standoff distance for isotopic analysis. Double pulsing, where the first pulse is used for LA while the second pulse is used for increasing the persistence of both excited and ground state populations, may also be useful in this context.

Finally, when considering the unique capabilities of LA tools for standoff plasma generation and recent developments in optical spectroscopy tools, one can easily conclude that the extensive use of such a technology is imminent in the near future for rapid and non-contact isotopic analysis of solids in numerous fields.

ACKNOWLEDGMENTS

The authors thank DOE Office of Defense Nuclear Nonproliferation (DNN) (NA-22) for funding support.

The authors are thankful to Bret Cannon, Norm Anheier, Bruce Bushaw, and Jeremy Yeak for their interest, help, and support. Also, thanks to Bruce Bernacki for proofreading and suggestions. Pacific Northwest National Laboratory is operated for the U.S. DOE by the Battelle Memorial Institute under Contract No. DE-AC05-76RLO1830.

- ¹G. Faure and T. M. Mensing, *Isotopes: Principles and Applications* (John Wiley & Sons, New Jersey, 2005).
- ²B. S. Chisholm, D. E. Nelson, and H. P. Schwarcz, *Science* **216**, 1131 (1982).
- ³H. W. Krueger and C. H. Sullivan, *ACS Sym. Ser.* **258**, 205 (1984).
- ⁴B. A. Alex, D. L. Nichols, and M. D. Glascock, *Archaeometry* **54**, 821 (2012).
- ⁵V. Renson *et al.*, *Appl. Geochem.* **28**, 220 (2013).
- ⁶M. Ganio, K. Latruwe, D. Brems, P. Muchez, F. Vanhaecke, and P. Degryse, *J. Anal. At. Spectrom.* **27**, 1335 (2012).
- ⁷A. Bayliss, *Radiocarbon* **51**, 123 (2009).
- ⁸Z. Varga, A. Nichol, M. Wallenius, and K. Mayer, *Anal. Chim. Acta* **718**, 25 (2012).
- ⁹U. Schaltegger, A. Schmitt, and M. Horstwood, *Chem. Geol.* **402**, 89 (2015).
- ¹⁰M. Chiaradia, U. Schaltegger, R. Spikings, J. Wotzlaw, and M. Ovtcharova, *Econ. Geol.* **108**, 565 (2013).
- ¹¹J. Steeb, C. Mertz, G. Sandi, D. Bass, D. Graczyk, and M. Goldberg, *J. Radioanal. Nucl. Chem.* **292**, 757 (2012).
- ¹²C. Paton, M. Schiller, D. Ulfbeck, and M. Bizzarro, *J. Anal. At. Spectrom.* **27**, 644 (2012).
- ¹³S. Chernonozhkin, S. Goderis, L. Lobo, P. Claeys, and F. Vanhaecke, *J. Anal. At. Spectrom.* **30**, 1518 (2015).
- ¹⁴J. Kosler *et al.*, *Geostand. Geoanal. Res.* **37**, 243 (2013).
- ¹⁵M. Ogasawara, M. Fukuyama, K. Horie, T. Sumii, M. Takehara, and M. Sudo, *Island Arc* **22**, 306 (2013).
- ¹⁶J. Eiler *et al.*, *Chem. Geol.* **372**, 119 (2014).
- ¹⁷Q. Chang, J. Kimura, and B. Vaglarov, *J. Anal. At. Spectrom.* **30**, 515 (2015).
- ¹⁸A. Godon, N. Jendrzejewski, H. Eggenkamp, D. Banks, M. Ader, M. Coleman, and F. Pineau, *Chem. Geol.* **207**, 1 (2004).
- ¹⁹S. Bourke, J. Turczenek, E. Schmeling, F. Mahmood, B. Olson, and M. Hendry, *Ground Water Monit. Rem.* **35**, 110 (2015).
- ²⁰O. Lebeau, V. Busigny, C. Chaduteau, and M. Ader, *Chem. Geol.* **372**, 54 (2014).
- ²¹G. Ratie *et al.*, *Chem. Geol.* **402**, 68 (2015).
- ²²N. Estrade, C. Cloquet, G. Echevarria, T. Sterckeman, T. Deng, Y. Tang, and J. Morel, *Earth Planet. Sci. Lett.* **423**, 24 (2015).
- ²³Z. Sharp, J. Barnes, A. Bearley, M. Chaussidon, T. Fischer, and V. Kamenetsky, *Nature* **446**, 1062 (2007).
- ²⁴Z. Abrego, A. Ugarte, N. Unceta, A. Fernandez-Isla, M. Goicolea, and R. Barrio, *Anal. Chem.* **84**, 2402 (2012).
- ²⁵S. J. Benson, C. J. Lennard, P. Maynard, D. M. Hill, A. S. Andrew, and C. Roux, *Sci. Justice* **49**, 73 (2009).
- ²⁶R. C. A. Schellekens, F. Stellaard, H. J. Woerdenbag, H. W. Frijlink, and J. G. W. Kosterink, *Brit. J. Clin. Pharm.* **72**, 879 (2011).
- ²⁷E. Evans, M. Horstwood, J. Pisonero, and C. Smith, *J. Anal. At. Spectrom.* **28**, 779 (2013).
- ²⁸K. Ariyama, M. Shinozaki, and A. Kawasaki, *J. Agric. Food Chem.* **60**, 1628 (2012).
- ²⁹S. Carter, A. Fisher, M. Hinds, S. Lancaster, and J. Marshall, *J. Anal. At. Spectrom.* **28**, 1814 (2013).
- ³⁰M. Miyabe, M. Oba, K. Jung, H. Iimura, K. Akoka, M. Kato, H. Otobe, A. Khumaeni, and I. Wakaida, *Spectrochim. Acta B* **134**, 42 (2017).
- ³¹J. Tarolli, B. Naes, B. Garcia, A. Fischer, and D. Willingham, *J. Anal. At. Spectrom.* **31**, 1472 (2016).
- ³²J. Zheng, W. Bu, K. Tagami, Y. Shikamori, K. Nakano, S. Uchida, and N. Ishii, *Anal. Chem.* **86**, 7103 (2014).
- ³³J. A. Vera, G. M. Murray, S. J. Weeks, and M. C. Edelson, *Spectrochim. Acta B* **46**, 1689 (1991).
- ³⁴S. Boulyga, S. Konegger-Kappel, S. Richter, and L. Sangely, *J. Anal. At. Spectrom.* **30**, 1469 (2015).
- ³⁵S. Horne, S. Landsberger, and B. Dickson, *J. Radioanal. Nucl. Chem.* **299**, 1171 (2014).
- ³⁶R. Marin, J. Sarkis, and M. Nascimento, *J. Radioanal. Nucl. Chem.* **295**, 99 (2013).
- ³⁷A. Huber *et al.*, *Fusion Eng. Des.* **86**, 1336 (2011).
- ³⁸E. Albalat *et al.*, *J. Anal. At. Spectrom.* **31**, 1002 (2016).
- ³⁹A. Taylor, M. Day, S. Hill, J. Marshall, M. Patriarca, and M. White, *J. Anal. At. Spectrom.* **29**, 386 (2014).
- ⁴⁰M. Resano, M. Aramendia, L. Rello, M. Calvo, S. Berail, and C. Pechevran, *J. Anal. At. Spectrom.* **28**, 98 (2013).
- ⁴¹M. Aramendia, L. Rello, M. Resano, and F. Vanhaecke, *J. Anal. At. Spectrom.* **28**, 675 (2013).
- ⁴²H. Gonzalez-Iglesias, M. Fernandez-Sanchez, J. Lopez-Sastre, and A. Sanz-Medel, *Electrophoresis* **33**, 2407 (2012).
- ⁴³J. Chen, S. Shahnavas, N. Singh, W. Ong, and T. Walczyk, *Metalloomics* **5**, 167 (2013).
- ⁴⁴D. Urgast, S. Hill, I. Kwun, J. Beattie, H. Goenaga-Infante, and J. Feldmann, *Metalloomics* **4**, 1057 (2012).
- ⁴⁵J. M. Eiler, in *Annual Review of Earth and Planetary Sciences*, edited by R. Jeanloz (Annual Reviews, Palo Alto, 2013), Vol. 41, p. 411.
- ⁴⁶E. S. F. Berman, N. E. Levin, A. Landais, S. N. Li, and T. Owano, *Anal. Chem.* **85**, 10392 (2013).
- ⁴⁷R. Q. Iannone, D. Romanini, O. Cattani, H. A. J. Meijer, and E. R. T. Kerstel, *J. Geophys. Res.* **115**, D10111, <https://doi.org/10.1029/2009JD012895> (2010).
- ⁴⁸S. N. Vardag, S. Hammer, M. Sabasch, D. W. T. Griffith, and I. Levin, *Atmos. Meas. Technol.* **8**, 579 (2015).
- ⁴⁹J. Heil, B. Wolf, N. Bruggemann, L. Emmenegger, B. Tuzson, H. Vereeken, and J. Mohn, *Geochim. Cosmochim. Acta* **139**, 72 (2014).
- ⁵⁰B. Tuzson, M. J. Zeeman, M. S. Zahniser, and L. Emmenegger, *Infrared Phys. Technol.* **51**, 198 (2008).
- ⁵¹A. Castrillo, G. Casa, and L. Gianfrani, *Opt. Lett.* **32**, 3047 (2007).
- ⁵²J. L. Gottfried, F. C. De Lucia, C. A. Munson, and A. W. Mizolek, *Anal. Bioanal. Chem.* **395**, 283 (2009).
- ⁵³S. A. Kalam, E. N. Rao, and S. V. Rao, *Laser Focus World* **53**, 24 (2017).
- ⁵⁴I. Gaona, J. Serrano, J. Moros, and J. J. Laserna, *Spectrochim. Acta B* **96**, 12 (2014).
- ⁵⁵G. Herzberg, *Spectra of Diatomic Molecules* (Van Nostrand Reinhold Company, Inc., NY, 1950), Vol. 1.
- ⁵⁶W. H. King, *Isotope Shifts in Atomic Spectra* (Springer Sciences, NY, 1984).
- ⁵⁷D. N. Stacey, *Rep. Prog. Phys.* **29**, 171 (1966).
- ⁵⁸P. Jacquinet and R. Klapisch, *Rep. Prog. Phys.* **42**, 773 (1979).
- ⁵⁹K. Heilig and A. Steudel, *At. Data Nucl. Data Tables* **14**, 613 (1974).
- ⁶⁰A. Palfy, *Contemp. Phys.* **51**, 471 (2010).
- ⁶¹G. F. Drake, *Springer Handbook of Atomic, Molecular, and Optical Physics* (Springer, NY, 2006).
- ⁶²O. Axner, J. Gustafsson, N. Omenetto, and J. D. Winefordner, *Spectrochim. Acta B* **59**, 1 (2004).
- ⁶³P. G. Schumann, K. D. A. Wendt, and B. A. Bushaw, *Spectrochim. Acta B* **60**, 1402 (2005).
- ⁶⁴R. C. Stern and B. B. Snavely, *Ann. NY Acad. Sci.* **267**, 71 (1976).
- ⁶⁵J. Blaise and L. J. Radziemski, Jr., *J. Opt. Soc. Am.* **66**, 644 (1976).
- ⁶⁶C. H. Corliss, *J. Res. Natl. Bur. Stand. A* **80A**, 1 (1976).
- ⁶⁷J. Blaise, J.-F. Wyart, J. Vergès, R. Engleman, B. A. Palmer, and L. J. Radziemski, *J. Opt. Soc. Am. B* **11**, 1897 (1994).
- ⁶⁸C. H. Corliss, *J. Res. Natl. Bur. Stand. A* **80**, 429 (1976).
- ⁶⁹M. Singh and N. A. Narasimham, *J. Phys. B* **2**, 119 (1969).
- ⁷⁰See <http://webbook.nist.gov/chemistry/> for NIST Chemistry WebBook.
- ⁷¹W. Opechowski and D. A. De Vries, *Physica* **6**, 913 (1939).
- ⁷²W. J. Childs, O. Poulsen, and L. S. Goodman, *Opt. Lett.* **4**, 35 (1979).
- ⁷³W. J. Childs, O. Poulsen, and L. S. Goodman, *Opt. Lett.* **4**, 63 (1979).
- ⁷⁴G. C. Y. Chan, I. Choi, X. L. Mao, V. Zorba, O. P. Lam, D. K. Shuh, and R. E. Russo, *Spectrochim. Acta B* **122**, 31 (2016).
- ⁷⁵M. C. Phillips, B. E. Brumfield, N. L. LaHaye, S. S. Harilal, K. C. Hartig, and I. Jovanovic, *Sci. Rep.* **7**, 3784 (2017).
- ⁷⁶L. Radziemski and D. Cremers, *Laser Induced Plasma and Applications* (Marcel Dekker, Inc., NY, 1989).
- ⁷⁷S. S. Harilal, P. Skordzki, A. Miloshevsky, B. Brumfield, M. C. Phillips, and G. Miloshevsky, *Phys. Plasmas* **24**, 063304 (2017).
- ⁷⁸D. A. Cremers and L. J. Radziemski, *Handbook of Laser-Induced Breakdown Spectroscopy* (John Wiley & Sons, NJ, 2013).
- ⁷⁹D. W. Hahn and N. Omenetto, *Appl. Spectrosc.* **66**, 347 (2012).
- ⁸⁰S. S. Harilal, C. V. Bindhu, R. C. Issac, V. P. N. Nampoori, and C. P. G. Vallabhan, *J. Appl. Phys.* **82**, 2140 (1997).
- ⁸¹J. R. Freeman, S. S. Harilal, P. K. Diwakar, B. Verhoff, and A. Hassanein, *Spectrochim. Acta B* **87**, 43 (2013).

- ⁸²Y. Tao, M. S. Tillack, S. S. Harilal, K. L. Sequoia, and F. Najmabadi, *J. Appl. Phys.* **101**, 023305 (2007).
- ⁸³C. Phipps, *Laser Ablation and Applications* (Springer, Heidelberg, 2007).
- ⁸⁴S. S. Harilal, in *Laser-Induced Breakdown Spectroscopy—Fundamentals and Applications*, edited by S. Musazzi and U. Perini, Springer Series in Optical Sciences, Vol. 182 (Springer, 2014), p. 143.
- ⁸⁵S. S. Harilal, C. V. Bindhu, M. S. Tillack, F. Najmabadi, and A. C. Gaeris, *J. Appl. Phys.* **93**, 2380 (2003).
- ⁸⁶R. K. Singh, O. W. Holland, and J. Narayan, *J. Appl. Phys.* **68**, 233 (1990).
- ⁸⁷S. A. Irimiciuc, S. Gurlui, G. Bulai, P. Nica, M. Agop, and C. Focsa, *Appl. Surf. Sci.* **417**, 108 (2017).
- ⁸⁸R. A. Burdt, S. Yuspeh, K. L. Sequoia, Y. Z. Tao, M. S. Tillack, and F. Najmabadi, *J. Appl. Phys.* **106**, 033310 (2009).
- ⁸⁹E. L. Gurevich and R. Hergenroder, *Appl. Spectrosc.* **61**, 233A (2007).
- ⁹⁰D. W. Hahn and N. Omenetto, *Appl. Spectrosc.* **64**, 335 (2010).
- ⁹¹S. S. Harilal, C. V. Bindhu, V. P. N. Nampoori, and C. P. G. Vallabhan, *Appl. Phys. Lett.* **72**, 167 (1998).
- ⁹²J. A. Aguilera and C. Aragón, *Appl. Surf. Sci.* **197-198**, 273 (2002).
- ⁹³A. V. Bulgakov and N. M. Bulgakova, *J. Phys. D* **31**, 693 (1998).
- ⁹⁴P. K. Diwakar, S. S. Harilal, and M. C. Phillips, *J. Appl. Phys.* **118**, 043305 (2015).
- ⁹⁵S. S. Harilal, M. S. Tillack, B. O’Shay, C. V. Bindhu, and F. Najmabadi, *Phys. Rev. E* **69**, 026413 (2004).
- ⁹⁶K. S. Singh and A. K. Sharma, *Phys. Plasmas* **23**, 123514 (2016).
- ⁹⁷V. N. Rai, A. K. Rai, F. Y. Yueh, and J. P. Singh, *Appl. Opt.* **42**, 2085 (2003).
- ⁹⁸T. A. Labutin, V. N. Lednev, A. A. Ilyin, and A. M. Popov, *J. Anal. At. Spectrom.* **31**, 90 (2016).
- ⁹⁹N. Smijesh, K. Chandrasekharan, J. C. Joshi, and R. Philip, *J. Appl. Phys.* **116**, 013301 (2014).
- ¹⁰⁰S. Sunku, M. K. Gundawar, A. K. Myakalwar, P. P. Kiran, S. P. Tewari, and S. V. Rao, *Spectrochim. Acta B* **79**, 31 (2013).
- ¹⁰¹P. Rohwetter et al., *Spectrochim. Acta B* **60**, 1025 (2005).
- ¹⁰²M. Durand et al., *Opt. Express* **21**, 26836 (2013).
- ¹⁰³M. Sababi, in *Laser-Induced Breakdown Spectroscopy*, edited by J. P. Singh and S. N. Thakur (Elsevier, Amsterdam, 2007).
- ¹⁰⁴B. Rethfeld, K. Sokolowski-Tinten, D. von der Linde, and S. I. Anisimov, *Appl. Phys. A* **79**, 767 (2004).
- ¹⁰⁵E. G. Gamaly, A. V. Rode, B. Luther-Davies, and V. T. Tikhonchuk, *Phys. Plasmas* **9**, 949 (2002).
- ¹⁰⁶B. N. Chichkov, C. Momma, S. Nolte, F. von Alvensleben, and A. Tunnermann, *Appl. Phys. A* **63**, 109 (1996).
- ¹⁰⁷P. Sankar, J. J. J. Nivas, N. Smijesh, G. K. Tiwari, and R. Philip, *J. Anal. At. Spectrom.* **32**, 1177 (2017).
- ¹⁰⁸V. Margetic, A. Pakulev, A. Stockhaus, M. Bolshov, K. Niemax, and R. Hergenroder, *Spectrochim. Acta B* **55**, 1771 (2000).
- ¹⁰⁹B. Verhoff, S. S. Harilal, and A. Hassanein, *J. Appl. Phys.* **111**, 123304 (2012).
- ¹¹⁰K. K. Anoop, X. C. Ni, M. Bianco, D. Paparo, X. Wang, R. Buzzese, and S. Amoruso, *Appl. Phys. A* **117**, 313 (2014).
- ¹¹¹A. Miloshevsky, M. C. Phillips, S. S. Harilal, P. Dressman, and G. Miloshevsky, *Phys. Rev. Mater.* **1**, 063602 (2017).
- ¹¹²O. Albert, S. Roger, Y. Glinec, J. C. Loulergue, J. Etchepare, C. Boulmer-Leborgne, J. Perriere, and E. Millon, *Appl. Phys. A* **76**, 319 (2003).
- ¹¹³M. D. Perry, B. C. Stuart, P. S. Banks, M. D. Feit, V. Yanovsky, and A. M. Rubenchik, *J. Appl. Phys.* **85**, 6803 (1999).
- ¹¹⁴A. Bogaerts, Z. Y. Chen, R. Gijbels, and A. Vertes, *Spectrochim. Acta B* **58**, 1867 (2003).
- ¹¹⁵N. M. Shaikh, B. Rashid, S. Hafeez, Y. Jamil, and M. A. Baig, *J. Phys. D* **39**, 1384 (2006).
- ¹¹⁶J. Hoffman, T. Moscicki, and Z. Szymanski, *Appl. Phys. A* **104**, 815 (2011).
- ¹¹⁷G. Olivie, D. Giguere, F. Vidal, T. Ozaki, J. C. Kieffer, O. Nada, and I. Brunette, *Opt. Express* **16**, 4121 (2008).
- ¹¹⁸N. L. LaHaye, S. S. Harilal, P. K. Diwakar, A. Hassanein, and P. Kulkarni, *J. Appl. Phys.* **114**, 023103 (2013).
- ¹¹⁹B. Rethfeld, D. S. Ivanov, M. E. Garcia, and S. I. Anisimov, *J. Phys. D* **50**, 193001 (2017).
- ¹²⁰R. Stoian, D. Ashkenasi, A. Rosenfeld, and E. E. B. Campbell, *Phys. Rev. B* **62**, 13167 (2000).
- ¹²¹J. A. Aguilera and C. Aragon, *Spectrochim. Acta B* **63**, 793 (2008).
- ¹²²R. A. Multari, L. E. Foster, D. A. Cremers, and M. J. Ferris, *Appl. Spectrosc.* **50**, 1483 (1996).
- ¹²³X. W. Li, W. F. Wei, J. Wu, S. L. Jia, and A. C. Qiu, *J. Appl. Phys.* **113**, 243304 (2013).
- ¹²⁴S. I. Anisimov, B. S. Lukyanchuk, and A. Luches, *Appl. Surf. Sci.* **96-98**, 24 (1996).
- ¹²⁵S. S. Harilal, *J. Appl. Phys.* **102**, 123306 (2007).
- ¹²⁶B. Toftmann, B. Doggett, C. B. J. Rgensen, J. Schou, and J. G. Lunney, *J. Appl. Phys.* **113**, 083304 (2013).
- ¹²⁷R. Teghil, L. D’Alessio, A. Santagata, M. Zaccagnino, D. Ferro, and D. J. Sordellet, *Appl. Surf. Sci.* **210**, 307 (2003).
- ¹²⁸S. S. Harilal, N. Farid, J. F. Freeman, P. K. Diwakar, N. L. LaHaye, and A. Hassanein, *Appl. Phys. A* **117**, 319 (2014).
- ¹²⁹A. Hayat, S. Bashir, M. S. Rafique, R. Ahmad, M. Akram, K. Mahmood, and A. Zaheer, *Appl. Phys. A* **123**, 505 (2017).
- ¹³⁰J. Guo, J. Shao, T. Wang, C. Zheng, A. Chen, and M. Jin, *J. Anal. At. Spectrom.* **32**, 367 (2017).
- ¹³¹S. S. Harilal, P. K. Diwakar, M. P. Polek, and M. C. Phillips, *Opt. Express* **23**, 15608 (2015).
- ¹³²S. L. Chin, *Femtosecond Laser Filamentation* (Springer-Verlag, NY, 2010).
- ¹³³B. La Fontaine et al., *Phys. Plasmas* **6**, 1615 (1999).
- ¹³⁴G. Mechain et al., *Appl. Phys. B* **79**, 379 (2004).
- ¹³⁵G. Mechain et al., *Opt. Commun.* **247**, 171 (2005).
- ¹³⁶M. Rodriguez et al., *Phys. Rev. E* **69**, 036607 (2004).
- ¹³⁷A. Couairon and A. Mysyrowicz, *Phys. Rep.* **441**, 47 (2007).
- ¹³⁸S. S. Harilal, J. Yeak, and M. C. Phillips, *Opt. Express* **23**, 27113 (2015).
- ¹³⁹A. Braun, G. Korn, X. Liu, D. Du, J. Squier, and G. Mourou, *Opt. Lett.* **20**, 73 (1995).
- ¹⁴⁰L. Berge, S. Skupin, R. Nuter, J. Kasparian, and J. P. Wolf, *Rep. Prog. Phys.* **70**, 1633 (2007).
- ¹⁴¹J. V. Moloney, *Proc. SPIE* **6261**, 626102 (2006).
- ¹⁴²M. Mlejnek, M. Kolesik, J. V. Moloney, and E. M. Wright, *Phys. Rev. Lett.* **83**, 2938 (1999).
- ¹⁴³I. Ghebregziabher, K. C. Hartig, and I. Jovanovic, *Opt. Express* **24**, 5263 (2016).
- ¹⁴⁴A. Valenzuela, C. Munson, A. Porwitzky, M. Weidman, and M. Richardson, *Appl. Phys. B* **116**, 485 (2014).
- ¹⁴⁵M. Weidman, K. Lim, M. Ramm, M. Durand, M. Baudelet, and M. Richardson, *Appl. Phys. Lett.* **101**, 034101 (2012).
- ¹⁴⁶S. S. Harilal, J. Yeak, B. E. Brumfield, and M. C. Phillips, *Opt. Express* **24**, 17941 (2016).
- ¹⁴⁷J. S. Cowpe, R. D. Pilkington, J. S. Astin, and A. E. Hill, *J. Phys. D* **42**, 165202 (2009).
- ¹⁴⁸G. Cristoforetti, S. Legnaioli, V. Palleschi, A. Salvetti, and E. Tognoni, *Spectrochim. Acta B* **59**, 1907 (2004).
- ¹⁴⁹R. K. Singh, A. Kumar, B. G. Patel, and K. P. Subramanian, *J. Appl. Phys.* **101**, 103301 (2007).
- ¹⁵⁰S. D. Zhang, X. H. Wang, M. H. He, Y. B. Jiang, B. C. Zhang, W. Hang, and B. L. Huang, *Spectrochim. Acta B* **97**, 13 (2014).
- ¹⁵¹J. Hermann and C. Dutouquet, *J. Phys. D* **32**, 2707 (1999).
- ¹⁵²D. Liu, C. S. Chen, X. Gao, J. Q. Lin, B. Y. Man, Y. N. Sun, and F. F. Li, *Eur. Phys. J. D* **70**, 245 (2016).
- ¹⁵³M. C. Spadaro, E. Fazio, F. Neri, S. Trusso, and P. M. Ossi, *EPL* **109**, 25002 (2015).
- ¹⁵⁴J. Wu, W. F. Wei, X. W. Li, S. L. Jia, and A. C. Qiu, *Appl. Phys. Lett.* **102**, 164104 (2013).
- ¹⁵⁵J. Hermann, A. Lorusso, A. Perrone, F. Strafella, C. Dutouquet, and B. Torralba, *Phys. Rev. E* **92**, 053103 (2015).
- ¹⁵⁶S. S. Harilal, R. C. Issac, C. V. Bindhu, P. Gopinath, V. P. N. Nampoori, and C. P. G. Vallabhan, *Spectrochim. Acta A* **53**, 1527 (1997).
- ¹⁵⁷A. De Giacomo and J. Hermann, *J. Phys. D* **50**, 183002 (2017).
- ¹⁵⁸N. Glumac and G. Elliott, *Opt. Laser Eng.* **45**, 27 (2007).
- ¹⁵⁹S. Mahmood, R. S. Rawat, M. Zakaullah, J. J. Lin, S. V. Springham, T. L. Tan, and P. Lee, *J. Phys. D* **42**, 135504 (2009).
- ¹⁶⁰J. L. Gottfried, *Phys. Chem. Chem. Phys.* **16**, 21452 (2014).
- ¹⁶¹T. E. Itina, J. Hermann, P. Delaporte, and M. Sentis, *Phys. Rev. E* **66**, 066406 (2002).
- ¹⁶²Q. L. Ma, V. Motto-Ros, W. Q. Lei, M. Boueri, X. S. Bai, L. J. Zheng, H. P. Zeng, and J. Yu, *Spectrochim. Acta B* **65**, 896 (2010).
- ¹⁶³S. S. Harilal, B. E. Brumfield, B. Cannon, and M. C. Phillips, *Anal. Chem.* **88**, 2296 (2016).
- ¹⁶⁴R. Glauz, J. Riedel, and I. Gornushkin, *Anal. Chem.* **87**, 10131 (2015).
- ¹⁶⁵J. Serrano, J. Moros, and J. J. Laserna, *Anal. Chem.* **87**, 2794 (2015).

- ¹⁶⁶S. Sreedhar, E. N. Rao, G. M. Kumar, S. P. Tewari, and S. V. Rao, *Spectrochim. Acta B* **87**, 121 (2013).
- ¹⁶⁷X. L. Mao, G. C. Y. Chan, I. Choi, V. Zorba, R. E. Russo, and J. Radanal, *Nucl. Chem.* **312**, 121 (2017).
- ¹⁶⁸K. Hartig, S. S. Harilal, M. C. Phillips, B. E. Brumfield, and I. Jovanovic, *Opt. Express* **25**, 11477 (2017).
- ¹⁶⁹K. Hartig, B. Brumfield, M. C. Phillips, and S. S. Harilal, *Spectrochim. Acta B* **135**, 54 (2017).
- ¹⁷⁰K. F. Al-Shboul, S. M. Hassan, and S. S. Harilal, *Plasma Sources Sci. Technol.* **25**, 065017 (2016).
- ¹⁷¹A. Kushwaha and R. K. Thareja, *Appl. Opt.* **47**, G65 (2008).
- ¹⁷²S. Trautner, J. Jasik, C. G. Parigger, J. D. Pedarnig, W. Spendelhofer, J. Lackner, P. Veis, and J. Heitz, *Spectrochim. Acta A* **174**, 331 (2017).
- ¹⁷³C. M. Ahamer, S. Eschlbock-Fuchs, P. J. Kolmhofer, R. Rossler, N. Huber, and J. D. Pedarnig, *Spectrochim. Acta B* **122**, 157 (2016).
- ¹⁷⁴P. J. Skordzki *et al.*, *Spectrochim. Acta B* **125**, 112 (2016).
- ¹⁷⁵H. M. Hou, X. L. Mao, V. Zorba, and R. E. Russo, *Anal. Chem.* **89**, 7750 (2017).
- ¹⁷⁶A. A. Bol'shakov, X. L. Mao, J. J. Gonzalez, and R. E. Russo, *J. Anal. At. Spectrom.* **31**, 119 (2016).
- ¹⁷⁷H. R. Griem, *Spectral Line Broadening by Plasmas* (Academic Press, New York, 1974).
- ¹⁷⁸H.-J. Kunze, *Introduction to Plasma Spectroscopy* (Springer, Heidelberg, 2009).
- ¹⁷⁹N. Konjević, *Phys. Rep.* **316**, 339 (1999).
- ¹⁸⁰C. Aragón and J. A. Aguilera, *Spectrochim. Acta B* **63**, 893 (2008).
- ¹⁸¹I. B. Gornushkin, L. A. King, B. W. Smith, N. Omenetto, and J. D. Winefordner, *Spectrochim. Acta B* **54**, 1207 (1999).
- ¹⁸²T. N. Anderson, J. K. Magnuson, and R. P. Lucht, *Appl. Phys. B* **87**, 341 (2007).
- ¹⁸³K. S. Bond *et al.*, *Appl. Phys. B* **90**, 255 (2008).
- ¹⁸⁴H. R. Griem, *Phys. Rev.* **165**, 258 (1968).
- ¹⁸⁵H. R. Griem, *Plasma Spectroscopy* (McGraw-Hill, NY 1964).
- ¹⁸⁶see <https://www.nist.gov/pml/atomic-spectra-database> for NIST Atomic database, version 5.
- ¹⁸⁷N. Konjević, A. Lesage, J. R. Fuhr, and W. L. Wiese, *J. Phys. Chem. Ref. Data* **31**, 819 (2002).
- ¹⁸⁸G. Cristoforetti and E. Tognoni, *Spectrochim. Acta B* **79-80**, 63 (2013).
- ¹⁸⁹C. D'Angelo, M. Garcimuno, D. Pace, and G. Bertuccelli, *JQSRT* **164**, 89 (2015).
- ¹⁹⁰N. V. Vitanov, B. W. Shore, L. Yatsenko, K. Bohmer, T. Halfmann, T. Rickes, and K. Bergmann, *Opt. Commun.* **199**, 117 (2001).
- ¹⁹¹S. S. Harilal, J. Yeak, B. E. Brumfield, and M. C. Phillips, *J. Anal. At. Spectrom.* **31**, 1192 (2016).
- ¹⁹²C. G. Parigger, M. Dackman, and J. O. Hornkohl, *Appl. Opt.* **47**, G1 (2008).
- ¹⁹³N. D. Zameroski, G. D. Hager, W. Rudolph, C. J. Erickson, and D. A. Hostutler, *JQSRT* **112**, 59 (2011).
- ¹⁹⁴G. A. Pitz, A. J. Sandoval, N. D. Zameroski, W. L. Klemmert, and D. A. Hostutler, *JQSRT* **113**, 387 (2012).
- ¹⁹⁵N. R. Taylor and M. C. Phillips, *Opt. Lett.* **39**, 594 (2014).
- ¹⁹⁶F. R. Doucet, G. Lithgow, R. Kosierb, P. Bouchard, and M. Sabsabi, *J. Anal. At. Spectrom.* **26**, 536 (2011).
- ¹⁹⁷W. Demtroder, *Laser Spectroscopy* (Springer, 2008), Vol. 2.
- ¹⁹⁸M. W. Sigrist, *Rev. Sci. Instrum.* **74**, 486 (2003).
- ¹⁹⁹N. Krstulović, N. Čutić, and S. Milosević, *Spectrochim. Acta B* **63**, 1233 (2008).
- ²⁰⁰M. C. Phillips and M. S. Taubman, *Opt. Lett.* **37**, 2664 (2012).
- ²⁰¹I. Labazan, N. Krstulovic, and S. Milosevic, *J. Phys. D* **36**, 2465 (2003).
- ²⁰²M. Burger, D. Pantic, Z. Nikolic, and S. Djenize, *Eur. Phys. J. D* **71**, 123 (2017).
- ²⁰³A. W. Miziolek, V. Palleschi, and I. Schechter, *Laser-Induced Breakdown Spectroscopy (LIBS): Fundamentals and Applications* (Cambridge University Press, Cambridge, 2006).
- ²⁰⁴S. Musazzi and U. Perini, *Laser-Induced Breakdown Spectroscopy: Theory and Applications* (Springer, Heidelberg, 2014).
- ²⁰⁵J. P. Singh and S. N. Thakur, *Laser Induced Breakdown Spectroscopy* (Elsevier, Amsterdam, 2007).
- ²⁰⁶J. J. Camacho, L. Diaz, M. Santos, L. J. Juan, and J. M. L. Poyato, *J. Appl. Phys.* **106**, 033306 (2009).
- ²⁰⁷N. M. Shaikh, M. S. Kalhoro, A. Hussain, and M. A. Baig, *Spectrochim. Acta B* **88**, 198 (2013).
- ²⁰⁸K. Yahiaoui, S. Abdelli-Messaci, S. Messaoud-Aberkane, T. Kerdja, and H. Kellou, *Spectrochim. Acta B* **93**, 20 (2014).
- ²⁰⁹J. F. Y. Gravel, F. R. Doucet, P. Bouchard, and M. Sabsabi, *J. Anal. At. Spectrom.* **26**, 1354 (2011).
- ²¹⁰A. Sarkar, D. Alamelu, and S. K. Aggarwal, *Appl. Opt.* **47**, G58 (2008).
- ²¹¹A. Sarkar, D. Alamelu, and S. K. Aggarwal, *Talanta* **78**, 800 (2009).
- ²¹²A. J. R. Bauer and S. G. Buckley, *Appl. Spectrosc.* **71**, 553 (2017).
- ²¹³J. D. Hybl, G. A. Lithgow, and S. G. Buckley, *Appl. Spectrosc.* **57**, 1207 (2003).
- ²¹⁴S. A. Davari, S. Hu, R. Pamu, and D. Mukherjee, *J. Anal. At. Spectrom.* **32**, 1378 (2017).
- ²¹⁵C. R. Bhatt, C. L. Goueguel, J. C. Jain, H. M. Edenborn, and D. L. McIntyre, *Appl. Opt.* **56**, 7789 (2017).
- ²¹⁶H. K. Sanghani *et al.*, *Spectrochim. Acta B* **115**, 40 (2016).
- ²¹⁷A. El-Hussein, A. Marzouk, and M. A. Harith, *Spectrochim. Acta B* **113**, 93 (2015).
- ²¹⁸M. Z. Martin, S. Allman, D. J. Brice, R. C. Martin, and N. O. Andre, *Spectrochim. Acta B* **74-75**, 177 (2012).
- ²¹⁹A. I. Whitehouse, J. Young, I. M. Botheroyd, S. Lawson, C. P. Evans, and J. Wright, *Spectrochim. Acta B* **56**, 821 (2001).
- ²²⁰J. E. Barefield *et al.*, *Spectrochim. Acta B* **120**, 1 (2016).
- ²²¹A. A. I. Khalil, M. A. Gondal, M. Shemis, and I. S. Khan, *Appl. Opt.* **54**, 2123 (2015).
- ²²²R. Noll, *Laser-Induced Breakdown Spectroscopy: Fundamentals and Applications* (Springer-Verlag, Berlin, 2012).
- ²²³E. Tognoni, V. Palleschi, M. Corsi, and G. Cristoforetti, *Spectrochim. Acta B* **57**, 1115 (2002).
- ²²⁴M. Kuzuya and O. Mikami, *Jpn. J. Appl. Phys., Part 1* **29**, 1568 (1990).
- ²²⁵S. S. Harilal, *Appl. Opt.* **43**, 3931 (2004).
- ²²⁶S. S. Harilal, P. K. Diwakar, N. L. LaHaye, and M. C. Phillips, *Spectrochim. Acta B* **111**, 1 (2015).
- ²²⁷P. K. Diwakar, S. S. Harilal, and M. C. Phillips, *J. Appl. Phys.* **116**, 133301 (2014).
- ²²⁸S. Merk, A. Demidov, D. Shelby, I. B. Gornushkin, U. Panne, B. W. Smith, and N. Omenetto, *Appl. Spectrosc.* **67**, 851 (2013).
- ²²⁹S. S. Harilal, P. Radhakrishnan, V. P. N. Nampoori, and C. P. G. Vallabhan, *Appl. Phys. Lett.* **64**, 3377 (1994).
- ²³⁰S. S. Harilal, *Appl. Surf. Sci.* **172**, 103 (2001).
- ²³¹N. L. LaHaye, M. C. Phillips, A. Duffin, G. Eiden, and S. S. Harilal, *J. Anal. At. Spectrom.* **31**, 515 (2016).
- ²³²A. De Giacomo, R. Gaudiuso, M. Dell'Aglio, and A. Santagata, *Spectrochim. Acta B* **65**, 385 (2010).
- ²³³A. Tarifa and J. R. Almirall, *Sci. Justice* **55**, 168 (2015).
- ²³⁴M. Tampo, M. Miyabe, K. Akaoka, M. Oba, H. Ohba, Y. Maruyama, and I. Wakaida, *J. Anal. At. Spectrom.* **29**, 886 (2014).
- ²³⁵Y. Liu, B. Bousquet, M. Baudelet, and M. Richardson, *Spectrochim. Acta B* **73**, 89 (2012).
- ²³⁶V. I. Babushok, F. C. DeLucia, Jr., J. L. Gottfried, C. A. Munson, and A. W. Miziolek, *Spectrochim. Acta B* **61**, 999 (2006).
- ²³⁷G. Cristoforetti, S. Legnaioli, L. Pardini, V. Palleschi, A. Salvetti, and E. Tognoni, *Spectrochim. Acta B* **61**, 340 (2006).
- ²³⁸Y. Wang, A. M. Chen, L. Z. Sui, S. Y. Li, D. L. Liu, X. W. Wang, Y. F. Jiang, X. R. Huang, and M. X. Jin, *Phys. Plasmas* **23**, 113105 (2016).
- ²³⁹O. A. Nassef and H. E. Elsayed-Ali, *Spectrochim. Acta B* **60**, 1564 (2005).
- ²⁴⁰C. Koral, A. De Giacomo, X. L. Mao, V. Zorba, and R. E. Russo, *Spectrochim. Acta B* **125**, 11 (2016).
- ²⁴¹E. Tognoni and G. Cristoforetti, *J. Anal. At. Spectrom.* **29**, 1318 (2014).
- ²⁴²B. Yee, K. C. Hartig, P. Ko, J. McNutt, and I. Jovanovic, *Spectrochim. Acta B* **79-80**, 72 (2013).
- ²⁴³J. Merten and B. Johnson, *Spectrochim. Acta B* **139**, 38 (2018).
- ²⁴⁴L. A. King, I. B. Gornushkin, D. Pappas, B. W. Smith, and J. D. Winefordner, *Spectrochim. Acta B* **54**, 1771 (1999).
- ²⁴⁵J. Koch, A. Zybin, and K. Niemax, *Spectrochim. Acta B* **57**, 1547 (2002).
- ²⁴⁶M. Miyabe, M. Oba, H. Iimura, K. Akaoka, Y. Maruyama, H. Ohba, M. Tampo, and I. Wakaida, *Appl. Phys. A* **112**, 87 (2013).
- ²⁴⁷H. Liu, A. Quentmeier, and K. Niemax, *Spectrochim. Acta B* **57**, 1611 (2002).
- ²⁴⁸M. Miyabe, M. Oba, H. Iimura, K. Akaoka, Y. Maruyama, H. Ohba, M. Tampo, and I. Wakaida, *Hyperfine Interact.* **216**, 71 (2013).
- ²⁴⁹A. Quentmeier, M. Bolshov, and K. Niemax, *Spectrochim. Acta B* **56**, 45 (2001).
- ²⁵⁰B. W. Smith, A. Quentmeier, M. Bolshov, and K. Niemax, *Spectrochim. Acta B* **54**, 943 (1999).
- ²⁵¹B. A. Bushaw and N. C. Anheier, *Spectrochim. Acta B* **64**, 1259 (2009).
- ²⁵²B. A. Bushaw and M. L. Alexander, *Appl. Surf. Sci.* **127**, 935 (1998).

- ²⁵³A. Neogi, E. T. Kennedy, J. P. Mosnier, P. van Kampen, J. T. Costello, C. McGuinness, and G. O'Sullivan, *J. Phys. B* **34**, L651 (2001).
- ²⁵⁴C. McGuinness *et al.*, *J. Phys. B* **33**, 5077 (2000).
- ²⁵⁵M. Ribiere and B. G. Cheron, *Spectrochim. Acta B* **65**, 524 (2010).
- ²⁵⁶R. A. AlWazzan, C. L. S. Lewis, and T. Morrow, *Rev. Sci. Instrum.* **67**, 85 (1996).
- ²⁵⁷G. W. Martin, L. A. Doyle, A. Al-Khateeb, I. Weaver, D. Riley, M. J. Lamb, T. Morrow, and C. L. S. Lewis, *Appl. Surf. Sci.* **127**, 710 (1998).
- ²⁵⁸S. S. Harilal, N. L. LaHaye, and M. C. Phillips, *Opt. Express* **25**, 2312 (2017).
- ²⁵⁹S. S. Harilal, N. L. LaHaye, and M. C. Phillips, *Opt. Lett.* **41**, 3547 (2016).
- ²⁶⁰P. Stchur, K. X. Yang, X. D. Hou, T. Sun, and R. G. Michel, *Spectrochim. Acta B* **56**, 1565 (2001).
- ²⁶¹S. Laville, C. Goueguel, H. Loudy, F. Vidal, M. Chaker, and M. Sabsabi, *Spectrochim. Acta B* **64**, 347 (2009).
- ²⁶²H. S. Kwong and R. M. Measures, *Anal. Chem.* **51**, 428 (1979).
- ²⁶³R. M. Measures and H. S. Kwong, *Appl. Opt.* **18**, 281 (1979).
- ²⁶⁴K. Niemax and W. Sdorra, *Appl. Opt.* **29**, 5000 (1990).
- ²⁶⁵I. B. Gornushkin, S. A. Baker, B. W. Smith, and J. D. Winefordner, *Spectrochim. Acta B* **52**, 1653 (1997).
- ²⁶⁶H. Loudy, K. Rifai, S. Laville, F. Vidal, M. Chaker, and M. Sabsabi, *J. Anal. At. Spectrom.* **24**, 1421 (2009).
- ²⁶⁷J. Kang, R. Li, Y. Wang, Y. Chen, and Y. Yang, *J. Anal. At. Spectrom.* **32**, 2292 (2017).
- ²⁶⁸B. W. Smith, I. B. Gornushkin, L. A. King, and J. D. Winefordner, *Spectrochim. Acta B* **53**, 1131 (1998).
- ²⁶⁹F. Hilbk-Kortenbruck, R. Noll, P. Wintjens, H. Falk, and C. Becker, *Spectrochim. Acta B* **56**, 933 (2001).
- ²⁷⁰C. M. Li, Z. Q. Hao, Z. M. Zou, R. Zhou, J. M. Li, L. B. Guo, X. Y. Li, Y. F. Lu, and X. Y. Zeng, *Opt. Express* **24**, 7850 (2016).
- ²⁷¹H. H. Telle, D. C. S. Beddows, G. W. Morris, and O. Samek, *Spectrochim. Acta B* **56**, 947 (2001).
- ²⁷²X. Wang, Z. Huang, P.-C. Chu, Y. Cai, K. S. Y. Leung, J. T. S. Lum, and N.-H. Cheung, *J. Anal. At. Spectrom.* **31**, 2363 (2016).
- ²⁷³J. A. Merten, C. A. Jones, and P. D. Tribbett, *J. Anal. At. Spectrom.* **32**, 1697 (2017).
- ²⁷⁴C. Goueguel, S. Laville, F. Vidal, M. Sabsabi, and M. Chaker, *J. Anal. At. Spectrom.* **25**, 635 (2010).
- ²⁷⁵C. Goueguel, S. Laville, F. Vidal, M. Chaker, and M. Sabsabi, *J. Anal. At. Spectrom.* **26**, 2452 (2011).
- ²⁷⁶S. Y. Chan and N. H. Cheung, *Anal. Chem.* **72**, 2087 (2000).
- ²⁷⁷N. H. Cheung, *Appl. Spectrosc. Rev.* **42**, 235 (2007).
- ²⁷⁸S. L. Lui, Y. Godwal, M. T. Taschuk, Y. Y. Tsui, and R. Fedosejevs, *Anal. Chem.* **80**, 1995 (2008).
- ²⁷⁹X. K. Shen and Y. F. Lu, *Appl. Opt.* **47**, 1810 (2008).
- ²⁸⁰E. Stoffels, P. van de Weijer, and J. van der Mullen, *Spectrochim. Acta B* **46**, 1459 (1991).
- ²⁸¹M. Miyabe, M. Oba, H. Iimura, K. Akaoka, A. Khumaeni, M. Kato, and I. Wakaida, *Spectrochim. Acta B* **110**, 101 (2015).
- ²⁸²Y. Nakata, T. Okada, and M. Maeda, *Opt. Lett.* **24**, 1765 (1999).
- ²⁸³K. Orsel, R. Groenen, H. M. J. Bastiaens, G. Koster, G. Rijnders, and K. J. Boller, *J. Instrum.* **8**, C10021 (2013).
- ²⁸⁴J. Muramoto, T. Inmaru, Y. Nakata, T. Okada, and M. Maeda, *Appl. Phys. Lett.* **77**, 2334 (2000).
- ²⁸⁵S. S. Harilal, B. E. Brumfield, and M. C. Phillips, *Opt. Lett.* **43**, 1055 (2018).
- ²⁸⁶L. Nagli and M. Gaft, *Appl. Spectrosc.* **70**, 585 (2016).
- ²⁸⁷Y. Matsuo, T. Nakajima, T. Kobayashi, and M. Takami, *Appl. Phys. Lett.* **71**, 996 (1997).
- ²⁸⁸C. E. Otis, A. Gupta, and B. Braren, *Appl. Phys. Lett.* **62**, 102 (1993).
- ²⁸⁹R. W. Dreyfus, *Appl. Phys. A* **55**, 335 (1992).
- ²⁹⁰M. He, H. X. Wang, and B. R. Weiner, *Chem. Phys. Lett.* **204**, 563 (1993).
- ²⁹¹D. A. Cremers, A. Beddingfield, R. Smithwick, R. C. Chinni, C. R. Jones, B. Beardsley, and L. Karch, *Appl. Spectrosc.* **66**, 250 (2012).
- ²⁹²C. A. Smith, M. A. Martinez, D. K. Veirs, and D. A. Cremers, *Spectrochim. Acta B* **57**, 929 (2002).
- ²⁹³C. Li, C. L. Feng, H. Y. Oderji, G. N. Luo, and H. B. Ding, *Front. Phys.* **11**, 114214 (2016).
- ²⁹⁴L. Mercadier, J. Hermann, C. Grisolia, and A. Semerok, *Spectrochim. Acta B* **65**, 715 (2010).
- ²⁹⁵A. D'Ulivo *et al.*, *Spectrochim. Acta B* **61**, 797 (2006).
- ²⁹⁶G. T. Razdobarin, G. Federici, V. M. Kozhevnik, E. E. Mukhin, V. V. Semenov, and S. Y. Tolstyakov, *Fus. Sci. Technol.* **41**, 32 (2002).
- ²⁹⁷R. Fantoni, S. Almaviva, L. Caneve, F. Colao, G. Maddaluno, P. Gasior, and M. Kubkowska, *Spectrochim. Acta B* **129**, 8 (2017).
- ²⁹⁸P. Paris, J. Butikova, M. Laan, M. Aints, A. Hakola, K. Piip, I. Tu fail, and P. Veis, *Phys. Scr.* **2017**, 014003.
- ²⁹⁹W. Pietsch, A. Petit, and A. Briand, *Spectrochim. Acta B* **53**, 751 (1998).
- ³⁰⁰R. C. Chinni, D. A. Cremers, L. J. Radziemski, M. Bostian, and C. Navarro-Northrup, *Appl. Spectrosc.* **63**, 1238 (2009).
- ³⁰¹G. C. Y. Chan, X. Mao, I. Choi, A. Sarkar, O. P. Lam, D. K. Shuh, and R. E. Russo, *Spectrochim. Acta B* **89**, 40 (2013).
- ³⁰²H. Niki, T. Yasuda, and I. Kitazima, *J. Nucl. Sci. Technol.* **35**, 34 (1998).
- ³⁰³S. Brown, A. Ford, C. A. Akpovo, and L. Johnson, *Spectrochim. Acta B* **122**, 178 (2016).
- ³⁰⁴S. Brown, A. Ford, C. C. Akpovo, J. Martinez, and L. Johnson, *Spectrochim. Acta B* **101**, 204 (2014).
- ³⁰⁵M. R. Dong, G. C. Y. Chan, X. L. Mao, J. J. Gonzalez, J. D. Lu, and R. E. Russo, *Spectrochim. Acta B* **100**, 62 (2014).
- ³⁰⁶P. Ko and I. Jovanovic, *Spectrochim. Acta B* **90**, 68 (2013).
- ³⁰⁷K. C. Hartig, I. Ghebregziabher, and I. Jovanovic, *Sci. Rep.* **7**, 43852 (2017).
- ³⁰⁸D. G. Weisz *et al.*, *Appl. Phys. Lett.* **111**, 034101 (2017).
- ³⁰⁹R. E. Russo, A. A. Bol'shakov, X. L. Mao, C. P. McKay, D. L. Perry, and O. Sorkhabi, *Spectrochim. Acta B* **66**, 99 (2011).
- ³¹⁰H. D. Wizemann and K. Niemax, *Mikrochim. Acta* **129**, 209 (1998).
- ³¹¹J. Bergevin, T.-H. Wu, J. Yeak, B. E. Brumfield, S. S. Harilal, M. C. Phillips, and R. J. Jones, *Nat. Commun.* **9**, 1273 (2018).
- ³¹²J. J. Laserna, R. F. Reyes, R. Gonzalez, L. Tobarria, and P. Lucena, *Opt. Express* **17**, 10265 (2009).
- ³¹³P. D. Barnett, N. Lamsal, and S. M. Angel, *Appl. Spectrosc.* **71**, 583 (2017).
- ³¹⁴I. B. Gornushkin, B. W. Smith, U. Panne, and N. Omenetto, *Appl. Spectrosc.* **68**, 1076 (2014).
- ³¹⁵D. A. Cremers, *Appl. Spectrosc.* **41**, 572 (1987).
- ³¹⁶A. Ferrero and J. J. Laserna, *Spectrochim. Acta B* **63**, 305 (2008).
- ³¹⁷B. Sallé, P. Mauchien, and S. Maurice, *Spectrochim. Acta B* **62**, 739 (2007).
- ³¹⁸S. Palanco, C. Lopez-Moreno, and J. J. Laserna, *Spectrochim. Acta B* **61**, 88 (2006).
- ³¹⁹B. Salle, D. A. Cremers, S. Maurice, R. C. Wiens, and P. Fichet, *Spectrochim. Acta B* **60**, 805 (2005).
- ³²⁰B. Salle, J. L. Lacour, E. Vors, P. Fichet, S. Maurice, D. A. Cremers, and R. C. Wiens, *Spectrochim. Acta B* **59**, 1413 (2004).
- ³²¹S. Palanco and J. J. Laserna, *Rev. Sci. Instrum.* **75**, 2068 (2004).
- ³²²J. L. Gottfried, F. C. De Lucia, C. A. Munson, and A. W. Mizolek, *Appl. Spectrosc.* **62**, 353 (2008).
- ³²³C. López-Moreno, S. Palanco, and J. J. Laserna, *J. Anal. Atom. Spectrosc.* **22**, 84 (2007).
- ³²⁴F. J. Fortes and J. J. Laserna, *Spectrochim. Acta B* **65**, 975 (2010).
- ³²⁵S. Wallin, A. Pettersson, H. Ostmark, and A. Hobro, *Anal. Bioanal. Chem.* **395**, 259 (2009).
- ³²⁶R. C. Wiens *et al.*, *Space Sci. Rev.* **170**, 167 (2012).
- ³²⁷S. M. Clegg *et al.*, *Spectrochim. Acta B* **129**, 64 (2017).
- ³²⁸J. Scaffidi, S. M. Angel, and D. A. Cremers, *Anal. Chem.* **78**, 24 (2006).
- ³²⁹J. Uebbing, J. Brust, W. Sdorra, F. Leis, and K. Niemax, *Appl. Spectrosc.* **45**, 1419 (1991).
- ³³⁰D. N. Stratis, K. L. Eland, and S. M. Angel, *Appl. Spectrosc.* **55**, 1297 (2001).
- ³³¹R. Sattmann, V. Sturm, and R. Noll, *J. Phys. D* **28**, 2181 (1995).
- ³³²F. Colao, V. Lazić, R. Fantoni, and S. Pershin, *Spectrochim. Acta B* **57**, 1167 (2002).
- ³³³A. Kuwako, Y. Uchida, and K. Maeda, *Appl. Opt.* **42**, 6052 (2003).
- ³³⁴P. Rohwetter *et al.*, *J. Anal. Atom. Spectrosc.* **19**, 437 (2004).
- ³³⁵K. Stelmaszczyk *et al.*, *Appl. Phys. Lett.* **85**, 3977 (2004).
- ³³⁶H. Wille *et al.*, *Eur. Phys. J.: Appl. Phys.* **20**, 183 (2002).
- ³³⁷S. Tzortzakis, D. Anglos, and D. Gray, *Opt. Lett.* **31**, 1139 (2006).
- ³³⁸H. L. Xu, W. Liu, and S. L. Chin, *Opt. Lett.* **31**, 1540 (2006).
- ³³⁹E. J. Judge, G. Heck, E. B. Cerkez, and R. J. Levis, *Anal. Chem.* **81**, 2658 (2009).
- ³⁴⁰H. L. Xu, J. Bernhardt, P. Mathieu, G. Roy, and S. L. Chin, *J. Appl. Phys.* **101**, 033124 (2007).
- ³⁴¹B. Beardsley, private communication (2017).